PLANT DEFENSE SIGNALING MECHANISMS AND EVOLUTION

A Dissertation

by

SHAN JIANG

Submitted to the Office of Graduate and Professional Studies of
Texas A & M University
in partial fulfillment of the requirements for the degree of

DOCTOR OF PHILOSOPHY

Chair of Committee,	Libo Shan
Committee Members,	Ping He
	Charles Kenerley
	Paul de Figueiredo
Head of Department,	Leland S. Pierson III

August 2015

Major Subject: Plant Pathology

ABSTRACT

Plant innate immunity has been classified into two layers of defense systems. Nucleotide-binding domain leucine-rich repeat (NLR) protein complexes activated by pathogen effectors launches effector-triggered immunity (ETI). A forward genetic screen using the ETI marker gene *WRKY46* promoter fused with a firefly luciferase gene (*pWRKY46::LUC*) as a reporter identified five *ARABIDOPSIS* GENES GOVERNING IMMUNE GENE EXPRESSION (*aggie*) mutants, named as *aggie4-8*. Though with elevated *pWRKY46::LUC* activity, *aggie4* showed enhanced resistance to avirulent bacterial infections, yet delayed hypersensitive response (HR), while *aggie5* exhibited compromised disease resistance and delayed HR. Map-based cloning coupled with next generation sequencing (NGS) suggests that causal mutations of *aggie4* and *aggie5* locate in different regions of chromosome 5. In addition, *pWRKY46::LUC* activity is elevated in *aggie6* and *aggie7*, while suppressed in *aggie8*.

Perception of microbe-associated molecular patterns (MAMPs) by pattern recognition receptors (PRRs) triggers another tier of innate immunity, termed as pattern-triggered immunity (PTI). The *Arabidopsis* SOMATIC EMBRYOGENESIS RECEPTOR KINASE (SERK) family plays important roles in plant defense responses. It remains unknown how SERK members have evolved. Here, three SERK homologs, Pp1s35_219V6.1, Pp1s96_90V6.1 and Pp1s118_79V6.1 were identified in *P. Patens* with 60%-80% amino acid identify to AtSERKs and were named as PpSERK1.1, PpSERK1.2 and PpSERK2 respectively. In vitro kinase assay revealed that PpSERK1.1

and PpSERK1.2, but not PpSERK2, possess strong kinase activity. Functional complementation analysis suggested that PpSERK1.1 and PpSERK1.2 but not PpSERK2 regulate FLS2-mediated plant defense, and PpSERK1.2 but not PpSERK1.1 also regulates cell death in *Arabidopsis*.

PTI induces a rapid and profound transcriptional reprograming via concerted actions of specific transcription factors and general transcription machinery. *Arabidopsis* SH4-related 3 (ASR3), a plant specific trihelix family of transcription factors, is rapidly phosphorylated by MPK4 at Threonine 189 residue upon multiple MAMP treatments but not upon elicitation of ETI. Genetic and biochemical data suggests that phosphorylation of ASR3 enhances its DNA binding activity to suppress immune genes expression. Importantly, the *asr3* mutant shows higher immune gene activation and enhanced disease resistance, while transgenic plants overexpressing ASR3 exhibit compromised PTI responses. This study reveals that ASR3 functions as a transcription repressor regulated by MPK4 to fine-tune plant defense.

To mom & dad

ACKNOWLEDGEMENTS

I would like to thank my committee chair, Dr. Libo Shan, co-chair Dr. Ping He, and my committee members, Dr. Charles Kenerley and Dr. Paul de Figueiredo, for their patient guidance and support throughout the course of this research. Dr. Kenerley is a great gentleman that he raised the question of what contribution I can make to the field in order to encourage me to think about future career. Dr. de Figueiredo is the man who helped me build up confidence in research. He "required" me to raise a question in every single seminar and that is the moment I started to be actively engaged in the scientific discussion.

Special thanks go to my advisors, Dr. Shan and co-chair Dr. He for the great opportunity of my Ph.D. study in the exciting field of molecular plant microbe interaction. Without their generous tolerance, forgiveness and strong support, I would not have overcome the difficulties and frustration I met during my abroad studies.

Tremendous thanks also go to the world's greatest and most lovely colleagues in Dr. Shan and Dr. He's Lab. I am extremely thankful to Dr. Bo Li and Dr. Xiao Yu, without whom the ASR3 project couldn't be accepted smoothly by the *Journal of the Plant Cell*. I would like to thank Dr. Cheng Cheng for initiating the ASR3 project and guiding me through the dark time. Moreover, I sincerely appreciate the cooperation of Ana Marcia Manhaes for her tremendous effort in the Moss SERK and forward genetic screen projects. In addition, I would like to thank Robert Justin Dorosky and Ken Wang for the generation of Moss SERKs knock-out constructs in *Physcomitrella patens*. I

would like to thank Dr. Fangjun Li for taking care of me and always sharing her food generously.

Sincere thanks go to the faculty and staff in the Norman Borlaug Institute and the Department of Plant Pathology for making my time at Texas AandM University a great and unforgettable experience. I also want to extend my gratitude to the China Scholarship Council for the scholarship.

Finally, I would like to thank my parents for their endless love and support and all my friends for their encouragement throughout my doctoral program.

.

TABLE OF CONTENTS

Page

LIST OF FIGURES

FIGURE Page

LIST OF TABLES

CHAPTER I

INTRODUCTION

Plants and animals are at the constant risk for infections from various microorganisms in their natural habitats. In contrast to animals, however, plants lack specialized mobile immune cells and an adaptive immune system (Ausubel, 2005; Jones and Dangl, 2006). In addition to preformed physical barriers, sessile plants largely rely on the innate immune system to launch prompt defense responses in situ to fend off potential infections (Spoel and Dong, 2012). Plant innate immunity has been classified as a two-tier defense system (Dodds and Rathjen, 2010; Jones and Dangl, 2006) (Fig. 1.1).

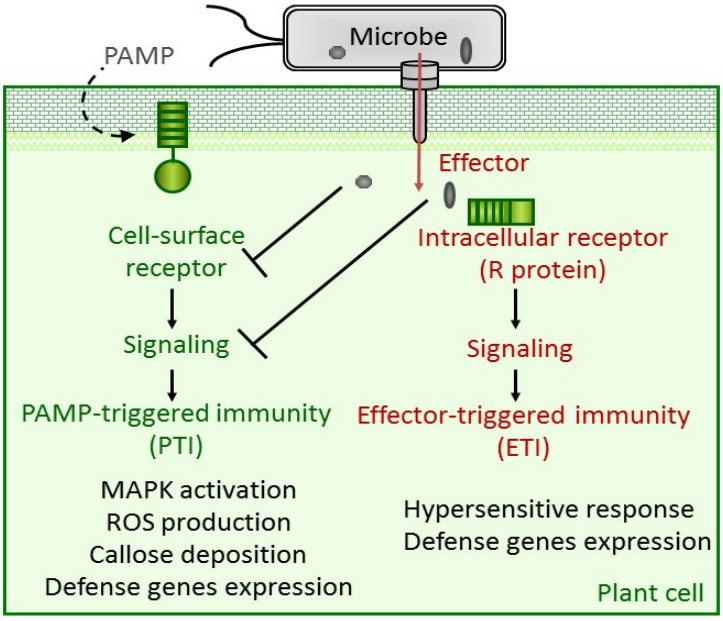

Fig. 1.1 Model of plant innate immunity. Plant innate immunity comprises of two branches, PTI and ETI.

1.1 Pattern-triggered immunity

Perception of MAMPs by PM-resident PRRs activates the first line of innate immunity, termed as PTI. This response mainly wards off the attack from host non-adapted pathogens (Bohm et al., 2014; Schwessinger and Ronald, 2012).

Even though the full repertoire of MAMPs perceived by plants remains unknown, several MAMPs, including bacterial flagellin, lipopolysaccharide (LPS), peptidoglycan (PGN), elongation factor Tu (EF-Tu), and fungal chitin, have been well characterized and shown to elicit various defense responses in plant cells (Bohm et al., 2014; Boller and Felix, 2009; Schwessinger and Ronald, 2012). A 22-amino-acid peptide corresponding to a region near the amino-terminus of flagellin, flg22, is perceived by *Arabidopsis thaliana* PRR FLAGELLIN-SENSING 2 (FLS2), a leucine-rich repeat RLK (LRR-RLK), and initiates immune signaling by instantaneous heterodimerization with another LRR-RLK BRASSINOSTEROID INSENSITIVE 1 - ASSOCIATED KINASE 1 (BAK1) (Chinchilla et al., 2007; Heese et al., 2007; Sun et al., 2013). BOTRYTIS-INDUCED KINASE 1 (BIK1), a receptor-like cytoplasmic kinase (RLCK), and its homolog PBS1-LIKE 1 (PBL1), constitutively associate with FLS2 and BAK1, and are rapidly phosphorylated and released from the receptor complex upon flg22 perception (Lu et al., 2010; Zhang et al., 2010). BIK1 directly phosphorylates PM-resident NADPH oxidase RESPIRATORY BURST OXIDASE HOMOLOG D (RBOHD) for transient production of reactive oxygen species (ROS), an early event triggered by multiple MAMPs (Kadota et al., 2014; Li et al., 2014). The FLS2 complex is also negatively regulated via various mechanisms to fine-tune PTI

responses. Two closely related plant U-box E3 ubiquitin ligases (PUB) 12 and 13 are recruited to the FLS2 complex via interaction with BAK1 upon flg22 perception, directly ubiquitinate FLS2 and lead to flg22-induced FLS2 degradation (Lu et al., 2011). BIR2 (BAK1-INTERACTING RLK 2), an LRR-RLK without detectable kinase activity, constitutively interacts with BAK1 and negatively regulates flg22-induced heterodimerization of FLS2 and BAK1 (Halter et al., 2014). In addition, PROTEIN PHOSPHATASE 2A (PP2A) controls activation of the PRR complexes likely by modulating the phosphorylation status of BAK1 (Segonzac et al., 2014).

Rapid activation of mitogen-activated protein kinase (MAPK) cascades has been observed upon multiple MAMP perceptions (Meng and Zhang, 2013; Pitzschke, et al., 2009; Rodriguez et al., 2010; Tena et al., 2011). A typical MAPK cascade is composed of three sequentially activated kinases consisting of a MAPK kinase kinase (MAP3K or MEKK), a MAPK kinase (MAP2K, or MKK) and a MAPK, which links upstream signals to downstream targets (Rodriguez et al., 2010). In Arabidopsis, two MAPK signaling pathways have been identified with one branch of MEKK-MKK4/MKK5-MPK3/MPK6 acting as positive regulators and another branch of MEKK1-MKK1/MKK2-MPK4 as negative regulators in plant immunity (Meng and Zhang, 2013; Tena et al., 2011). In general, MAPKs regulate gene expression through phosphorylation of downstream transcription factors. WRKY and ERF transcription factors are two major defense-related transcription factors in plants and some of them have been shown to be phosphorylated by MAPKs. Ethylene responsive factor104 (ERF 104) is a substrate of MPK6 activated by flg22, and phosphorylation induces its release from MPK6 to

regulate target gene expression (Bethke et al., 2009). WRKY33 is phosphorylated by MPK3 and MPK6 in vivo upon *Botrytis cinerea* infection, thereby inducing camalexin biosynthetic gene expression to promote phytoalexin biosynthesis (Mao et al., 2011). In addition, ERF6 is also phosphorylated by MPK3 and MPK6 and plays an important role in plant defense against fungal pathogen (Meng and Zhang, 2013).

1.2 Effector-triggered immunity

Adapted pathogens deploy various virulence factors to interfere with PTI and establish successful infections (Block et al., 2008; Dou and Zhou, 2012; Mudgett, 2005; Xin and He, 2013). In particular, many pathogenic bacteria inject a plethora of effector proteins into host cells through type III secretion system (T3SS), which favors pathogen survival and multiplication and mediates effector-triggered susceptibility (ETS). Many of these effectors target important host components to interfere host immune responses and physiology. (Cui et al., 2013; Feng and Zhou, 2012). Multiple effectors, including AvrPto, AvrPtoB and HopF2 target PRR co-receptor BAK1 to dampen PTI (Zhou et al., 2014). Host plants further evolved the intracellular receptors often encoded by NLR, also named as disease resistance (R) proteins, to recognize virulence effectors or sense effector-mediated perturbations of host targets and elicit the second tier of defense responses, termed as ETI (Bonardi and Dangl, 2012; Gassmann and Bhattacharjee, 2012; Qi and Innes, 2013).

Plant NLR proteins share the structural similarity with mammalian (nucleotide-binding oligomerization domain) NOD-like receptors that perceive intracellular MAMPs

and danger signals to initiate inflammation and immunity (Maekawa et al., 2011). *Pseudomonas syringae* effector AvrRpt2 is recognized by *Arabidopsis* NLR protein RESISTANCE TO PSEUDOMONAS SYRINGAE 2 (RPS2), whereas two sequence-unrelated effectors, AvrRpm1 and AvrB, are recognized by RESISTANCE to PSEUDOMONAS SYRINGAE PV. MACULICOLA 1 (RPM1) to initiate ETI responses including transcriptional reprogramming and localized programmed cell death (PCD) termed as HR. Instead of direct NLR-effector interaction, RPS2 and RPM1 monitor the perturbation of host protein RPM1-INTERACTING PROTEIN 4 (RIN4) targeted by pathogen effectors to mount defense responses (Axtell and Staskawicz, 2003; Mackey et al., 2003). Specific calcium-dependent protein kinases (CDPKs) downstream of NLR proteins sense sustained increase of cytosolic Ca^{2+} concentration and regulate the bifurcate defense responses via phosphorylation of different substrates and subcellular dynamics (Gao et al., 2013).

CHAPTER II

GENETIC DISSECTION OF PLANT INNATE IMMUNE SIGNALING NETWORKS

2.1 Summary

Effector recognition by host R proteins activates ETI. However, the molecular signaling networks underlying ETI remain fragmented. A forward genetic screen for mutants with altered ETI response was conducted. WRKY46 is an early and specific ETI marker in response to multiple effectors. Transgenic plants carrying WRKY46 promoter fused with a luciferase gene were generated. Mutants with altered effector-triggered *pWRKY46::LUC* activity were selected. Five mutants with altered *pWRKY46::LUC* activity were identified and named as *aggie4-8*. The *aggie4* mutant displays elevated effector-triggered *pWRKY46::LUC* activity and resistance to avirulent *Pseudomonas sryingae* pv *sryingae* carrying (*Pst*) avrRpt2 or *Pst* avrRpm1, but delayed HR. The *aggie5* mutant displays elevated effector-triggered *pWRKY46::LUC* activity, but delayed HR and compromised disease resistance to virulent *Pseudomonas sryingae* pv *maculicola* (*Psm*) and avirulent *Pst* avrRpt2. In addition, flg22-triggered MAPKs activation, a PTI early response, is further enhanced in *aggie5*. Map-based cloning coupled with NGS revealed that *aggie4* and *aggie5* causal genes locate in the regions on chromosome 5. Characterization of the *aggie* mutants will provide important insights in dissecting plant immune signaling.

2.2 Introduction

H.H. Flor's observation that certain groups of flax were susceptible to one type of rust, whereas other groups were not, lead to the "gene-for-gene" theory. This theory describes the one for one relationship between an avirulence gene (Avr gene) in the pathogen and a resistance R gene in the host (Flor et al., 1971). Specific Avr proteins could be recognized by R proteins in the host, and trigger defense responses. Two independent cases, the cloning of Avr genes from *Pseudomonas syringae* pv. *glycinea* race 6 (Staskawicz et al., 1984) and the cloning of the R gene *Pto* from tomato (Martin et al., 1993), confirmed the gene-for-gene theory. Direct R protein-effector interactions were detected and supported by yeast two-hybrid and in vitro interaction assays (Catanzariti et al., 2010; Dodds and Rathjen, 2010).

However, indirect R-effector interactions appear to be the more prevalent cases for many Arv-R pairs. Two models were postulated to explain the indirect R-effector interaction. In the guard hypothesis model, the receptor is activated when a host guardee is modified by a pathogen effector (Bhattacharjee et al., 2011; Mackey et al., 2003). Plant R proteins, RPM1 and RPS2 constitutively guard a host protein, RIN4. AvrB- or AvrRpm1- induced phosphorylation of RIN4 is sensed by RPM1 to activate immune signaling pathway (Liu et al., 2011). RIN4 cleavage by AvrRpt2 activates RPS2 to trigger downstream defense response (Axtell and Staskawicz, 2003; Mackey et al., 2003). In the absence of RPM1 or RPS2, RIN4 acts as a negative regulator of basal resistance (Kim et al., 2005; Liu et al., 2009).

In the decoy hypothesis model, plants are believed to deploy a host factor of not measurable resistance function as a decoy to trap pathogen effectors that target structurally related basal defense components, thereby triggering ETI (Collier and Moffett, 2009). The protein kinase AVRPPHB SUSCEPTIBLE 1 (PBS1) has no obvious function in basal resistance. PBS1 cleavage by *P. syringae* effector AvrPphB activates RPS5-mediated resistance.

In order to dissect ETI pathway, our lab initiated a forward genetic screen in search of mutants with altered ETI response indicated by *pWRKY46::LUC* activity. *WRKY46* is an early and effector-induced gene. *pWRKY46::LUC* was generated by fusing WRKY46 promoter with a luciferase gene (Fig. 2.1A). Transgenic plant seeds carrying *pWRKY46::LUC* were subjected to mutagen ethyl methanesulfonate (EMS) treatment to generate random mutations. *pWRKY46::LUC* activity was measured via a luminometer machine (Fig. 2.1B). Five mutants out of ~5,000 with altered *pWRKY46::LUC* activity were selected for further study.

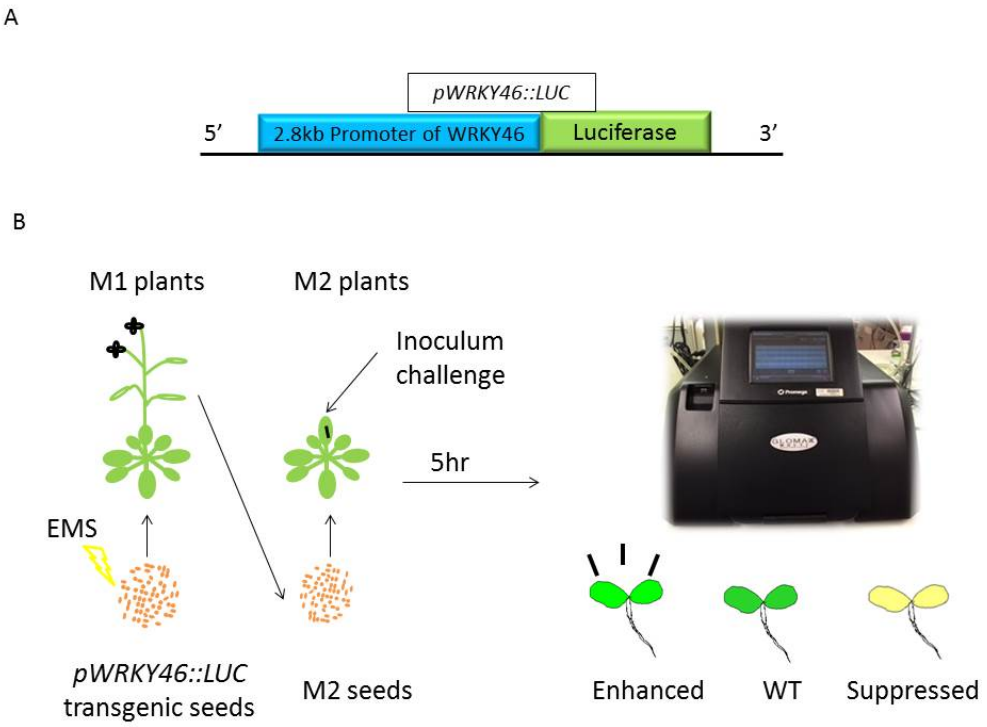

Fig. 2.1 Schematic design of screening *pWRKY46::LUC* transgenic mutants. (A) Model of *pWRKY46::LUC* construct used for generating *pWRKY46:LUC* transgenic plants. (B) Scheme displays steps of *pWRKY46::LUC* mutant screening.

Forward genetics has been proven as an effective method to identify causal mutations for certain phenotypes. Map-based cloning is widely used to locate the mutation to the chromosomal region harboring the mutation. To generate the mapping population, the mutant of interest usually in Col-0 ecotype is outcrossed to another *Arabidopsis* ecotype, *Landsberg. Erecta* (Ler). Seeds obtained from outcross siliques are named as F1, which followed by a self-cross to yield F2 seeds. F2 recombinants that show the mutant phenotype will be selected. A series of genetic markers are identified as polymorphisms between the two *Arabidopsis* ecotypes. Less frequent recombinations occur between the causal mutation and the nearby genetic markers, while random recombinations happen between the causal mutation and the non-linked markers.

Genotyping analyses will reveal over-representation of causal mutations within markers from the selected F2 recombinants. The putative causal gene linked genetic markers will enable the identification of a broad chromosome region that harbors the causal mutation. Traditionally, Sanger sequencing of individual genes in the mutant within the mapping interval is used to detect the true mutation in the mutant. This method has proven to successfully identify causal mutations across species. One disadvantage is that Sanger sequencing of an individual putative gene is time and labor intensive when many putative genes are included within the final mapping interval.

NGS is also known as high-throughput sequencing, which allows DNA and RNA sequencing much more quickly than Sanger sequencing. With the development of NGS, map-based cloning coupled with whole genome sequencing allows the rapid identification of the causal mutation (Metzker, 2010; Shendure and Ji, 2008).

2.3 Material and methods

2.3.1 Plant growth conditions and bacterial inoculation

Arabidopsis WT (Col-0) and other plants were grown in pots containing soil (Metro Mix 360) in a growth room at 23°C, 60% relative humidity and 75 μE $m^{-2}\cdot s^{-1}$ light with a 12 hr photoperiod for approximate 4 weeks before bacterial inoculation.

2.3.2 Map-based cloning

Approximately 125,000 seeds containing the *WRKY46::LUC* transgenic seeds were treated with 0.4% EMS for 8 hours. Approximately 5,000 M2 plants were screened

for *aggie* mutants with the high or low luciferase activity based upon *Pst* avrRpt2 infection. The F2 populations for mapping the *aggie4* and *aggie5* mutations were derived from genetic crossing between the mutants in the Col-0 background to WT plants in the Ler background. Bulked segregation analysis was performed on pools of 40 plants with INDEL markers between Col-0 and Ler. Fine mapping with 180 homozygotes revealed 25 recombinants.

2.3.3 Disease assay and HR assay

Pst AvrRpt2, *Pst* AvrRpm1, *Pst* AvrRps4 strains were grown overnight at 28°C in the King's medium B (KB) containing rifamycin and kanamycin (each at 50 μg $\cdot ml^{-1}$). *Psm* strain was grown overnight at 28°C in the KB medium containing rifamycin (50 μg $\cdot ml^{-1}$). Bacteria were pelleted by centrifugation, washed, and diluted to the desired density (OD=0.01 for HR, $5*10^{-4}$ for disease assay). The leaves were hand-inoculated with bacteria using a needleless syringe, and collected at the indicated time (0dpi, 3dpi) for bacterial counting, HR phenotype recording. To measure bacterial growth, two leaf discs were ground in 100 μl water and serial dilutions were plated on TSA (1% Bacto tryptone, 1% sucrose, 0.1% glutamic acid, 1.5% agar) medium with appropriate antibiotics. Bacterial colony forming units (cfus) were determined after incubation at 28°C.

At least three independent experiments were performed for all experiments. A one-way ANOVA analysis was performed with SPSS software with (SPSS Inc., Chicago).

2.3.4 MAPK activation

To detect MAPK activity, 10-day-old WT, *aggie4* and *aggie5* seedlings grown on ½ MS medium were transferred to water, incubated overnight and then treated with 100 nM flg22 or water for indicated time points (0, 15, 45min) and frozen in liquid nitrogen. The seedlings were homogenized in an extraction buffer (20 mM Tris-HCl, pH7.5, 100 mM NaCl, 1 mM EDTA, 10% Glycerol, 1% Triton X-100). Supernatant after centrifugation was transferred into a new tube. Equal amount of total proteins were electrophoresed on 10% SDS–PAGE. A α-pERK antibody (Cell Signaling) was used to detect phosphorylation status of MPK3 and MPK6 with an immunoblot. For different treatments, the seedlings were treated with 100 nM flg22 for indicated length of time.

2.4 Results

2.4.1 Five mutants of *pWRKY46::LUC* transgenic plants were identified with altered *pWRKY46::LUC* activity

To elucidate the signaling networks regulating immune gene activation, we developed a high throughput genetic screen. *WRKY46* represents a specific and early immune responsive gene activated by multiple effectors, including AvrRpt2, AvrRpm1 and AvrRps4. Transgenic plants were generated by *Agrobacteria tumefaciens* transformation with the construct *pWRKY46::LUC* containing WRKY46 promoter fused with a luciferase reporter gene. EMS mutagenized population of transgenic plants seeds carrying *pWRKY46::LUC* were subjected to a genetic screen. M1 plants were grown to obtain M2 seeds, and then the soil grown M2 plants were infiltrated with *Pst* avrRpt2.

Five hours post inoculation, the inoculated leaves were cut and placed into 96-well plate. After spraying with luciferin, the substrate of luciferase enzyme, the plate was measured via a luminometer.

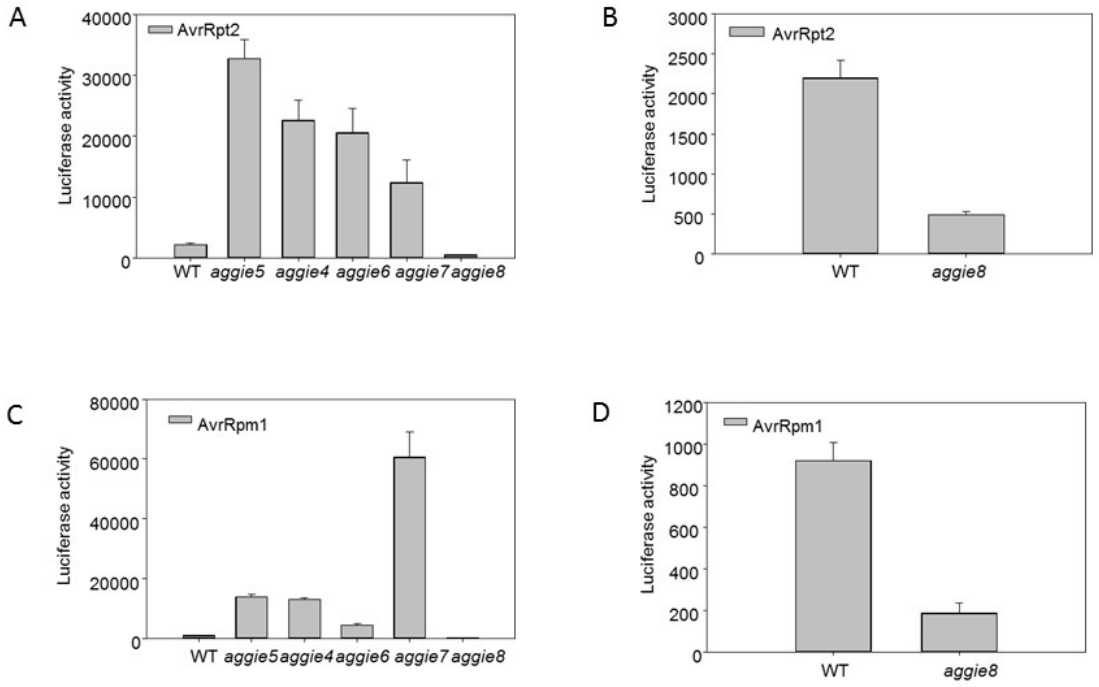

Fig. 2.2 Altered *pWRKY46::LUC* activity in *aggie4-8*. (A,B) *aggie4-7* displayed enhanced AvrRpt2-induced *pWRKY46::LUC* activity while *aggie8* displayed suppressed AvrRpt2-induced *pWRKY46::LUC* activity. (C,D) *aggie4-7* displayed enhanced AvrRpm1-induced *pWRKY46::LUC* activity while *aggie8* displayed suppressed AvrRpm1-induced *pWRKY46::LUC* activity. 4-week-old soil-grown adult plants were subjected to hand inoculation of *Pst* avrRpt2 at OD=0.01 with a needleless syringe, and luciferase activity was measured 5 hr after infiltration.

Five *pWRKY46::LUC* transgenic mutants out of 5,000 plants were selected with altered *pWRKY46::LUC* activity and named as *aggie4-8*. *aggie4-7* displayed enhanced AvrRpt2 and AvrRpm1-induced *pWRKY46::LUC* activity while *aggie8* displayed compromised AvrRpt2 and AvrRpm1-induced *pWRKY46::LUC* activity (Fig. 2.2).

2.4.2 Elevated *pWRKY46::LUC* activity and disease resistance in *aggie4* mutant

Upon *Pst* AvrRpt2 infiltration, *aggie4* displayed elevated *pWRKY46::LUC* promoter activity detected by CDD camera (Fig. 2.3A) and luminometer (Fig. 2.3B). Notably, the *aggie4* mutant significantly activated *pWRKY46::LUC* promoter in the absence of effector infiltration, suggesting constitutive immune response in *aggie4*. Notably, the *aggie4* mutant displayed morphological differences such as wrinkled leaf edges and hypersensitive to mechanical damage compared to WT plants. In addition to AvrRpt2, the *aggie4* mutant exhibited enhanced *pWRKY46::LUC* activity in response to other effectors, including AvrRpm1 and AvrRps4 (Fig. 2.3B). As multiple effector-induced *pWRKY46::LUC* was elevated in *aggie4*, the *aggie4* mutant may affect a downstream convergent component regulating ETI. Consistent with the enhanced *pWRKY46::LUC* activity, *aggie4* was more resistant to avirulent *Pst* avrRpt2 and *Pst* avrRpm1 infections. The bacterial multiplication in *aggie4* was less than that in WT plants at 3 days post infection (dpi) (Fig. 2.3C, D).

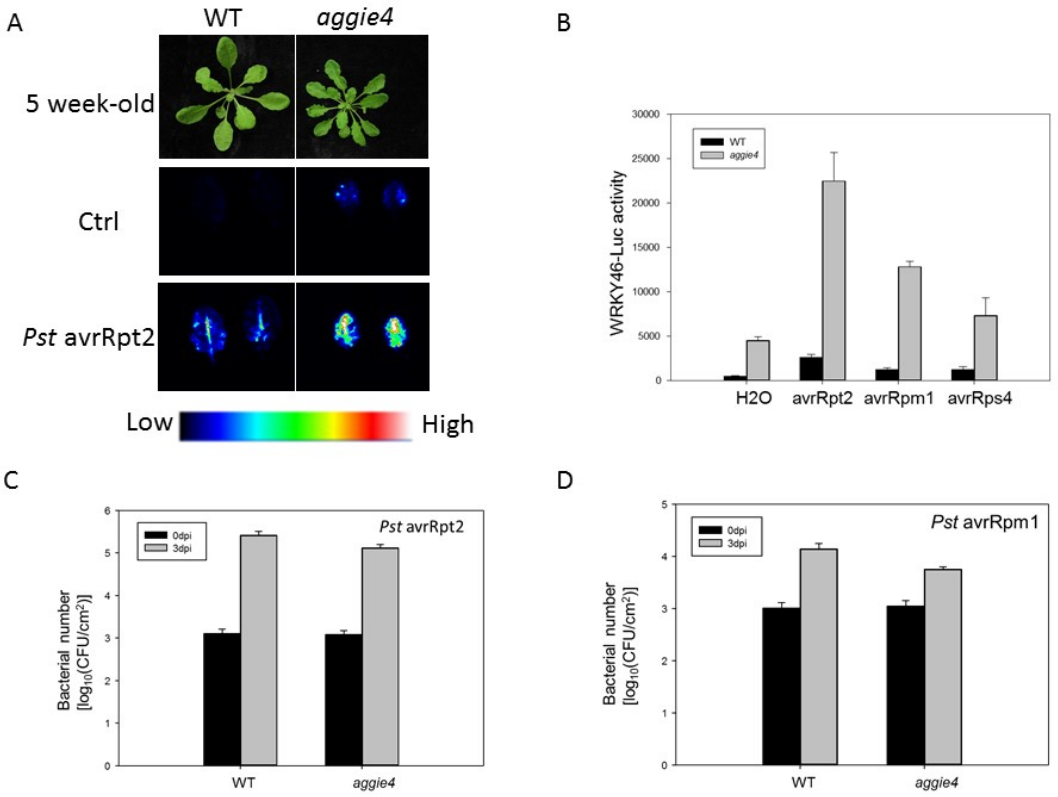

Fig. 2.3 Elevated *pWRKY46::LUC* activity and disease resistance in *aggie4* mutant. (A) 5-week-old wild-type *pWRKY46::LUC* transgenic plants and *aggie4* were analyzed without treatment (control) and with *Pst* avrRpt2 infiltration under CCD camera. (B) The *pWRKY46::LUC* activity was enhanced in *aggie4* mutant upon infiltration of multiple strains *Pst* avrRpt2, *Pst* avrRpm1 and *Pst* avrRps4. (C)The *aggie4* mutants are more resistant to *Pst* avrRpt2 infection. The plants were hand-inoculated with *Pst* avrRpt2 at 2 x 10^8 cfu/ml and bacterial growth assay was performed at 0dpi and 3dpi. (D)The *aggie4* mutant was more resistant to *Pst* avrRpm1 infection. The plants were hand-inoculated with *Pst* avrRpm1 at 2 x 10^8 cfu/ml and bacterial growth assay was performed at 0dpi and 3dpi.

2.4.3 Delayed HR response and unaltered PTI response in *aggie4* mutant

ETI responses are often accompanied with HR. Although effector-induced *pWRKY46::LUC* activity was elevated, *aggie4* displayed delayed HR response to *Pst* avrRpt2 and *Pst* avrRpm1 infections (Fig.2.4A, B), which suggest that the different mechanisms of regulating defense transcriptome profile and HR response.

MAPK activation represents one of early PTI signaling events. The flg22-induced MAPK activation detected by a α-pERK antibody in WT and *aggie4* seedlings

suggested that *aggie4* did not affect flg22-induced MAPK activation (Fig. 2.4C). The results suggest that *aggie4* functions specifically in ETI but not PTI.

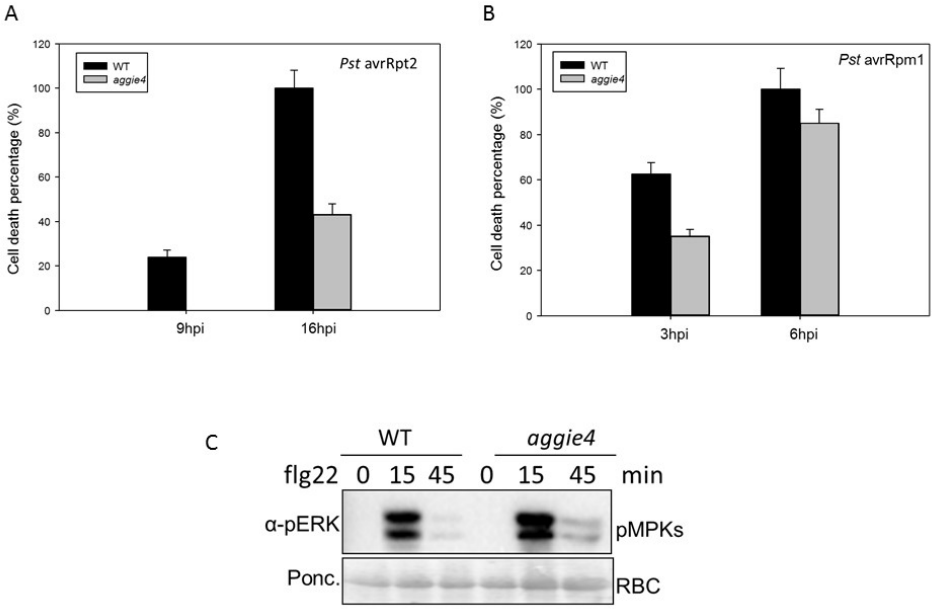

Fig. 2.4 Delayed HR response but unaltered PTI response in *aggie4* mutant. (A) 4-week-old WT and *aggie4* were hand-inoculated with *Pst* avrRpt2 at OD=0.1. Numbers of leaves display HR were recorded for a time series of 8 hour post inoculation (hpi) to 16hpi. Proportions of leaves showing HR were calculated and two timepoints (9hpi and 16hpi) were shown in the Fig.. (B) 4-week-old WT and *aggie4* were hand-inoculated with *Pst* avrRpm1 at OD=0.1. Numbers of leaves display HR were recorded for a time series of 2 hpi to 8hpi. Proportions of leaves showing HR were calculated and two timepoints (3hpi and 6hpi) were shown in the Fig.. (C) Unaltered flg22-triggered MAPKs activation in *aggie4*. Twelve-day old WT or *aggie4* seedlings were treated with 100nM flg22 for different time points. MAPK activation was analyzed with a α-pERK antibody (top panel), and the protein loading was shown by Coomassie blue staining (CBS) (bottom panel).

2.4.4 The *aggie4* was mapped to *Arabidopsis* choromosome 5

Genetic analysis indicated that the causal mutation in *aggie4* is recessive as F1 plants obtained by *aggie4* backcrossing with WT showed similar *pWRKY46::LUC* activity compared to the WT plants upon infiltration of *Pst* avrRpt2 (Fig 2.5A). Map-based cloning was applied to locate the causal mutation. F1 plants were obtained by outcrossing *aggie4* (in WT Col-0 background) with the WT *Ler*. After one generation of self-crossing, F2 plants were subjected to screen of homozygotes, which displayed

enhanced AvrRpt2-mediated *pWRKY46::LUC* activity. Phenotypic analysis of 1800 F2 plants leads to finding of 180 homozygotes. Bulked segregation analysis was performed on pools of 40 plants with INDEL markers between Col-0 and Ler. (Fig. 2.5B). Fine mapping with 180 homozygotes revealed 25 recombinants. Genetic analysis with the homozygous recombinants demonstrated that *aggie4* causal mutation is located within a region between genetic marker T31B5 and MTG13 (4.2Mb to 5.4Mb) on *Arabidopsis* choromosome 5 (Fig. 2.5C). NGS suggests G to A point mutations of three genes within the final mapping interval of 100% frequency. We Sanger sequenced the three individual genes and confirmed the G to A point mutations resulting in amino acid changes. Complementation assay needs to be performed to determine which the bona fide causal gene accounting for the altered ETI responses in *aggie4*.

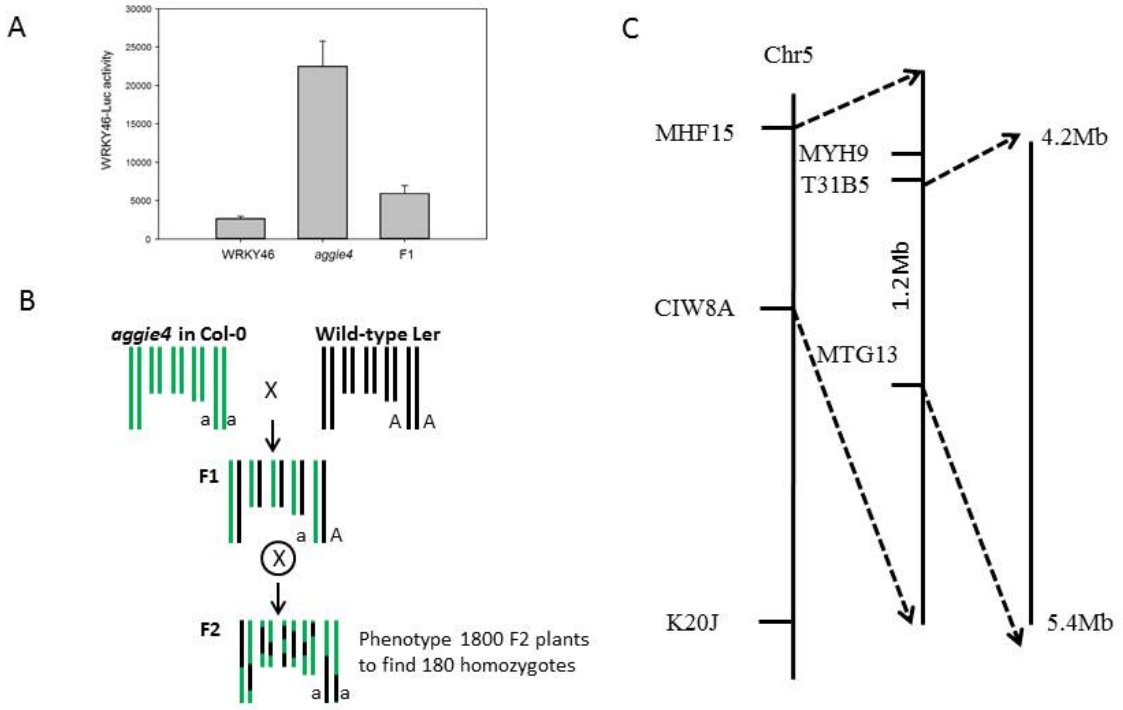

Fig. 2.5 The *aggie4* was mapped to *Arabidopsis* choromosome 5. (A) Causal mutation in *aggie4* is recessive. The F1 plants crossed from *aggie4* and WT Col-0 showed *pWRKY46::LUC* activity similar to WT upon infiltration of *Pst* avrRpt2. (B) Scheme displays map-based cloning of *aggie4*. F1 plants were obtained by outcrossing *aggie4* (in Col-0 background) with another WT Ler. After one generation of self-crossing, F2 plants were subjected to screen of homozygotes, which displayed enhanced AvrRpt2-mediated *pWRKY46::LUC* activity. (C) *aggie4* causal mutation was mapped to a region between genetic marker T31B5 and MTG13 (4.2Mb to 5.4Mb) on *Arabidopsis* choromosome 5.

2.4.5 Elevated *pWRKY46::LUC* activity in *aggie5* mutant

The *aggie5* displays morphological differences with smaller leaves and pentagon leaf shape, compared to WT plants (Fig. 2.6A). The *aggie5* exhibited enhanced *pWRKY46::LUC* activity in response to multiple effectors such as AvrRpt2, AvrRpm1 or AvrRps4 (Fig. 2.6B). As multiple-effector-induced *pWRKY46::LUC* was elevated in *aggie5*, the *aggie5* mutant may affect a downstream convergent component regulating ETI.

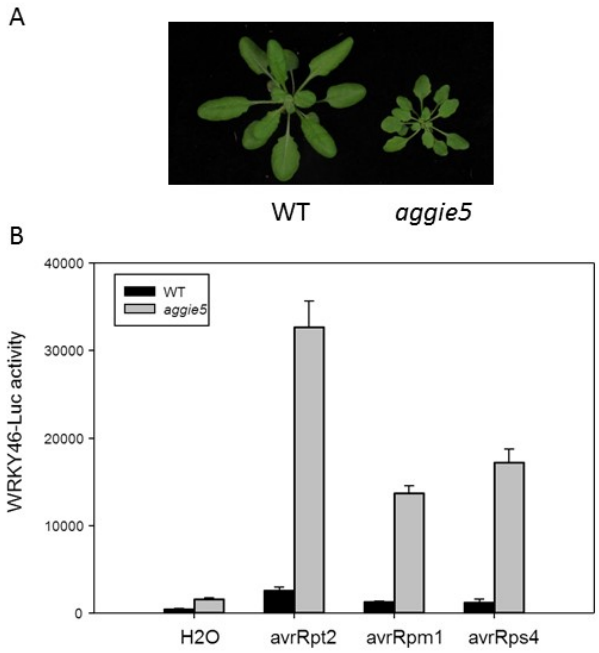

Fig. 2.6 Elevated *pWRKY46::LUC* activity in *aggie5* mutant. (A) Photograph of 5-week-old WT plants and *aggie5*. (B) The *pWRKY46::LUC* activity was enhanced in *aggie5* mutant upon infiltration of multiple strains *Pst* avrRpt2, *Pst* avrRpm1 and *Pst* avrRps4.

2.4.6 The *aggie5* display compromised ETI response and disease resistance but enhanced PTI response

In contrast to the enhanced effector-triggered *pWRKY46::LUC* activity, AvrRpt2- and AvrRpm1-triggered HR responses in *aggie5* were much delayed compared with WT (Fig. 2.7A, B). The *aggie5* mutant was more susceptible to avirulent *Pst* avrRpt2 and virulent *Psm* infections, as more bacterial multiplication and more severe yellowish disease symptom compared to WT (Fig. 2.7 C, D). In addition, flg22-induced MAPK activation was further enhanced in *aggie5*, suggesting *aggie5* affects both ETI and PTI. The underlining mechanisms suggest the existence of crosstalk between PTI and ETI pathway.

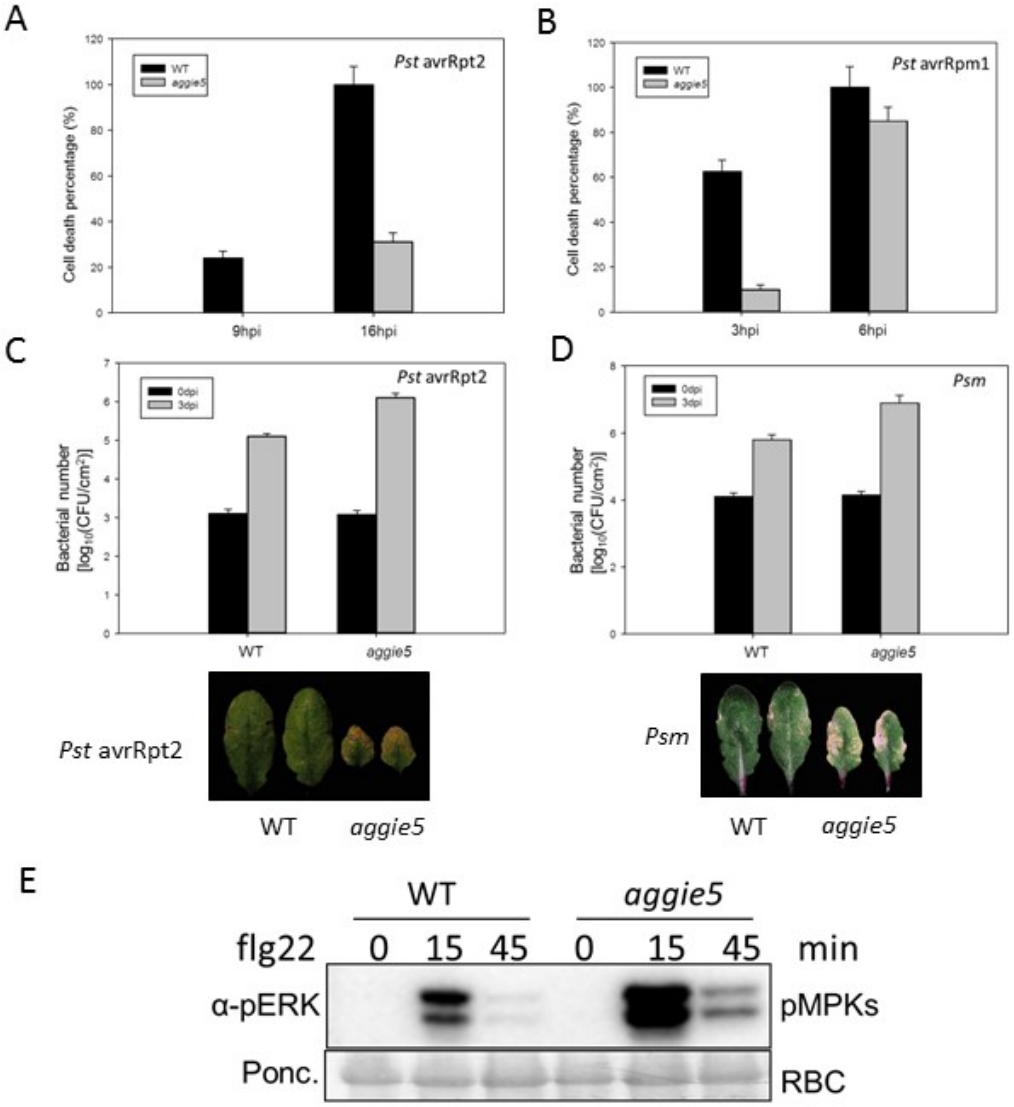

Fig. 2.7 Compromised ETI but enhanced PTI response in *aggie5*. (A) 4-week-old WT plants and *aggie5* were hand-inoculated with *Pst* avrRpt2 at OD_{600}=0.1. Numbers of leaves displaying HR were recorded for a time series of 8hpi to 16hpi. Proportions of leaves showing HR were calculated and results at two timepoints (9hpi and 16hpi) were shown in the Fig.. (B) 4-week-old WT plants and *aggie5* were hand-inoculated with *Pst* avrRpm1 at OD_{600}=0.1. Numbers of leaves displaying HR were recorded for a time series of 2hpi to 8hpi. Proportions of leaves showing HR were calculated and results at two timepoints (3hpi and 6hpi) were shown in the Fig.. (C)The *aggie5* mutant was more susceptible to *Pst* avrRpt2 infection. The plants were hand-inoculated with *Pst* avrRpt2 at $OD_{600}=5*10^{-4}$ ($2 * 10^8$) cfu/ml and bacterial growth assay was performed at 0dpi and 3dpi. Photograph showed disease symptom of *Pst* avrRpt2 infected WT and *aggie5* mutant at 3dpi. (D)The *aggie5* mutant was more susceptible to *Psm* infection. The plants was hand-inoculated with *Psm* at $OD_{600}=5*10^{-4}$ ($2 * 10^8$) cfu/ml and bacterial growth assay was performed at 0dpi and 3dpi. Photograph showed disease symptom of *Psm* infected WT and *aggie5* mutant at 3dpi. (E) Enhanced flg22-triggered MAPKs activation in *aggie5*. Twelve-day old WT or *aggie5* seedlings were treated with 100nM flg22 for different time points. MAPK activation was analyzed with a α-pERK antibody (top panel), and the protein loading was shown by CBS (bottom panel).

2.5 Discussion

Specific R proteins in an adapted host could recognize cognate effectors to launch ETI, which is often associated with HR and defense genes activation. However, the underlying mechanism remains unknown. WRKY46 is a specific and early marker gene in ETI pathway. Forward genetic screen by utilizing *pWRKY46::LUC* transgenic plants have proved to be an effective and powerful way to study plant defense signaling pathways. Luciferase activity detected via a luminometer enables the quantitative measurement of the reporter gene expression activity. In addition, colleagues from our lab have identified mutants carrying mutations in either RPS2 or RPM1, which were unresponsive to AvrRpt2/AvrRpm1-mediated *pWRKY46::LUC* activity respectively. Hence, the results suggest that the forward genetic screen of using *pWRKY46::LUC* transgenic plants is likely to be effective. In addition, the procedure of screening is readily carried out in a relatively short time frame. Map-based cloning coupled with NGS analysis, instead of individual Sanger sequencing, also largely speed up the map-based cloning process.

As the mutants display multiple altered ETI responses, they could be of great important materials to study ETI signaling pathway. However, the apparent contradictory phenotype of *aggie4* and *aggie5* suggest a likely complex mechanism underlying ETI pathway. With elevated *pWRKY46::LUC activity*, *aggie4* was expected to be more resistant. However, *aggie4* displayed delayed HR in response to AvrRpt2 and AvrRpm1, which often serves as a sign of compromised ETI. Surprisingly, *aggie4* is more resistant to avirulent strain *Pst* avrRpt2 and *Pst* avrRpm1. The seemingly

contradictory defense responses in *aggie4* suggest that underlying mechanisms may be different from the conventional defense pathway, or the responses are controlled by parallel or overlapping pathways. Similar to *aggie4*, elevated AvrRpt2-triggered *pWRKY46::LUC* activity was enhanced in *aggie5*. However, *aggie5* displayed delayed HR in response to AvrRpt2 and AvrRpm1, and more susceptible to both *Pst* avrRpt2 and *Psm* infections compared to WT plants. Interestingly, besides ETI, *aggie5* exhibited altered PTI responses, as flg22-triggered MAPK activation is further enhanced in *aggie5* seedlings. Thus, *aggie5* affects both PTI and ETI antagonistically. Although the two-tier theory of plant defense has been proposed for plant innate immunity, mounting evidence suggests blur boundary between two branches. Characterization of *aggie5* function will shed light on research of crosstalk between PTI and ETI.

To test the hypothesis, cloning of the bona fide causal genes of *aggie4* and *aggie5* is necessary. Complementation assay of transforming the candidate genes back into the *aggie4* mutant is ongoing. In addition, additional knock-out mutants of candidate genes will be very useful to validate whether the function of the genes leads to *aggie4* phenotype. Genetic analysis suggest the causal mutation in *aggie5* is also recessive as F1 plants obtained by backcrossing *aggie5* with WT showed similar *pWRKY46::LUC* activity as the WT upon infiltration of *Pst* avrRpt2 (Fig. 2.8). 1200 F2 plants of outcrossing *aggie5* (in Col-0 background) with another ecotype *Ler* were tested, and 120 plants with high *pWRKY46::LUC* activity were selected. Fine mapping with 120 plants via using markers, which show polymorphism between Col-0 and Ler, and span trhougth the different chromosomes of Arabidopsis, revealed 18 recombinants.

Genetic analysis with the recombinants revealed that *aggie5* causal mutation located within a region about 0.4Mb to 1.3Mb on *Arabidopsis* choromosome 3. However, NGS identified no mutations located within this region of 100% frequency. Whole genome sequence analysis revealed that the *pWRKY46::LUC* was integrated to the *Arabidopsis* choromosome 3, which should be considered as a putative co-segregate factor. The traditional mapping requires the use of a segregating population from a cross of *aggie5* mutant in one accession Col-0 with a different accession, *Ler*. However, *aggie5* phenotype in *Ler* may be modified and thus limit mapping accuracy. To determine the causal mutation in *aggie5*, a new mapping method, using NGS on bulked segregants of *aggie5* backcross F2 offsprings was applied. Sequencing analysis was carried out by aligning the readings to the reference genome. SNP/INDEL were called and filtered by using SAMTOOLS. SNP ratios were plotted and peaks indicate *aggie5* causal mutation locates on chromosome 5. Complementation and knockout assay will be carried out to confirm the causal mutation (Zhu et al., 2012).

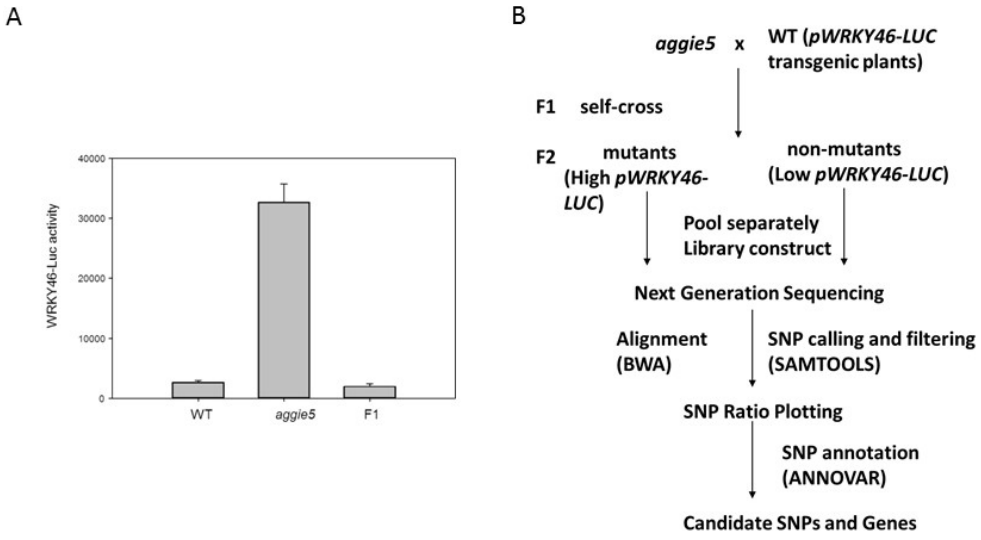

Fig. 2.8 Mapping and cloning strategy for *aggie5* causal mutation. (A) Causal mutation in *aggie5* is recessive. The F1 plants crossed from *aggie5* and WT showed similar *pWRKY46::LUC* activity to WT upon infiltration of *Pst* avrRpt2. (B) Scheme display the mapping and cloning strategy for *aggie5* with bulked segregants in backcross progenies. *aggie5* will be backcrossed to its original starting strain *pWRKY46::LUC* transgenic plants and F2 progenies will be scored for mutant phenotypes. Mutant plants with high *pWRKY46::LUC* activity and non-mutant plants with low *pWRKY46::LUC* activity will be separately pooled. DNAs from mutants and non-mutants pools will be used for library construct and subjected to NGS separately. After aligning the sequence reads to the reference genome, SNP/INDEL were called and filtered by using SAMTOOLS. SNP ratios will be plotted and peaks indicate mutation locations.

CHAPTER III

STUDY OF THE ORIGIN OF THE SERK FAMILY

3.1 Summary

PTI responses depend on the perception of MAMPs by PM-localized PRRs. PRRs in plants are often RLKs or Receptor Like Proteins (RLPs). The *Arabidopsis* SERK family is comprised of five RLKs with specific and overlapping functions involved in diverse cellular processes ranging from male microsporogenesis, plant growth hormone Brassinosteroid signaling, and cell death to PRR-mediated innate immunity. Despite the ubiquitous presence of their homologous sequences across different plant species, how SERK members have evolved with redundant and distinct functions remains unknown. Three SERK homologs in *Physcomitrella patens*, Pp1s35_219V6.1, Pp1s96_90V6.1 and Pp1s118_79V6.1 were identified as they share 60%-80% identity at the amino acid sequence level to individual SERKs and were named as PpSERK1.1, PpSERK1.2, and PpSERK2 respectively. In addition, PpSERK1.1 and PpSERK1.2 are more closely related to each other with 97% identity, and bear 82% and 86% identity with SERK1 and SERK2, respectively. Blast of the amino acid sequence of PpSERK1.1 and PpSERK1.2 cytosolic kinase domains reveals only one amino acid difference. In consistent, in vitro kinase assay revealed that PpSERK1.1 and PpSERK1.2 possess strong kinase activity, while PpSERK2 possesses weaker kinase activity. Functional analysis suggested that PpSERK1.1 and PpSERK1.2, but not PpSERK2, regulate FLS2-mediated plant defense; and PpSERK1.2, but not

PpSERK1.1, regulates cell death in *Arabidopsis*. As the SERK family plays multifaceted roles in plant defense and development, study on SERK family origin will shed light on the evolution of plant innate immunity.

3.2 Introduction

3.2.1 *Physcomitrella patens*

3.2.1.1 Classification and significance

Physcomitrella patens is a member of the Bryophytes, which are amongst the earliest land plants. *Physcomitrella* are believed to deviate from vascular plants such as *Arabidopsis* more than 450MYA (Fig. 3.1). Among the early land plants, *Physcomitrella* serves as a very important node to link the green algae and seed plants (Clarke et al., 2011; Lewis and McCourt, 2004). Thus, *Physcomitrella* is thought to be an ideal model plant for evolutionary study (Hedges, 2002). A transcriptome comparison studies suggest that at least 66% of *A. thaliana* genes have homologues in *P. patens* (Nishiyama et al., 2003; Prigge and Bezanilla, 2010; Rensing et al., 2008). The transition of a living environment from water to land is associated with drastic changes in plants. The plants face challenges, such as low humidity, ultraviolet exposure stress and airborne pathogens, which strongly demands evolutionary changes in their defense systems. Thus, *Physcomitrella* stands on an important evolutionary node, and the study of defense in *Physcomitrella* will provide vital insights in plant defense signaling origins.

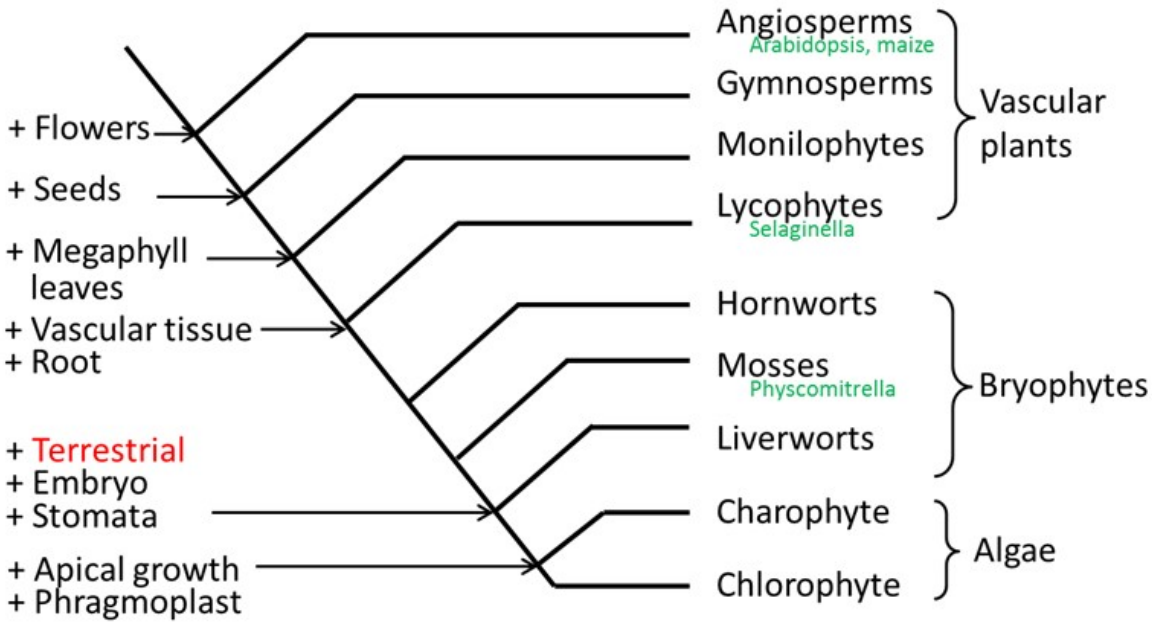

Fig. 3.1 Scheme of plant evolution. *Physcomitrella* is amongst the earliest land plants. "+" represents new characteristic appear through evolution.

3.2.1.2 *Physcomitrella* life cycle

Both haploid gametophyte and diploid sporophyte generations are found in *Physcomitrella*. In contrast to ferns and seed plants, the haploid gametophyte is the dominant phase in *Physcomitrella*, which makes the plants easier for genetic studies.

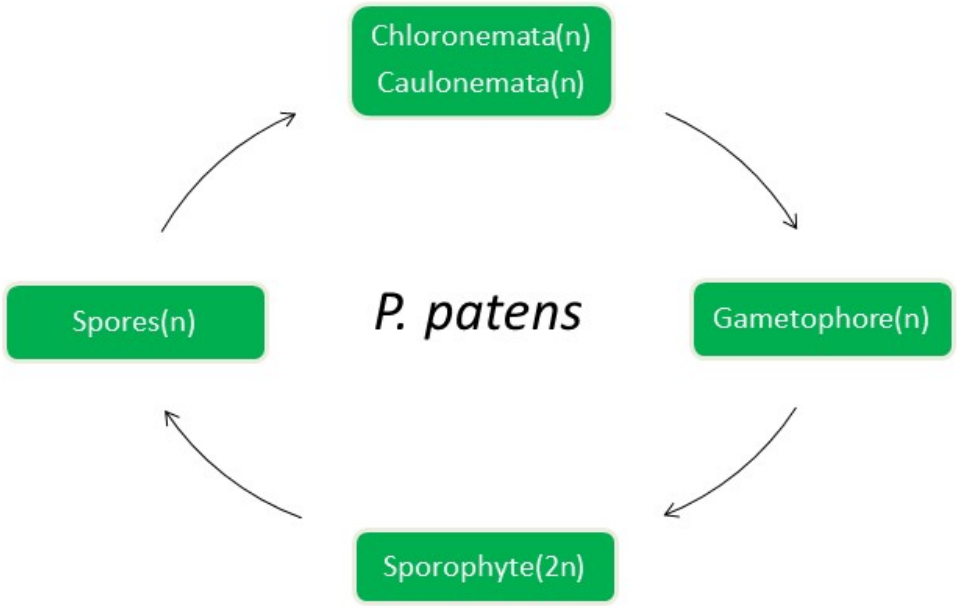

Fig. 3.2 Life cycle of *Physcomitrella.* A haploid spore germinates into slow-growing chloronemal cells, which continue to grow and differentiate into rapidly growing caulonemal cells. Gametophores, or shoots, emerge off protonemal filaments and are ultimately anchored by rhizoids. Sexual organs, both female, archegonia and male, antheridia form at the apex of the gametophore. A motile flagellate sperm fertilizes the egg with the help of water, and the sporophyte develops at the apex of the gametophore.

Gransden WT is the widely used *Physcomitrella* strain. The life cycle of the Gransden strain usually takes 3 to 4 months (Fig. 3.2). Gametophyte stage starts when spores germinate to produce the filamentous protonemata. The first protonemata consist of choloronematal cells, which continue to grow and differentiate caulonemal cells. Choloronema are slow-growing filaments, which contain many cells with large chloroplasts and serve as the assimilatory component in the protonema. Caulonema are rapidly growing filaments, of which cells contain few not well developed chloroplasts and serve as an adventitious component of the protonema. Protonemal filaments are anchored by rhizoids. Gametophore and shoots emerge from the protonema. Both archegonia, the female organ, and antheridia, the male organ, form at the apex of

gametophore. A motile flagella sperm from the antheridia fertilizes the egg in the archegonia. The fertilized zygote that develops into a sporophyte consists of a short seta bearing a spore capsule. When mature, the capsule contains about 4000 spores (Cove et al., 1997; Prigge and Bezanilla, 2010; Rensing et al., 2008).

3.2.1.3 The genome of *Physcomitrella*

Physcomitrella patens genome was published in 2008 (Rensing et al., 2008). The genome size is 480Mb and consists of 27 chromosomes, while the *Arabidopsis thaliana* genome is 125Mb in size and contains 5 chromosomes.

Evolution suggests that whole genome duplications occur in both the *Arabidopsis* and *Physcomitrella*. Researchers hypothesized that originally seven chromosomes in *Physcomitrella*, and four times of whole genome duplication and one chromosome lost leads to 27 chromosomes in *Physcomitrella* now(Hedges, 2002; Rensing et al., 2008). The evolutionary distance between *Physcomitrella* and *Arabidopsis* is believed to be similar to that of fishes and humans. A transcriptome comparison study suggest that at least 66% of *A. thaliana* genes have homologues in *P. patens* (Nishiyama et al., 2003).

3.2.2 SERK family

There are five SERKs in *Arabidopsis*, SERK1 to SERK5 (Hecht et al., 2001). SERK5 is believed to be not functional. SERK1 to SERK4 function redundantly in multiple ways, including regulation of male microsporogenesis, plant growth hormone BR signaling, cell death and PRR-mediated innate immunity (Fig. 3.3) (Li et al., 2002;

Nam and Li, 2002; He et al., 2007; Chinchilla et al., 2007; Heese et al., 2007; Gao et al., 2009; Postel et al., 2010; Roux et al., 2011).

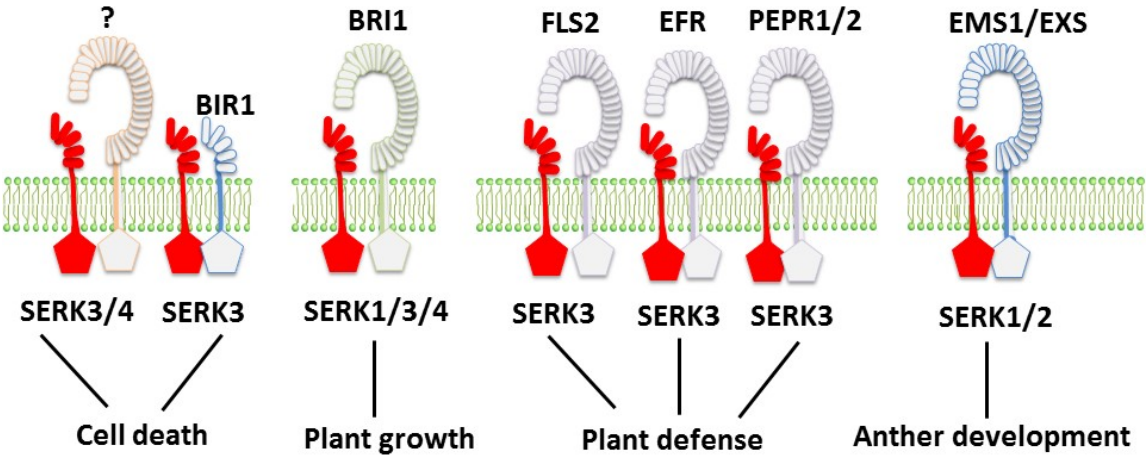

Fig. 3.3 Schematic illustrations of SERK family functions. SERKs function in multiple signaling pathways ranging from cell death regulation, plant development and defense.

3.2.2.1 SERKs function as co-receptors for multiple PRRs to modulate plant defense

FLS2 and EFR sense the conserved 22-amino-acid peptide of bacterial flagellin, named flg22, and the N-terminal 18-amino-acid peptide of EF-Tu called elf18, respectively (Gómez-Gómez and Boller, 2000; C. Zipfel et al., 2006). FLS2 and EFR belong to the LRR-RLK XII subfamily. Upon flg22 or elf18 treatment, BAK1 forms a ligand-induced receptor respective complex with FLS2 and EFR in a rapid fashion, which occurs within 1 or 5 min after treatment (Chinchilla et al., 2007; Heese et al., 2007).

PEPR1/2 are the receptors of the AtPEP1 ligand, which is a wound-induced and plant derived endogenous peptide. PEPR1/2 belong to the LRR-RLK XI subfamily (Krol

et al., 2010). A yeast-two-hybrid assay revealed that BAK1 also serves as a co-receptor for PEPR1/2 (Postel et al., 2010). Recognition of AtPEP1 by the PEPR1 receptor enhances plant resistance against *Pythium irregular* infection (Huffaker et al., 2006; Yamaguchi et al., 2006).

BAK1 is a positive regulator of PTI as the *bak1-4* null mutant display dramatic defects in plant defense responses such as oxidative burst, MAPK activation and seedling growth inhibition upon flg22 and elf18 treatment (Chinchilla et al., 2007; Heese et al., 2007).

3.2.2.2 SERKs function as cell death regulator

BAK1 null mutant *bak1-3* and *bak1-4* exhibited uncontrolled cell death upon infection by virulent bacterial *Pst* DC3000, indicating that BAK1 is involved in the negatively regulating cell death. BAK1 function in negative regulation of cell death is supported in the *bak1-4*$^{-/-}$*serk4*$^{-/-}$ double mutant, which displays reduced growth and seedling lethality accompanied by excessive ROS production and constitutive expression of defense genes (He et al., 2007).

BAK1-INTERACTING RECEPTOR-LIKE KINASE 1 (BIR1) negatively regulates cell death as *bir1-1* mutant displays seedling lethality at 22°C due to excessive salicylic acid accumulation (Gao et al., 2009). Interestingly, BIR1 association with BAK1, SERK1, SERK2, or SERK4 can be detected via BiFC assay (Gao et al., 2009). Taken together, these results suggest that BAK1 and SERKs play a role in BIR1 mediate cell death.

3.2.2.3 SERKs function in BR signaling

The brassinosteroid (BR) class of steroid hormones is known to be the key phytohormone that regulates multiple stages of plant development and defense against biotic and abiotic stresses. Mutants in BR signaling are defective, displaying extreme dwarfism, reduced seed germination, and photomorphogenesis in the dark. BRI1 is the main receptor to perceive BR molecules in *Arabidpsis* (Fàbregas et al., 2013). BAK1 was originally identified to function in regulating BR signaling through a yeast-two-hybrid screen for Bri1 interacting proteins (Nam and Li, 2002), and by an activation tagging genetic screen for BRI1 weak allele *bri1-5* mutant suppressor (Li et al., 2002; Noguchi et al., 1999).

BRI1 is activated and forms a ligand-induced complex with BAK1 upon the binding of BL, the most active BR. A series of trans-phosphorylation events between the two components amplify the signal (Gou et al., 2012; Nam and Li, 2002). In parallel, the activated BRI1 phosphorylates a RLCK BR SIGNALING KINASE 1 (BSK1) and Constitutive Differential Growth 1 (CDG1) (Kim et al., 2011; Tang et al., 2008). Phosphorylated BSK1 subsequently phosphorylates and activates a phosphatase bri1 SUPPRESSOR 1 (BSU1) (Kim et al., 2011; Kim et al., 2009; Mora-García et al., 2004). Activated BSU1 dephosphorylates and inactivates a BR negative regulator GSK3 type kinase, BR-INSENSITIVE 2 (BIN2) (Kim and Wang, 2010). The inactive BIN2 allows downstream transcription factors BRASSINAZOLE RESISTANT 1 (BZR1) and BRI1–EMS-suppressor 1 (BES1) to bind to the promoter of the BR induced genes to activate BR signaling (He et al., 2005; Y. Sun et al., 2010; Yin et al., 2005; Yu et al., 2011).

BRI1 null mutants exhibit an extreme dwarf stature with epinastic leaves, reduced male fertility, and more compact rosette leaves. Over-expression of BAK1 suppress a weak bri1 allele, *bri1-5* (Li et al., 2002). Furthermore, overexpression of AtSERK1/2/3/4 suppresses *bir1-5* dwarf phenotype, and overexpression of the kinase dead version of these genes in *bri1-5* display a dominant negative phenotype, suggesting that multiple SERKs function redundantly in BR signaling (Gou et al., 2012).

As a dual co-receptor for both BRI1 and other PRRs and the potential redundancy of SERK family in regulating both pathways, the SERK family plays a critical role in understanding the crosstalk between plant development and innate immunity.

3.2.2.4 SERKs function in regulating anther development

Daucus carota SERK (DcSERK) was first found to function as a marker of embryogenesis in carrot (Schmidt et al., 1997). Since the identification of DcSERK1 in carrot, SERK homologs have been identified in many species, including *Dactylis glomerata, Medicago truncatula, Helianthus annuus, Ocotea catharinensi, Citrus unshiu* and *Arabidopsis* (Hecht et al., 2001; Schmidt et al., 1997). Based on the homology to DcSERK, there are five homologs in *Arabidopsis*, named as AtSERK1 to AtSERK5 (Hecht et al., 2001). All five *Arabidopsis* SERK members belong to subclass LRR II of the *Arabidopsis* RLK family (Shiu and Bleecker, 2001). AtSERK1, the closest homolog to DcSERK1 in *Arabidopsis*, was mainly expressed in developing ovules and early embryos and was proven to be a marker gene as overexpression of AtSERK1 enhance

embryogenic cell formation in response to the growth regulator 2,4-D (Hecht et al., 2001). The SERK2 gene bears 90% amino acid identity to SERK1 and is thus considered as the closest homolog to SERK1. Recent duplication is suggested from the phylogenic analysis (Hecht et al., 2001).

Fourteen stages are characterized for anther development via morphological landmarks or cellular events through microscopy analysis. In *Arabidopsis*, *serk1* or *serk2* single mutants didn't show defect in anther development. However, *serk1*$^{-/-}$*serk2*$^{-/-}$ double mutant is defective in anther development as the mutant develops normal inflorescence architecture and floral structures, but no siliques or pollen formation (Goldberg et al., 1993; Sanders et al., 1999). Detailed microscopic analysis reveals that *serk1*$^{-/-}$*serk2*$^{-/-}$ mutant develops normal cell layers up to stage 4. At anther development stage 5, WT anthers consist of five layers, the epidermis, endothecium, middle layer, tapetum, and microsporocytes. However, no tapetal layer but more microsporocytes were found in *serk1*$^{-/-}$*serk2*$^{-/-}$ compared with WT anther (Albrecht et al., 2005). Furthermore, an early tapetum marker, ATA7 (ARABIDOPSIS THALIANA ANTHER7) gene expression was not detected in *serk1*$^{-/-}$*serk2*$^{-/-}$ mutant (Rubinelli et al., 1998).

Taken all the results together, characterization of SERK family function in *Physcomitrella patens* will provide insight in evolution of innate immunity and plant growth.

3.3 Materials and methods

3.3.1 Plant growth conditions

Arabidopsis WT (Col-0), *bak1-4*$^{-/+}$*serk4*$^{-/-}$, *serk1-1*$^{-/-}$*serk2-2*$^{-/+}$, 35S::PpSERK1.2-HA/*bak1-4*$^{-/+}$*serk4*$^{-/-}$, 35S::PpSERK1.2-HA/*bak1-4*$^{-/-}$*serk4*$^{-/-}$, were grown in pots containing a soil mix (Metro Mix 360, Sun Gro Horticulture) in a growth room at 23°C, 65% relative humidity and 75 $\mu E \bullet m^{-2} \bullet s^{-1}$ light with a 12 hr photoperiod for approximately 4 weeks before protoplast isolation and *Agrobacterium* transformation.

3.3.2 Tissue culture of *P. patens*

WT *P. patens* cv Gransden (Ashton and Cove, 1977) was routinely grown on BCD plates (Roberts et al., 2011) overlaid with cellophane discs (AA Packaging) at 25ºC in continuous light following standard protocols (Roberts et al., 2011). Seven days before transformation, WT *P. patens* were passaged to BCD plates containing 5 mM diammonium tartrate.

3.3.3 Generation of transgenic Plants

The *Agrobacterium*-mediated transformation was used to introduce individual *pCB302-35S::PpSERK1.1-HA*, *pCB302-35S::PpSERK1.2-HA*, and *pCB302-35S::PpSERK2-HA* into *bak1-4*$^{-/+}$*serk4*$^{-/-}$, respectively; and introduce individual *pCB302-35S::PpSERK1.1-HA*, *pCB302-35S::PpSERK1.2-HA*, and *pCB302-35S::PpSERK2-HA* into *serk1-1*$^{-/-}$*serk2-2*$^{-/+}$ plants, respectively. To eliminate the C-terminal tag potential effect on SERKs function, non-tagged *pCB302-35S::PpSERK1.1,*

pCB302-35S::PpSERK1.2 or *pCB302-35S::PpSERK2* were introduced into *bak1-4*$^{-/+}$*serk4*$^{-/-}$ via *Agrobacterium* transformation, respectively. Similarly, Individual non-tagged *pCB302-35S::*PpSERK was introduced in to different background of *serk1-1*$^{-/-}$ *serk2-2*$^{-/+}$*, bak1-5serk4*, or *bri1-5* via *Agrobacterium* transformation, respectively. The transgenic plants were selected with Basta resistance and immunoblot using α-HA (Roche) antibodies.

3.3.4 Plasmid constructs, protoplast transient assay and elicitor treatments

Arabidopsis BAK1, *BIK1*, *ASR3* constructs were reported previously (Li et al., 2015; Lu et al., 2010; Shan et al., 2008). The *PpSERK1.1, PpSERK1.2* and *PpSERK2* full length genes were amplified by PCR from *Physcomitrella* cDNA and introduced into a plant expression vector with or without an HA epitope tag at the C terminus.

The kinase domain of *Arabidopsis BAK1* and full length *BIK1* in the *pMAL-c2* (New England Biolabs) or in the modified GST fusion protein expression vector *pGEX4T-1* (Pharmacia) were reported previously (D. P. Lu et al., 2010). The kinase domain of *PpSERK1.1, PpSERK1.2* and *PpSERK2* were amplified by PCR from *Physcomitrella* cDNA and introduced into the *pMAL-c2* (New England Biolabs) fusion protein expression vector.

Protoplasts isolation and transient expression assay were conducted as described (Asai et al., 2002; D. Lu et al., 2010; Shan et al., 2008). In general, 100 µl protoplasts at the density of 2 x 10^5 /ml and 20 µg DNA were used for transfection. The flagellin

peptide flg22 (Felix et al., 1999) were used in a final concentration of 100 μM unless stated otherwise. Protoplasts transfected with empty vector were used as a control.

3.3.5 BIK1, ASR3 phosphorylation assays and MAPK activity

For BIK1 phosphorylation assay, FLAG epitope-tagged BIK1 was co-transfected with individual *pHBT-BAK1-HA*, *pHBT-PpSERK1.1-HA*, *pHBT-PpSERK1.2-HA, pHBT-PpSERK2-HA* or non-tagged *pHBT-BAK1*, *pHBT-PpSERK1.1, pHBT-PpSERK1.2*, and *pHBT-PpSERK2* into *Arabidopsis* protoplasts. Transfected protoplasts were incubated at room temperature overnight, and then treated with 100 nM flg22 or water for 10 minutes. Protoplasts were harvested, and the total protein was separated by 10% SDS–PAGE gel followed by a α-HA immunoblot. Similar method was applied for ASR3 phosphorylation assay.

To detect MAPK activity, protoplasts were transfected with individual p*HBT-BAK1-HA, pHBT-PpSERK1.1-HA, pHBT-PpSERK1.2-HA*, *pHBT-PpSERK2-HA* or non-tagged *pHBT-BAK1, pHBT-PpSERK1.1, pHBT-PpSERK1.2*, or *pHBT-PpSERK2*. Transfected protoplasts were incubated at room temperature for overnight, and then treated with 100 nM flg22 or water for 15 minutes. Protoplasts were harvested and suspended in lysis buffer (20 mM Tris-HCl, pH7.5, 100 mM NaCl, 1 mM EDTA, 10% Glycerol, 1% Triton X-100), and the supernatant was collected after centrifugation. Protein samples with 1X SDS buffer were separated in 10% SDS-PAGE gel to detect pMPK3, pMPK6 and pMPK4 by Western blot with α-pErk1/2 antibody (Cell Signaling).

3.3.6 Protein expression and *in vitro* kinase assay

GST and MBP fusion proteins were purified with Pierce glutathione agarose (Thermo Scientific), and with amylose resin (New England Biolabs) respectively, according to the standard protocols from the company. The protein concentration was determined with the BioRad Quick Start Bradford Dye Reagent and confirmed by the NanoDrop ND-1000 Spectrophotometer. For in vitro kinase assay, reactions were performed in 30 μL kinase buffer (20 mM Tris•HCl, pH 7.5, 10 mM $MgCl_2$, 5 mM EGTA, 100 mM NaCl, and 1 mM DTT) containing 10 μg fusion proteins with 0.1 mM cold ATP and 5 μCi [32P]-γ-ATP at room temperature for 3 h with gentle shaking. The reactions were stopped by adding 4XSDS loading buffer. The phosphorylation of fusion proteins was analyzed by autoradiography after separation with 10% SDS/PAGE.

3.3.7 Genotyping

To determine the genotype of transgenic plants, PCR with Primer Left Border (LB) primer on the T-DNA and gene specific (Left Primer) LP and (Right Primer) RP were performed. The primers were designed by T-DNA Primer Design (http://signal.salk.edu/tdnaprimers.2.html) and the PCR reactions were carried out according to its protocol. The sequence of LB originated from the T-DNA fragment. The LP and RP are BAK1 gene specific primers. The product of the amplification of LB plus RP indicates the insertion of T-DNA fragment. The product of the amplification by using LP plus RP indicates the existence of BAK1.

3.4 Results

3.4.1 Identification of 3 SERKs homologs in *Physcomitrella* based on amino acid sequence

Three genes (Pp1s35_219V6.1, Pp1s96_90V6.1 and Pp1s118_79V6.1) were retrieved when blasted against the *P. patens* genome (http://www.cosmoss.org/) using the full-length amino acid sequences of SERKs. These three genes encode proteins with overall more than 60% identity at the amino acid sequence level to individual SERKs. Phylogenetic analysis suggested that they belong to the same clade with SERK1 and SERK2, distinct from the SERK3, SERK4 or SERK5 clade (Fig. 3.4A). The amino acid sequence analysis reveals that Pp1s35_219V6.1 and Pp1s96_90V6.1 are more closely related to each other with 97% identity, and bear 82% and 86% identity with SERK1 and SERK2, respectively. Pp1s118_79V6.1 shares 69% and 68% identity to SERK1 and SERK2, respectively. Apparently, there are three SERK1/SERK2 orthologs in the *P. patens* genome, but no *P. patens* ortholog of SERK3/SERK4/SERK5 was found. Therefore, we named Pp1s35_219V6.1 as PpSERK1.1, Pp1s96_90V6.1 as PpSERK1.2, and Pp1s118_79V6.1 as PpSERK2. Similar to the AtSERKs, the PpSERKs possess conserved SERK family featured domains such as a transmembrane domain, five leucine-rich repeats, a proline rich domain and a kinase domain with a conserved ATP-binding region and a protein kinase active site (Fig.3.4 B, C).

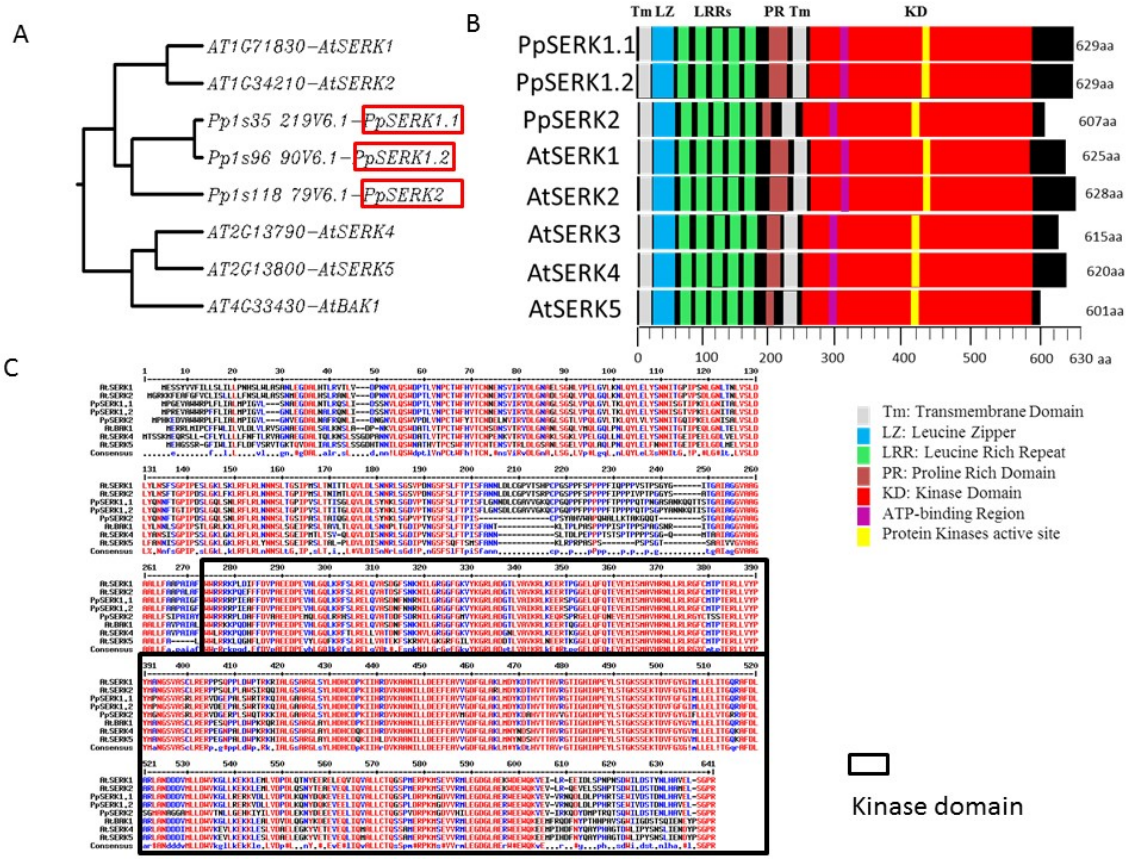

Fig. 3.4 Three SERK homologs identified in *Physcomitrella*. (A) Phylogenetic tree revealed that PpSERKs fall into the same clade with AtSERK1, AtSERK2, but not AtSERK3, AtSERK4 nor AtSERK5. (B) PpSERKs possess conserved transmembrane domains, LRR repeat, and kinase domain (adapted from PlantsP database and Clustaw). (C)PpSERKs share 60%-80% identity to AtSERKs based on amino acid sequence. (http://multalin.toulouse.inra.fr/multalin/multalin.html http://www.genome.jp/tools/clustalw/)

To examine whether PpSERKs are functional kinases, we cloned the cytosolic domains of *PpSERK1.1, PpSERK1.2* and *PpSERK2* into the bacterial protein expression vector *pMAL* fused with a MBP tag at the N-terminus. An in vitro kinase assay suggested that PpSERK1.1 and PpSERK1.2 displayed strong autophosphorylation activity, while PpSERK2 displayed moderate autophosphorylation activity (Fig. 3.5A). The in vitro kinase assay further suggested that PpSERK1.1 and PpSERK1.2 display strong transphosphorylation activity on AtBIK1, while PpSERK2 displayed moderate transphosphorylation activity (Fig. 3.5B). Taken together, the three PpSERK homologs

all possess kinase activity and PpSERK1.1 and PpSERK1.2 possess stronger kinase activity than PpSERK2. Since the BAK1 kinase activity is required for defense signaling (D. Chinchilla et al., 2007; A. Heese et al., 2007), the difference of the kinase activity may indicate that PpSERK2 functions differently from PpSERK1.1 or PpSERK1.2.

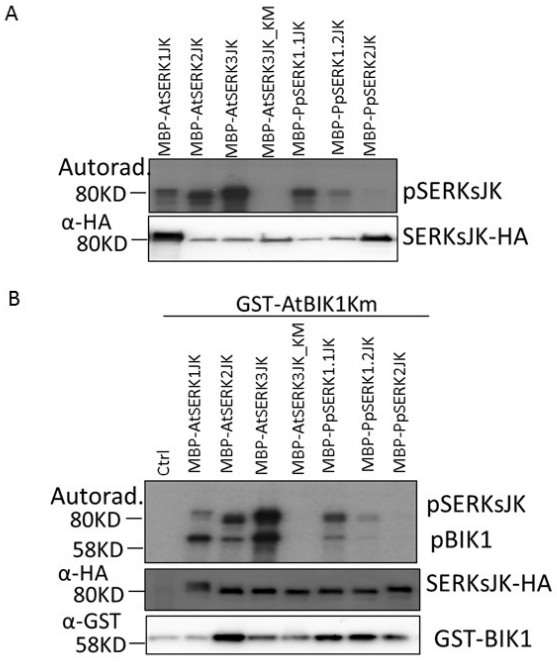

Fig. 3.5 PpSERKs possess kinase activity. (A)PpSERK1.1 and PpSERK1.2 display strong auto-phosphorylation activity in vitro, while PpSERK2 only possesses weak auto-phophorylation activity in vitro. An in vitro kinase assay was performed by incubating MBP-PpSERKsJK proteins in kinase assay buffer. Proteins were separated by 10% SDS/PAGE and analyzed by autoradiography (Upper), and the protein loading control was shown by CBS (Lower). MBP-AtSERK3JK kinase mutant serves as a negative control. (B)PpSERK1.1 and PpSERK1.2 strongly phosphorylates AtBIK1 in vitro, while PpSERK2 only slightly phosphorylates AtBIK1 in vitro. An in vitro kinase assay was performed as previously described. GST-AtBIK1Km only and MBP-AtSERK3JK kinase mutant serves as negative controls.

3.4.2 PpSERK1.1 and PpSERK1.2 are functional in regulation of plant defense in *Arabidopsis*

Even though PpSERKs possess kinase activity, their involvement in plant innate immunity remains unknown. Upon perception of flg22 by the FLS2/BAK1 receptor

complex, BIK1 is strongly phosphorylated and released from the complex. subsequently, MAPK cascades are activated through an unknown mechanism. The flg22-activated MPK4 strongly phosphorylates ASR3, a transcriptional repressor. The phosphorylation of ASR3 enhances its binding to the defense gene FRK1 to negatively regulate defense genes expression. The phosphorylation of BIK1 and ASR3 is evidenced by a protein mobility shift on SDS PAGE gel. Importantly, the flg22-induced phosphorylation of BIK1 and ASR3, and flg22-triggered MAPKs activation are largely dependent on BAK1.

To determine whether PpSERKs are functional in plant defense, a complementation assay was performed by overexpressing individual PpSERK with BIK1 or ASR3 in the *bak1-4* null mutant protoplasts. Interestingly, the complementation assay suggests that PpSERK1.1 and PpSERK1.2, but not PpSERK2 could also complement flg22-induced BIK1 and ASR3 phosphorylation in *bak1-4* protoplasts (Fig. 3.6 A, B), indicating that PpSERK1.1 and PpSERK1.2, but not PpSERK2 are functional in flg22-induced defense signaling.

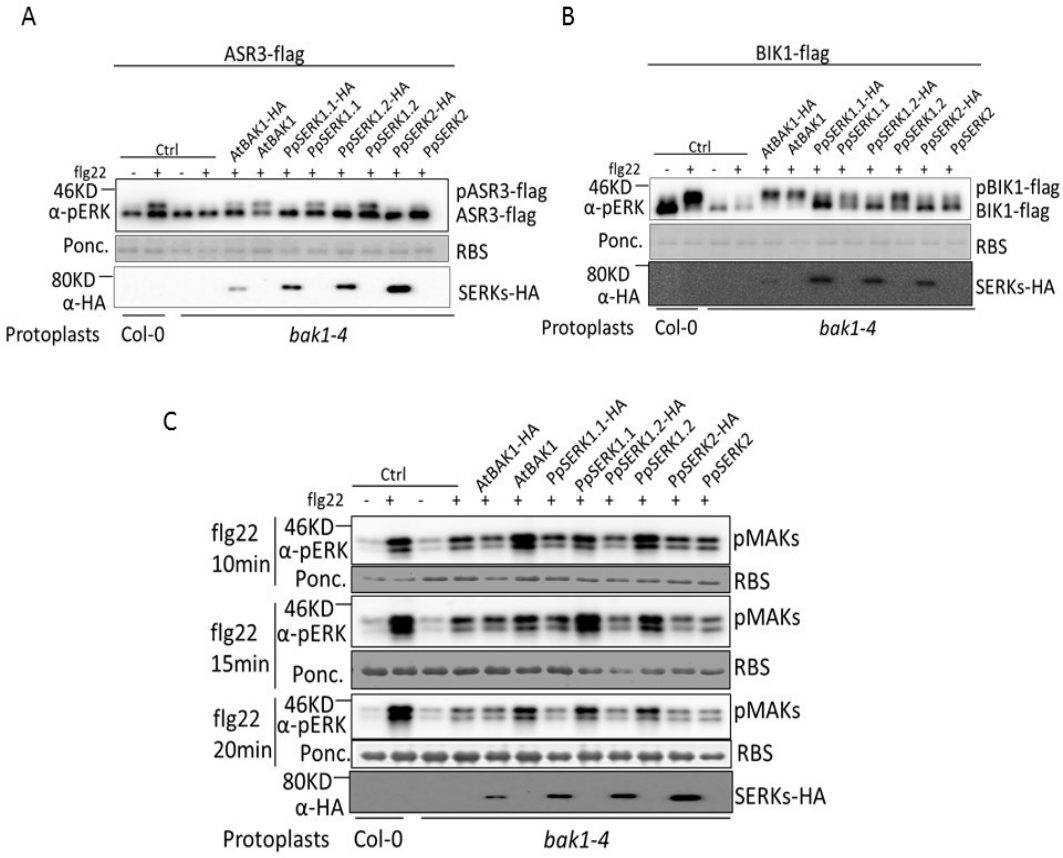

Fig. 3.6 PpSERK1.1 and PpSERK1.2 function in regulating plant defense. (A) PpSERK1.1 and PpSERK1.2 complement BIK1 phosphorylation in *bak1-4* protoplasts. BIK1-flag was co-expressed with control, non-tagged AtSERKs and PpSERKs or HA-tagged SERKs and PpSERKs in *Arabidopsis* WT and *bak1-4* protoplasts. Transfected protoplasts were incubated at room temperature for 6hr and were treated without or with 100nM flg22 for 15min. The proteins were analyzed by using Western blot with α-flag antibody. Top panel shows BIK1-flag and pBIK1-flag, middle panel shows the equal protein loading by CBS, and bottom panel shows expression of both SERKs-HA and PpSERKs-HA. (B) PpSERK1.1 and PpSERK1.2 complement ASR3 phosphorylation in *bak1-4* protoplasts. ASR3-flag was co-expressed with control, non-tagged AtSERKs and PpSERKs or HA-tagged SERKs and PpSERKs in *Arabidopsis* WT and *bak1-4* protoplasts. Transfected protoplasts were incubated at room temperature for 6hr and were treated without or with 100nM flg22 for 15min. The proteins were analyzed through a using Western blot with α-flag antibody. Top panel shows ASR3-flag and pASR3-flag, middle panel shows the equal protein loading by CBS, and bottom panel shows expression of both SERKs-HA and PpSERKs-HA. (C) PpSERK1.1 and PpSERK1.2 complement flg22-triggered MAPKs activation in *bak1-4* protoplasts. ASR3-flag was co-expressed with control, non-tagged SERKs and PpSERKs or HA-tagged SERKs and PpSERKs in *Arabidopsis* WT and *bak1-4* protoplasts. Transfected protoplasts were incubated at room temperature for 6hr and were treated without or with 100nM flg22 for the indicated length of time. The proteins were analyzed through a Western blot with α-pErk1/2 antibody. Within one set, the top panel shows flg22-triggered MAPK activation, middle panel shows the equal protein loading by Ponceau staining. The bottom panel shows expression of both SERKs-HA and PpSERKs-HA.

The complementation assay suggests that PpSERK1.1 and PpSERK1.2, but not PpSERK2 could also complement flg22-activated MAPK cascade (Fig. 3.6C). Taken together, PpSERK1.1 and PpSERK1.2, but not PpSERK2 are functional in FLS2-

mediated defense signaling. PpSERK2 failure to complement defense response in *bak1-4* mutant may be due to the relatively weak kinase activity. However, the potential role of PpSERK2 remains unknown.

Notably, C-terminal epitope tag affects BAK1 function in innate immunity but not cell death or BR signaling (Ntoukakis et al., 2011). Consistently, non-tagged BAK1, PpSERK1.1 and PpSERK1.2 could largely restore flg22-induced ASR3 phosphorylation while BAK1-HA, PpSERK1.1-HA or PpSERK1.2-HA failed to. However, BAK1 C-terminal HA tag may not affect all FLS2-mediated defense responses, as both non-tagged and HA-tagged BAK1 could complement BIK1 phosphorylation and MAPK activation in *bak1-4* mutants, while only non-tagged PpSERK1.1 and PpSERK1.2 could complement these two events. The results again call attention to the usage of epitope tag on the SERK family study.

This work here suggests that PpSERK1.1 and PpSERK1.2, but not PpSERK2 could complement FLS2 signaling events, as of BIK1 phosphorylation, MAPK activation and ASR3 phosphorylation in *bak1-4* mutant and also calls for a cautionary use of the HA tag in studies involving BAK1 study.

3.4.3 PpSERK1.2, but not PpSERK1.1 could suppress *bak1-4*$^{-/-}$*serk4*$^{-/-}$ seedling lethality

Cell death in HR is characterized as a defense response in which the plant carries out the abscission of infected leaf in order to survive. However, cell death needs to be regulated under strict control for appropriate defense and prevent potential harm to the plant (He et al., 2007).

To determine whether PpSERKs in *Physcomitrella* also regulate cell death, transgenic plants of overexpressing *35S::PpSERK1.1-HA, 35S::PpSERK1.2-HA* or *35S::PpSERK2-HA* in *bak1-4*$^{-/-}$*serk4*$^{-/-}$ plants were generated. Due to seedling lethality, *bak1-4*$^{-/-}$*serk4*$^{-/-}$ double mutants were not available for the transformation. Instead, plant of *bak1-4*$^{-/+}$*serk4*$^{-/-}$ were used for *Agrobacterium*-mediated transformation with *35S::PpSERK1.1-HA, 35S::PpSERK1.2-HA* or *35S::PpSERK2-HA* construct, respectively. Transgenic plants overexpressing *35S::PpSERK1.2-HA* carry the resistance to a herbicide BASTA. T_0 seeds were harvested and next generation T_1 true transformants that survived BASTA spray were obtained and subjected for genotyping in search of *bak1-4*$^{-/-}$*serk4*$^{-/-}$ double mutant. 33 transgenic plants survived after application of BASTA, among which, three lines were of *35S::PpSERK1.2-HA/bak1-4*$^{-/-}$*serk4*$^{-/-}$, ten were of *35S::PpSERK1.2-HA/bak1-4*$^{+/+}$*serk4*$^{-/-}$ and 20 were of *35S::PpSERK1.2-HA/bak1-4*$^{+/-}$*serk4*$^{-/-}$. The observation that *35S::PpSERK1.2-HA/bak1-4*$^{-/-}$*serk4*$^{-/-}$ survived for more than 11 weeks, and produced viable seeds (Fig. 3.7A,B), suggests that PpSERK1.2 negatively regulates the cell death pathway. Interestingly, the lines of *35S::PpSERK1.2-HA/bak1-4*$^{+/-}$*serk4*$^{-/-}$ #23 and *35S::PpSERK1.2-HA/bak1-4*$^{+/-}$*serk4*$^{-/-}$ #32 with high protein expression mimicked a BRI1 overexpression phenotype with elongated and edge-wrinkled leaves, while *35S::PpSERK1.2-HA/bak1-4*$^{+/-}$*serk4*$^{-/-}$ #21 with a lower PpSERK1.2-HA expression resembled WT phenotype, suggesting that PpSERK1.2 may also function in BR signaling (Fig. 3.7 C,D; Table 3.1).

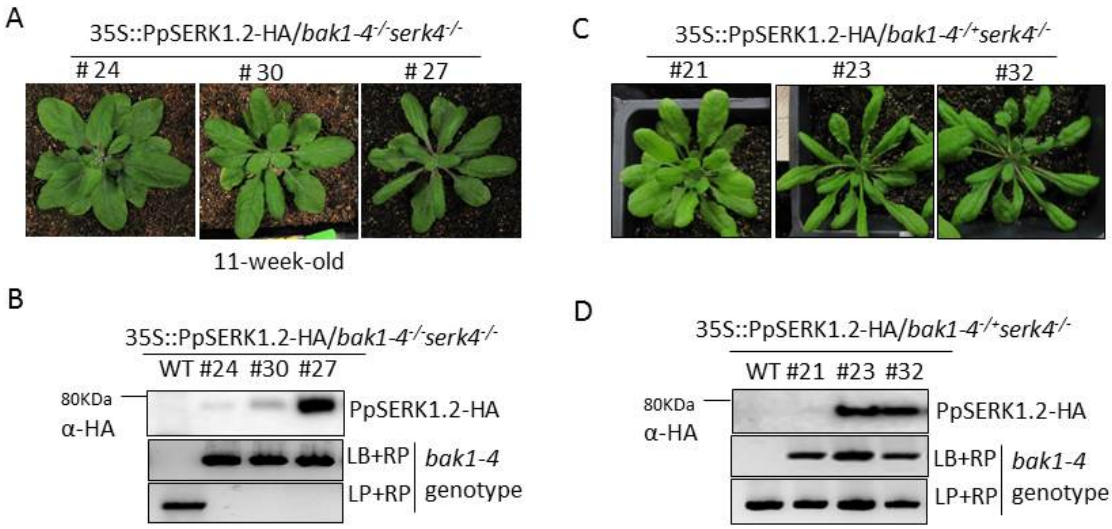

Fig. 3.7 PpSERK1.2 suppresses *bak1-4$^{+/-}$serk4$^{-/-}$* seedling lethality. (A) Photograph of 11 week-old *35S::PpSERK1.2-HA/bak1-4$^{-/-}$ serk4$^{-/-}$* transgenic plants. (B) The PpSERK1.2-HA expression was demonstrated by α-HA Western blotting. Agarose gels display the genotype of the transgenic plants. (C) Photograph of 11 week-old *35S::PpSERK1.2-HA/bak1-4$^{+/-}$serk4$^{-/-}$* transgenic plans. (D) The PpSERK1.2-HA expression was demonstrated by α-HA Western blotting. Agarose gels display the genotype of the transgenic plants.

Table 3.1 Chart of *35S::PpSERKs-HA/bak1-4$^{+/-}$serk4$^{-/-}$* segregation. Transgenic plants that survived from a herbicide BASTA application were subjected for genotyping analysis. Numbers of plants of different genotype and the total number used for genotyping were recorded in the chart. BBss represents *serk4* single mutant, Bbss represents *bak1-4$^{+/-}$serk4$^{-/-}$*, bbss represents *bak1-4$^{-/-}$serk4$^{-/-}$*.

	PpSERK1.1-HA	PpSERK1.2-HA	PpSERK2-HA
BBss	70	10	28
Bbss	110	20	17
bbss	0	3	0

3.4.4 PpSERK1.1, PpSERK1.2 or PpSERK2 failed to complement *serk1*$^{-/-}$*serk2*$^{-/-}$ pollen defective phenotype

SERK1 and SERK2 function redundantly in regulating male sporogenesis. *serk1* and *serk2* single mutants are normal in terms of seeds. However, *serk1*$^{-/-}$*serk2*$^{-/-}$ double mutant exhibit pollen defect (Albrecht et al., 2005).

In order to investigate whether PpSERKs function in regulation on pollen development, multiple transgenic plants of *35S::PpSERK1.1-HA*/*serk1*$^{-/-}$*serk2*$^{-/-}$, *35S::PpSERK1.2-HA/serk1*$^{-/-}$*serk2*$^{-/-}$, and *35S::PpSERK2-HA/serk1*$^{-/-}$*serk2*$^{-/-}$ were generated. As no seeds production from *serk1*$^{-/-}$*serk2*$^{-/-}$ double mutant, we transformed *35S::PpSERK1.1-HA*, *35S::PpSERK1.2-HA* and *35S::PpSERK2-HA* in to *serk1-1*$^{-/-}$ *serk2-2*$^{-/+}$ respectively. Multiple transgenic plants of *35S::PpSERK1.1-HA*/*serk1*$^{-/-}$*serk2*$^{-/-}$, *35S::PpSERK1.2-HA/serk1*$^{-/-}$*serk2*$^{-/-}$, and *35S::PpSERK2-HA/serk1*$^{-/-}$*serk2*$^{-/-}$ were obtained.

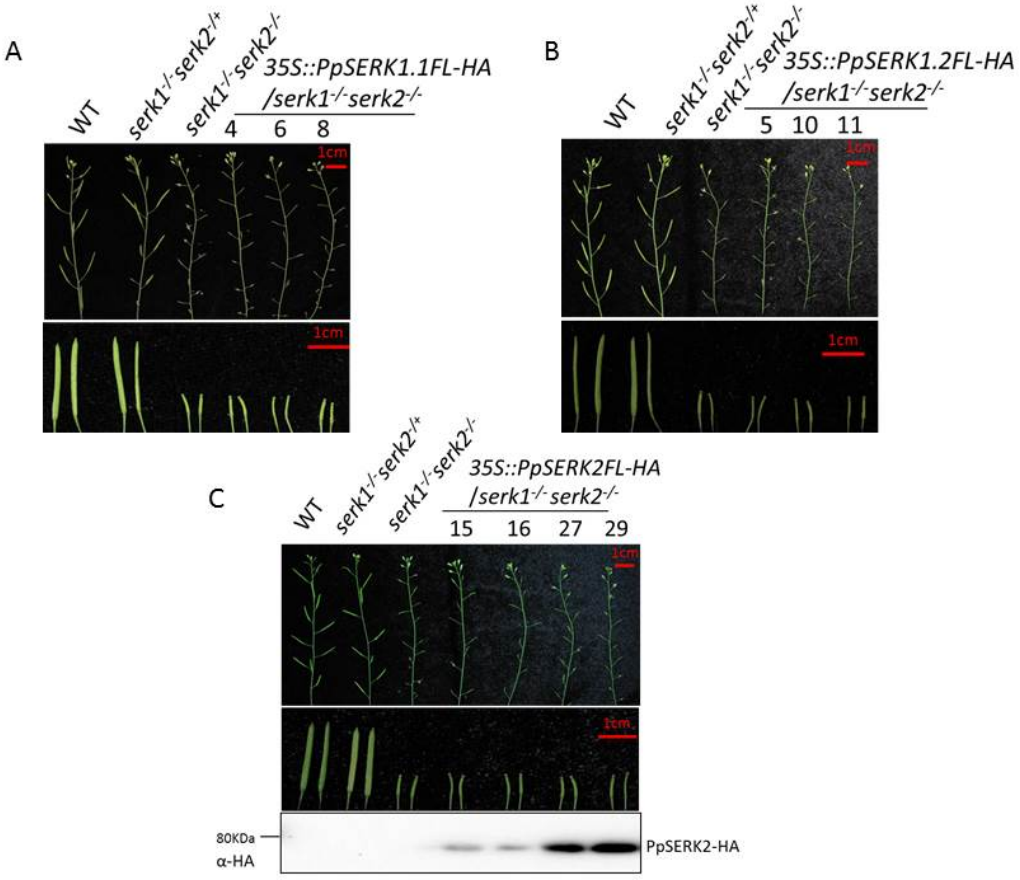

Fig. 3.8 Functional complementation assay in *serk1$^{-/-}$serk2$^{-/-}$*. (A) The top panel shows the inflorescence structure of 11 week-old WT, serk1$^{-/-}$serk2$^{+/-}$, serk1$^{-/-}$serk2$^{-/-}$ and three representative transgenic lines of 35S::PpSERK1.1-HA/serk1$^{-/-}$serk2$^{-/-}$. The bottom shows the closer look at the siliques of each line. (B) The top panel shows the inflorescence structure of 11 week-old WT, serk1$^{-/-}$serk2$^{+/-}$, serk1$^{-/-}$serk2$^{-/-}$ and three representative transgenic lines of 35S::PpSERK1.2-HA/serk1$^{-/-}$serk2$^{-/-}$. The bottom panel shows the closer look at the siliques of each line. (C) Top panel shows the inflorescence structure of 11 week-old WT, serk1$^{-/-}$serk2$^{+/-}$, serk1$^{-/-}$serk2$^{-/-}$ and three representative transgenic lines of 35S::PpSERK2-HA/serk1$^{-/-}$serk2$^{-/-}$. The middle panel shows the closer look at the siliques of each line. The bottom panel shows PpSERK2-HA expression in transgenic plants by western blot. Red bar indicates 1cm in each Figure.

Interestingly, protein level was not detectable by western blot for *35S::PpSERK1.1-HA/serk1$^{-/-}$serk2$^{-/-}$* or *35S::PpSERK1.2-HA/serk1$^{-/-}$serk2$^{-/-}$*, while decent protein expression was detected in multiple *35S::PpSERK2-HA/serk1$^{-/-}$serk2$^{-/-}$* transgenic plants #15, 16, 27, and 29 (Fig. 3.8A, B, C). However, no silique was obtained from *35S::PpSERK1.1-HA/serk1$^{-/-}$serk2$^{-/-}$*, *35S::PpSERK1.2-HA/serk1$^{-/-}$serk2$^{-/-}$* or *35S::PpSERK2-HA/serk1$^{-/-}$serk2$^{-/-}$* transgenic plants #15, 16, 27, and 29 (Fig. 3.8A, B,

C), indicating *35S::PpSERK2-HA* could not complement either SERK1 or SERK2 in regulating pollen development. The observation that no protein detected in *35S::PpSERK1.1-HA/serk1*$^{-/-}$*serk2*$^{-/-}$, *35S::PpSERK1.2-HA/serk1*$^{-/-}$*serk2*$^{-/-}$ raises the question whether it is caused by specific protein silencing for PpSERK1.1, PpSERK1.2 but not PpSERK2.

3.5 Discussion

Plants are at a constant risk of both biotic and abiotic stresses. Thus, plants are facing a question: to defend or to develop. Plants need to differentiate danger signals from the barrage of background noise and integrate key component to mobilize energy into costly defense systems to defend. SERKs, a RLK family in *Arabidopsis* share convergent and different roles in regulating from male sporogenesis, BR signaling, PRR-mediated plant defense to cell death. Research of the SERK family origin could provide an insight in innate immunity evolution and highlight the trade-off between plant defense and development.

Biochemical and genetic analyses suggest that PpSERK1.1 and PpSERK1.2 possess strong auto-phosphorylation and trans-phosphorylation activity, while PpSERK2 possesses weak auto-phosphorylation and trans-phosphorylation activity towards BIK1. The protoplast-based complementation assays suggests that PpSERK1.1 and PpSERK1.2, but not PpSERK2, function in FLS2-mediated plant defense, as overexpressing PpSERK1.1 and PpSERK1.2 can restore flg22-induced phosphorylation of BIK1 and ASR3, and MAPKs activation in the *bak1-4* null mutant. PpSERK2 lack of

function in FLS2-mediated plant defense responses may be due to the weaker kinase activity.

bak1-4serk4 seedling lethality circumvents research on redundancy of the SERK family function in plant defense. *bak1-5*, another *bak1* mutant allele, containing a Cys408Tyr point mutation, displays defects specifically in PTI responses but does not exhibit pleiotropic defects in BR signaling or cell death regulation (Roux et al., 2011). BAK1 and SERK4 function redundantly and additively in regulating immunity as early PTI responses like elf18- or flg22- induced ROS burst, MAPK activation, and defense genes expression were reduced in *bak1-4serk4* mutant compared with *bak1-5* single mutant. In addition, later responses like flg22/elf18-induced ethylene production were reduced in *bak1-5serk4* double mutant than single mutants; *bak1-5serk4* is insensitive to flg22 induced seedling growth inhibition compared to *bak1-4*, *bkk1* single mutant or Col-0. Overall, BAK1 and BKK1 are both required for full responses to flg22 or elf18. Thus, *bak1-5serk4* is more susceptible to virulent, non-host pathogens compared with *bak1-5, serk4* single mutant or WT (Roux et al., 2011).

In order to determine whether PpSERKs play a role in innate immunity, we overexpressed *35S::PpSERK1.1, 35S::PpSERK1.2* and *35S::PpSERK2* in *bak1-5serk4*. True transformants will be selected by BASTA application and PCR confirmation. Three representative transgenic lines with low, middle and high levels of PpSERK proteins will be saved for further study. Both early defense responses, including flg22-induced ROS burst, MAPK activation, defense gene expression, and late defense responses, including flg22-induced seedling inhibition assay and disease resistance assay to virulent

pathogens, are proposed to be tested in order to characterize PpSERKs function in plant defense.

In addition, PpSERK1.2, but not PpSERK1.1, also functions in cell death regulation as overexpression of PpSERK1.2 suppressed the *bak1-4*$^{-/-}$*serk4*$^{-/-}$ double mutant lethal phenotype. As the closet homolog of PpSERK1.2, PpSERK1.1 is only one amino acid change from PpSERK1.2. However, our results suggest that PpSERK1.1 may not be involved in cell death regulation as no plants of *35S::PpSERK1.1-HA/bak1-4*$^{-/-}$*serk4*$^{-/-}$ genotype were found in the 180 *35S::PpSERK1.1-HA* overexpressing T_1 plants we have tested so far (Fig. 3.6F). We hypothesize that PpSERK1.1 may be unable to suppress *bak1*$^{-/-}$*serk4*$^{-/-}$ seedling lethality. To prove this hypothesis, virus-induced gene silence (VIGS) of BAK1 in *35S::PpSERK1.1-HA/bak1-4*$^{+/-}$*serk4*$^{-/-}$ transgenic plants will be performed. Cell death after VIGS of BAK1 in *35S::PpSERK1.1-HA/bak1-4*$^{+/-}$*serk4*$^{-/-}$ transgenic plants will indicate that PpSERK1.1 could not suppress *bak1*$^{-/-}$*serk4*$^{-/-}$ seedling lethality, while survival after VIGS of BAK1 in *35S::PpSERK1.1-HA/bak1-4*$^{+/-}$ *serk4*$^{-/-}$ transgenic plants may suggest that PpSERK1.1 can suppress *bak1*$^{-/-}$*serk4*$^{-/-}$ seedling lethality and thus function as a negative regulator of cell death. Similar assays will be carried out for *35S::PpSERK2-HA/bak1-4*$^{+/-}$*serk4*$^{-/-}$ transgenic plants, as no plants of *35S::PpSERK2-HA/bak1-4*$^{-/-}$*serk4*$^{-/-}$ genotype plants were obtained either.

The observation that *35S::PpSERK1.2-HA/bak1-4*$^{+/-}$*serk4*$^{-/-}$ #23 and #32 transgenic lines with higher protein expression mimicked a BRI1 overexpression phenotype with elongated and edge-wrinkled leaves, while *35S::PpSERK1.2-HA/bak1-4*$^{+/-}$*serk4*$^{-/-}$ #21 transgenic lines with lower PpSERK1.2-HA expression resembled WT

phenotype, indicate that PpSERK1.2 may also be involved in BR signaling (Fig. 3.6 D, E). To test this hypothesis, transgenic plants overexpressing PpSERK1.1, PpSERK1.2 and PpSERK2 in the *bri1-5* null mutant are being generated to test whether PpSERKs positively regulates BR signaling by rescuing *bir1-5* extreme dwarf phenotype.

PpSERKs potential function in the regulating pollen development is still under instigation. The observation that no silique was obtained from *35S::PpSERK2-HA*/*serk1*$^{-/-}$*serk2*$^{-/-}$ transgenic plants #15, 16, 27, and 29, indicating *35S::PpSERK2-HA* could not complement either SERK1 or SERK2 in regulating pollen development. It also raises several hypotheses that the HA epitope tag or the 35S constitutive expression promoter disturb PpSERK1.2 function in pollen development. In order to eliminate the effect of 35S promoter and HA epitope tag, non-tagged genomic construct of each PpSERK is proposed to transform into *serk1*$^{-/-}$*serk2*$^{+/-}$. Once the *PpSERK1.1::PpSERK1.1/serk1*$^{-/-}$*serk2*$^{-/-}$, *PpSERK1.2::PpSERK1.2/serk1*$^{-/-}$*serk2*$^{-/-}$, and *PpSERK2::PpSERK2/serk1*$^{-/-}$*serk2*$^{-/-}$ obtained, pollen defective analysis will be carried out to determine the potential role of PpSERKs in pollen defective and anther development. Also, it is possible that SERK function in regulating pollen development is a new function gained after the differentiation between moss and other advanced land plants. If the latter hypothesis proved to be true, it is interesting to investigate why though more closed to AtSERK1/2 at protein level, PpSERKs do not function as AtSERK1/2 in regulating pollen development but function as AtBAK1 in FLS2-medited plant innate immunity. The observation that no protein detected in *35S::PpSERK1.1-HA*/*serk1*$^{-/-}$*serk2*$^{-/-}$, *35S::PpSERK1.2-HA/serk1*$^{-/-}$*serk2*$^{-/-}$ raises the question whether it is caused by specific

protein silencing for PpSERK1.1, PpSERK1.2 but not PpSERK2, which needs further investigation. Generations of multiple transgenic plants in multiple background mutants are still ongoing. More thorough tests will be carried out once the transgenic plants are available.

Knockout lines of individual PpSERK members in *Physcomitrella* will substantially benefit the characterization of PpSERKs function in *Physcomitrella*. In order to generate PpSERK knockout in *Physcomitrella*, *pBHRF* vector, derived from pMCS5 (MoBiTec), containing resistance to ampicillin in *E. coli* and hygromycine in moss, was used (Fig. 3.9A). In order to generate PpSERK1.1 knockout, a 1,057-nucleotide 5' targeting fragment was amplified from genomic DNA with primers of *PpSERK1.1-US-F-HIII* and *PpSERK1.1-US-R-XhoI* (Fig. 3.9B, Table 3.2) and cloned into the *Hind*III and *Xho*I sites of the vector *pBHRF* (Fig. 3.9A) upstream of *Hph*. Similarly, a 1,084-nucleotide 3' targeting fragment was amplified from genomic DNA with primers of *PpSERK1.1-DS-F-NotI* and *PpSERK1.1-DS-R-BglII* (Fig. 3.9B, Table 3.2) and cloned into the *Not*I and *Bgl*II sites of *pBHRF*, 3' to *Hph* (Fig. 3.9A). Minipreps of DNA were digested with HIII and XhoI, or NotI and BglII, which showed a predicted size of band with around 1 kb, respectively. Furthermore, Sanger sequencing confirmed the successful cloning of these genes into pHBRF vectors.

A

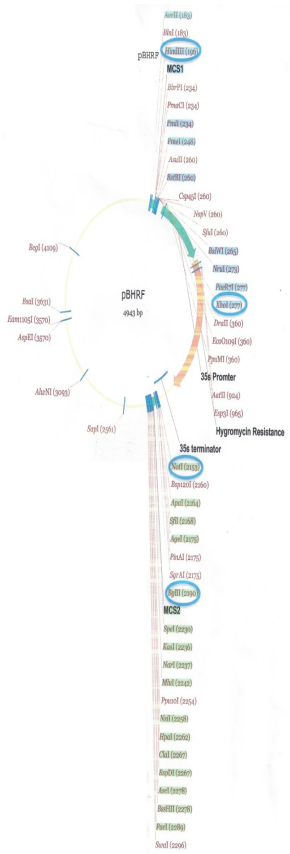

B

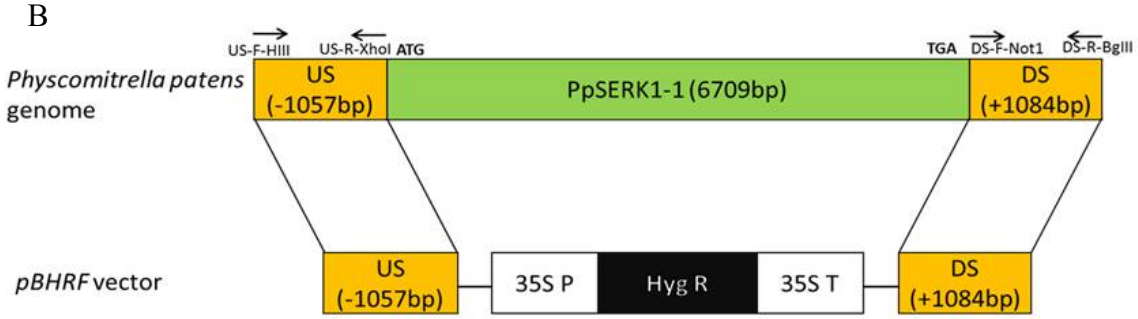

Fig. 3.9 Generation of PpSERK1-1 knock out in *Physcomitrella*. (A) Map of *pBHRF* vector with restriction enzyme sites shown. (B) Scheme of PpSERK1-1 knockout construct. US stands for sequence "upstream" of PpSERK1-1; DS stands for "downstream" sequence. A hygromycin (HygR) selection cassette, driven by 35S promoter and 35S terminator, is applied to knockout PpSERK1-1 through homologous recombination.

Table 3.2 PpSERKs knockout primers and sequences.

Primer	Sequence
PpSERK1.1-US-F-HIII	CCCAAGCTTCGTACACACATTTGAAGGAGG
PpSERK1.1-US-R-XhoI	CCG CTCGAG GCAACCAAGCCGTAAGTACCC
PpSERK1.1-DS-F-NotI	AGAATGCGGCCGCGACCAGGGAGGTTTTCATTG
PpSERK1.1-DS-R-BglII	GAAGATCTCTCGGCTATTGCACACACATG
PpSERK1.2-US-F-HIII	CCCAAGCTTTGTATTCTTTTAGCTGTCGG
PpSERK1.2-US-R-XhoI	GCCCTCGAGTCACTACAGCTG
PpSERK1.2-DS-F-BglII	GCCAGATCTTAGGTTTCGATC
PpSERK1.2-DS-R-SpeI	GACTAGTCTTACATCCAGTAGAAGACG
PpSERK2-US-F-HIII	CCCAAGCTTCTTGGTGCAATGTAATTGCTG
PpSERK2-US-R-XhoI	CCGCTCGAGGAGAAAGGATGGTGAAACCCC
PpSERK2-DS-F-NotI	ATAAGAATGCGGCCGCTATGCAGGTTTGTAATGTTACG
PpSERK2-DS-R-SpeI	GACTAGTCAACCACTGTACCACCGGTC

To transform *P. patens*, 50 mg of *PpSERK1.1* knockout construct was linearized by simultaneous digestion with *Hind*III and *Bgl*II overnight with 40uL 10X buffer, 15uL restriction enzyme *Hind*III, 15uL restriction enzyme *Bgl*II, and added water up to 400uL. Precipitated the mixture after digestion with isopropanol at -20ºC for 4 hours, and washed it twice with 70% EtOH and re-suspended the pellet in 50-100uL of water. The concentration of recovered plasmid was measured by running an Agarose gel. 60ug linearized DNA was introduced into WT *P. patens* cv Gransden protoplasts using a previously described polyethylene glycol transformation protocol. Transformants will be initially selected by 7 day of growth on plates containing 20 mg/mL hygromycin followed by 10 d of growth on nonselective plates and an additional 7 d of growth on hygromycin plates. Surviving colonies will be analyzed by genotyping PCR and

Southern blotting for knockout the PpSERK1.1 at the correct location in the genome. The generation of PpSERK1.2 and PpSERK2 knockout lines will be conducted in the same way with that of PpSERK1.1 knockout line by digestion with the corresponding enzymes (Table 3.2).

From biochemical and genetic studies, our work suggests that there are conserved functions for the SERK family in *Physcomitrella*, from regulating cell death to PTI defense. The study of PpSERKs function in growth, development and responses to pathogen infection will provide insights on the functional convergence and divergence in innate immunity.

CHAPTER IV

PHOSPHORYLATION OF TRIHELIX TRANSCRIPTION REPRESSOR ASR3 BY MPK4 NEGATIVELY REGULATES ARABIDOPSIS IMMUNITY AND CONCLUSIONS*

4.1 Summary

Proper control of immune-related gene expression is crucial for the host to launch an effective defense response. Perception of MAMPs induces a rapid and profound transcriptional reprograming via concerted actions of specific transcription factors and general transcription machinery in plants. Here we show that Arabidopsis SH4-related 3 (ASR3) functions as a transcription repressor and plays a negative role in regulating PTI in *Arabidopsis thaliana*. ASR3 belongs to a plant-specific trihelix transcription factor family for which functional studies are lacking. MAMP treatments induce rapid phosphorylation of ASR3 at threonine 189 via MPK4, a mitogen-activated protein kinase that negatively regulates PTI responses downstream of multiple MAMP receptors. ASR3 possesses transcriptional repressor activity via its ERF-associated amphiphilic repression motifs and negatively regulates a large subset of flg22-induced genes. Phosphorylation of ASR3 by MPK4 enhances its DNA binding activity to suppress gene expression. Importantly, the *asr3* mutant shows enhanced disease

---

* Reprinted with permission from "Phosphorylation of Trihelix Transcriptional Repressor ASR3 by MAP KINASE4 Negatively Regulates Arabidopsis Immunity" by Bo Li, Shan Jiang, Xiao Yu, Cheng Cheng, Sixue Chen, Yanbing Cheng, Joshua S. Yuan, Daohong Jiang, Ping He, and Libo Shan. *The Plant Cell*, Vol.27: 839-856.

resistance to virulent bacterial pathogen infection, whereas transgenic plants overexpressing the WT or phospho-mimetic form of ASR3 exhibit compromised PTI responses. Our studies reveal a function of the trihelix transcription factors in plant innate immunity and provide evidence that ASR3 functions as a transcriptional repressor regulated by MAMP-activated MPK4 to fine-tune plant immune gene expression.

4.2 Introduction

To elucidate the signaling networks orchestrating immune gene activation, we developed a genetic screen with an EMS-mutagenized population of *Arabidopsis pFRK1::LUC* transgenic plants expressing a firefly luciferase reporter gene under the control of FRK1 promoter. *FLG22-INDUCED RECEPTOR-LIKE KINASE 1(FRK1)* is a specific and early immune responsive gene activated by multiple MAMPs (Asai et al., 2002; He et al., 2006). A series of mutants with altered *FRK1* promoter activity upon flg22 treatment or nonpathogenic *Pseudomonas syringae* pv. *tomato* (*Pst*) DC3000 type III secretion mutant *hrcC* infection were identified and named as *aggies*. During map-based cloning of *aggie1* mutant, a collection of homozygous Salk T-DNA insertion mutants for individual genes located in 110 kilobase pair (kb) region on Chromosome 2 was analyzed for disease resistance to virulent bacterium *Pst* DC3000 infection and flg22-induced *FRK1* expression. Interestingly, a knockout line with a T-DNA insertion at *At2g33550* exhibited enhanced flg22-induced *FRK1* expression and elevated resistance to virulent bacterial pathogens. *At2g33550* encodes a plant-specific protein with no significant homology to any known proteins. The predicated gene product of

At2g33550 has two putative nuclear localization signals, a putative trihelix DNA binding motif at its N terminus and a loosely conserved coiled-coil motif at its C terminus. Based on these features, At2g33550 was classified to the SH4 (Shattering 4, a quantitative trait locus controlling grain shattering in rice [*Oryza satival*]) clade of trihelix transcription factor family (Kaplan-Levy et al., 2012). We named this gene as *ASR3* for *Arabidopsis SH4-related 3*. *SH4* was identified as a single dominant gene controlling seed shattering in the wild species of rice. The domesticated rice cultivars carry mutations in this gene, thus eliminating seed shattering (Li et al., 2006; Lin et al., 2007). Here, we report that Arabidopsis ASR3 is rapidly phosphorylated upon MAMP treatments downstream of MPK4. Our results provide genetic evidence that a trihelix family transcription factor functions in plant biotic stresses and identify a target of MPK4, which acts as a transcriptional repressor to negatively regulate plant innate immunity and immune gene expression.

4.3 Materials and methods

4.3.1 Plant materials and growth conditions

Arabidopsis thaliana accessions Col-0 and Ler, mutants *fls2* (Salk_141277), *bak1-4* (Salk_116202), *mpk4* (CS5205, in Ler background), *asr3-1* (SALK_112571C), and *asr3-2* (SALK_047951C) were obtained from ABRC. Transgenic plants *pASR3::ASR3-HA* in the background of *asr3-1* mutant, *p35S::ASR3-HA*, *p35S::ASR3*^{T189A}*-HA*, *p35S::ASR3*^{T189D}*-HA*, *p35S::ASR3-GFP* in the background of Col-0 are generated in the studies. Plants were grown in soil (Metro Mix 366) in a growth

room at 23°C, 45% humidity and 75μE $m^{-2}\cdot s^{-1}$ light with a 12-hr-light/12-hr-dark photoperiod. Four-week-old plants were used for protoplasts isolation, pathogen infection and ROS production assays. Seedlings were germinated on half-strength Murashige and Skoog plate containing 1% sucrose, 0.8% Agar, grown under the same condition as above for 10 d, transferred to a six-well tissue culture plate with 2ml water for overnight, and then treated with flg22 at indicated amount of time for MAPK and qRT-PCR assays.

4.3.2 Plasmid construction, protoplast transient assays and generation of transgenic plants

The *ASR3* gene was amplified from Col-0 cDNA with primers containing *Bam*HI and *Nco*I at N terminus and *Stu*I at C terminus (Supplemental Table 2), and introduced into the plant expression vector *pHBT* with an HA, FLAG or GFP epitope-tag at C terminus. The clone was sequenced to cover the entire *ASR3* gene. *Δ*C, *Δ*N, *Δ*C1, *Δ*C2, *Δ*C3, and *Δ*C4 were cloned using the above clone *pHBT-ASR3-HA* as template and primers as listed in the Supplemental table 2. The point mutations of $ASR3^{S169A}$, $ASR3^{S175A}$, $ASR3^{S182A}$, $ASR3^{T189A}$, $ASR3^{S182A/T189A}$, $ASR3^{T189D}$, $ASR3^{T196A}$ and $ASR3^{S230A}$ were generated by site-directed mutagenesis kit with primers listed in Supplemental Table 2. To make the *Escherichia.coli* fusion protein constructs, *ASR3,* $ASR3^{S182A}$, $ASR3^{T189A}$, $ASR3^{S182A/T189A}$ and $ASR3^{T189D}$ were subcloned into a modified pMAL-c2 vector (NEB) with *BamHI* and *StuI* digestion. To construct the *pCB302-35S::ASR3-GFP* binary vector for *Agrobacterium tumefaciens*-mediated transient expression assay in

Nicotiana benthamiana and *Arabidopsis* transformation, the *ASR3-GFP* fragment was released from *pHBT-35S::ASR3-GFP* using *Nco*I and *Pst*I digestion and ligated into *pCB302* binary vector. To construct the *pCB302-pASR3::ASR3-HA* binary vector, the native promoter of ASR3 (2.1 kp upstream of the start codon) was amplified from Col-0 genomic DNA with primers containing *Xho*I at the N terminus and *Bam*HI at the C terminus, and introduced into the vector *pHBT-ASR3-HA*. The *pASR3::ASR3* fragment was released via *XhoI* and *StuI* digestion and ligated into *pCB302* binary vector with an HA-tag at ASR3 C terminus. For yeast-two hybrid assay, *ASR3*, $ASR3^{T189A}$ and $ASR3^{T189D}$ were subcloned into a modified *pGBKT7* vector (Clontech) and a modified *pGADT7* vector (Clontech) with *Bam*HI and *Stu*I digestion. For transcriptional activity assay, different *ASR3* variants were subcloned into the effector vector containing 35S promoter-driven GAL4 DNA binding domain with *Bam*HI and *Stu*I digestion. *MEKK1*, *MEKK1Km*, and *MPK* clones in protoplast expression vector and protoplast transient assays were reported previously (He et al., 2006). For transgenic plant generation, a standard protocol for *Agrobacterium tumefaciens*-mediated floral dip method was used. The transgenic plants were selected by glufosinate-ammonium (50 μg/mL). Equal numbers of leaves from multiple transgenic plants were ground in 4 X SDS loading buffer, boiled samples were subjected to SDS-PAGE gel separation, and proteins were detected by immunoblotting with an a-HA antibody (Roche; 12013819001). Two lines with single insertions and similar protein expression levels were chosen for further assays.

4.3.3 Elicitor and chemical inhibitor treatments

The flagellin peptide flg22, EF-Tu peptide elf18, Chitin and LPS (Supplemental table 3) were used in the concentration as indicated. Chemical inhibitors Lanthanum chloride ($LaCl_3$), Gallium chloride ($GaCl_3$) and Ruthenium red (RR) were purchased from Sigma-Aldrich and K-252a, diphenylene iodonium (DPI), U0126 were purchased from A.G. Scientific. Chemical inhibitors used at a final concentration of 1 μM for K-252a, 5 μM for DPI, 0.5-1 mM for $LaCl_3$, 0.5-1 mM for $GaCl_3$, 0.1-0.2 mM for RR and 5 μM for U0126. Different chemical inhibitors were added to protoplasts 1 h before the flg22 treatment. Calf intestinal alkaline phosphatase (CIP) and the Lamda protein phosphatase (λPP) were purchased from New England BioLabs, and the treatments were performed following the manufacturer's instruction. A detailed summary on the chemical inhibitor usage was included as Supplemental Table 3.

4.3.4 MAPK assays

Ten-day-old seedlings were grounded in lysis buffer (20 mM Tris-HCl, pH7.5, 100 mM NaCl, 1 mM EDTA, 10% glycerol, 1% Triton X-100) and supernatant was collected after centrifugation. Protein samples with 1X SDS buffer were separated in 10% SDS-PAGE gel to detect pMPK3, pMPK6 and pMPK4 by immunoblotting with α-pERK1/2 antibody (Cell Signaling, #9101).

4.3.5 Liquid chromatography-MS/MS analysis

To obtain samples for mass spectrometry analysis, FLAG-tagged ASR3 was expressed in protoplasts for 12 h and treated with or without flg22 for 15 min. Protoplasts were lysed with buffer (20 mM Tris-HCl, pH7.5, 100 mM NaCl, 10% glycerol, 1% Triton X-100 and protease inhibitor cocktail) and immunoprecipitated with α -FLAG Agarose (Sigma-Aldrich). The immunoprecipitated ASR3 was separated in 10% SDS/PAGE gel followed by silver staining. A small aliquot of immunoprecipitated ASR3 was subjected for immunoblot using α -FLAG antibody. The corresponding bands were sliced and subjected for in-gel digestion with trypsin. The phosphor-peptides were enriched with a LTQ Orbitrap XL LC-MS/MS system (Thermo Scientific). The MS/MS spectra were analyzed with Mascot (Matrix Science; version 2.2.2), and the identified phosphorylated peptides were manually inspected to ensure confidence in phosphorylation site assignment.

4.3.6 RNA isolation and qRT-PCR analysis

Total RNA from ten-day-old seedlings was extracted by TRIzol reagent (Invitrogen) and quantified with NanoDrop (Thermo Scientific). RNA was then reverse transcribed to synthesize first strand cDNA with M-MuLV Reverse Transcriptase and oligo (dT) primer following RNase-free DNase I (New England Biolabs) treatment. Quantitative real-time polymerase chain reaction (qRT-PCR) analysis was performed using iTaq SYBR green Supermix (Bio-Rad) with an ABI GeneAmp® PCR System

9700 following standard protocol. The expression of each gene was normalized to the expression of *UBQ10*.

4.3.7 RNA-seq and data analysis

Two independent repeats were performed for RNA-seq analysis. For each repeat, equal amount of RNA from two biological replicates was pooled for RNA-seq library construction. RNA-seq library preparation and sequencing were performed at Texas AgriLife Genomics and Bioinformatics Service (College Station, TX). Approximately 15 million reads were obtained for each sample, which corresponds to 30 X coverage of the whole Arabidopsis transcriptome. RNA-seq reads with low sequencing quality or reads with sequencing adaptors were filtered from the raw data. The resulting clean reads were then aligned to the Arabidopsis reference genome (TAIR10) using TopHat (Trapnell et al., 2010) with default parameters. A GFF (general feature format) formatted gene model annotation file was provided for reads alignment. Following the alignments, Cuffdiff (Trapnell et al., 2010) was used to calculate the number of fragments per kilobase of exon per million fragments mapped (FPKM) and to find the significant differential gene expression. Genes with expression fold change $\geqslant$ 2 and P-value < 0.05 were considered as significantly different between samples with and without flg22 treatment. The differential expressed genes were chosen for the hierarchical clustering analysis. A clustering heat map was generated using the Mev software (Howe et al., 2011). GO term enriched in each genes list was identified using GO::Term Finder (Boyle et al., 2004) with the latest Arabidopsis GO term annotations. The cutoff for

significant enrichment is P value < 0.01 and calculation false discovery rate < 0.5. The fold enrichment was calculated based on the frequency of genes annotated to the term compared to their frequency in the genome.

4.3.8 ROS analysis

Around 25 leaves of 5-week-old soil-grown Arabidopsis plants for each genotype were excised into leaf discs (5-mm diameter) and then cut into leaf strips, followed by an overnight incubation with water in 96-well plate to eliminate the wounding effect. ROS burst was determined by a luminol-based assay. Leaf strips were soaked with solution containing 50 μM luminol and 10 μg/ml horseradish peroxidase (Sigma-Aldrich) supplemented with 100 nM flg22. The measurement was performed immediately after adding the solution with a Multilabel Plate Reader (PerkinElmer, Victor X3) for a period of 30 min. The values for ROS production from each line were indicated as means of Relative Light Units.

4.3.9 *In vivo* co-immunoprecipitation

Arabidopsis protoplasts were transfected with with a pair of constructs tested (empty vector as control) and incubated for 12 h. Samples were collected by centrifugation and lysed with co-IP buffer (20 mM Tris-HCl, pH7.5, 100 mM NaCl, 1 mM EDTA, 10% glycerol, 0.5% Triton X-100 and protease inhibitor cocktail) by vortexing. For *p35S::ASR3-HA* transgenic plants, 2-week-old seedlings were homogenized by mortar and pestle with liquid nitrogen, the fine powders were then

transferred into co-IP buffer for lysis. For the Co-IP assay, protein extract was pre-cleared with protein-G-agarose beads for 1 h at 4℃ with gentle shaking. Immunoprecipitation was performed with an α -HA or an α-FLAG antibody for 2 h and then with protein-G-agarose beads for another 2 h at 4℃. The beads were collected and washed three time with washing buffer (20 mM Tris-HCl, pH7.5, 100 mM NaCl, 0.1mM EDTA, 0.1% Triton X-100). The immunoprecipitated and input proteins were analyzed by immunoblot with indicated antibodies.

4.3.10 *In vitro* pull-down assay

Fusion proteins were expressed from bacterial protein expression vector in *E. coli* BL21 strain using Lysogeny broth medium supplemented with 0.25 mM isopropyl β-D-1-thiogalactopyranoside (IPTG). GST and GST-MPK4 were purified with Pierce glutathione agarose (Thermo Scientific), and MBP, MBP-ASR3, MBP-ASR3^{T189A} and MBP-ASR3^{T189D} proteins were purified using amylose resin (New England Biolabs) according to the standard protocols from the company. MBP fusion proteins (tagged with HA) as preys were pre-incubated with 5 μL prewashed glutathione agarose in 300 μL incubation buffer (20 mM Tris-HCl, pH7.5, 50 mM NaCl, 0.1mM EDTA, 0.5% Triton X-100) for 0.5 h at 4℃. After centrifugation, the supernatant was collected and incubated with prewashed GST or GST-MPK4 beads for another 1 h. The beads were collected and washed three times with washing buffer (20 mM Tris-HCl, pH7.5, 300 mM NaCl, 0.1mM EDTA, 0.1% Triton X-100). The pull-down proteins were detected with an α-HA antibody by immunoblot.

4.3.11 Subcellular localization

Agrobacterium strain GV3101 containing *pCB302-35S::ASR3-GFP* vector was cultured at 28℃ for overnight. Bacteria were harvested by centrifugation and re-suspended with buffer (10 mM MES pH5.7, 10 mM $MgCl_2$, 200 μM acetosyringone) at OD_{600}=0.75. Leaves of 3-week-old soil-grown *Nicotiana benthamian* were infiltrated with Agrobacterium cultures. Fluorescence signals were detected 2 days post-infiltration. Arabidopsis transgenic plants expressing *ASR3-GFP* were generated by Agrobacterium-mediated floral dipping transformation. For transient protoplast expression, protoplasts were co-transfected with GFP-tagged ASR3-ΔN or ASR3-ΔC vector and a nuclear-localized red fluorescence protein (NLS-RFP) and signals were observed 12 h after transfection. Fluorescence images were taken with Nikon-A1 confocal laser microscope systems and images were processed using NIS-Elements microscope imaging software. The excitation laser of 488 or 561nm was used for imaging GFP and RFP signals, respectively.

4.3.12 Transcriptional activity assay and *FRK1* reporter assay

Transcriptional activity assay was carried out by coexpression of the effector and the reporter constructs in Arabidopsis protoplasts. The effector vector containing GAL4 binding domain was used as the transcriptional activity control and *UBQ10-GUS* was included for all the samples as the internal transfection efficiency control. For *FRK1* reporter assay, protoplasts were cotransfected with empty vector, *35S:ASR3-HA*, *35S:ASR3*$^{ear\text{-}A}$*-HA*, or *35S:ASR3*$^{ear\text{-}B}$*-HA* and *pFRK1:LUC* for 4 h and then treated with

100 nM flg22 for another 4 h. The cells were collected and resuspended with cell lysis buffer (25 mM Tris-phosphate, pH7.8, 2 mM 1,2-Diaminocyclohexane -N,N,N',N'-tetraacetic acid, 10% glycerol, 1% Triton X-100, and 2 mM DTT). The luciferase activity was detected by Glomax Multi-Detection System (Promege) with the luciferase assay substrate (Promega). For the GUS activity, methylumbelliferyl-beta-D-glucuronide was mixed with the lysed cells and the fluorescence signals were analyzed with a Multilabel Plate Reader (PerkinElmer, Viktor X3).

4.3.13 Yeast two-hybrid assay

The different combination of ASR3 variants in *pGADT7* and *pGBKT7* as indicated in the Fig.s were cotransformed into the yeast AH109 strain. Polyethylene glycol/LiAc-mediated yeast transformation was performed according to the protocol of Yeastmaker Yeast Transformation System 2 (Clontech). Protein-protein interaction was tested by growing yeast colonies on the synthetic defined (SD) medium without histine, leucine or tryptophan (SD-H-L-T) and supplemented with 1 mM 3-amino-1, 2, 4-triazole.

4.3.14 Chromatin immunoprecipitation assay

Two-week-old seedlings from T3 homozygous transgenic lines of *35S::ASR3-HA., 35S::ASR3*^{T189A}*-HA, 35S::ASR3*^{T189D}*-HA* were used for ChIP assay following the protocol described previously (Kaufmann et al., 2010). Plant tissues were cross-linked with 1% formaldehyde under vacuum and quenched by glycine. Fixed samples were

ground in a mortar with liquid nitrogen and nuclei were extracted with fresh prepared buffer (15 mM Tris-HCl, pH 7.0, 0.25 M sucrose, 5 mM $MgCl_2$, 15 mM NaCl, 1 mM $CaCl_2$, 0.5% Triton X-100 and protease inhibitor cocktail). Chromatin was sheared into ~500-bp fragments by sonication, six times with Output 2, Duty cycle 3 (Brason Sonifier 250). Immunoprecipitation was performed with an α-HA antibody and protein G-Agrose (Roche). Immunoprecipitated DNA was precipitated with ethanol following proteinase K digestion. PCR amplification was performed with four pairs of primers amplifying different regions of FRK1 (Supplemental table 2).

4.3.15 Bacterial pathogen infection assay

Pst DC3000, *Psm* ES4326 or *Pst* DC3000 *avrRpt2* strains were cultured for overnight at 28°C in the King's B medium with appropriate antibiotics. Bacteria were harvested by centrifugation of 3500 rpm, washed with double distilled water, and adjusted to the density of 5×10^5 colony-forming units (cfu)/mL with 10 mM $MgCl_2$. Leaves of 4-week-old soil-grown plants were hand-infiltrated with bacterial suspension using a needleless syringe. For flg22 protection assay, leaves were preinoculated with 100 nM flg22 or double distilled water as control 24 h before bacterial pathogen infiltration. To measure in planta bacterial growth, six leaf discs separated as three repeats were ground and serial dilutions were plated on medium (1% tryptone, 1% sucrose, 0.1% glutamatic acid, 1.5% agra) with the corresponding antibiotics. Bacterial colony forming units were counted at 0, 2 and 4 day post inoculation.

4.4 Results

4.4.1 The *asr3* mutant shows enhanced immune gene activation and disease resistance

We initially isolated two *ASR3* T-DNA insertion lines *asr3-1* (SALK_112571C) and *asr3-2* (SALK_047951C) (Supplemental Fig. 1A). Genotyping and RT-PCR analysis confirmed that *asr3-1* is a knockout mutant with no detectable full-length transcript. However, *asr3-2* with the T-DNA insertion at the stop codon exhibited the same level of full length transcript as WT plants (Supplemental Fig. 1B). Accordingly, the *asr3-1* mutant was used for further studies. The *asr3-1* mutant displayed the elevated expression of several MAMP marker genes, including *FRK1*, *PP2C* (protein phosphatase 2C family protein) and *At2G17740* after flg22 treatment compared with WT plants (Fig. 4.1A). In addition, the *asr3-1* mutant was more resistant to infections by virulent bacteria *Pst* DC3000 and *Psm* ES4326 than were WT plants as indicated by a more than 5-fold smaller bacterial population in the mutant compared with that in WT plants 2 and 4 days post-inoculation (dpi) (Fig. 4.1B, C). The *asr3-1* mutant displayed unaltered disease resistance to avirulent strain *Pst* DC3000 carrying effector *avrRpt2* (Fig. 4.1D). To confirm that the *asr3-1* phenotypes were caused by mutation in the *ASR3* gene, we introduced HA epitope-tagged *ASR3* under the control of its native promoter (2.1 kb upstream of the translational start site) into *asr3-1* mutant. Two independent complementation lines with similar detectable ASR3 expression (Supplemental Fig. 1C) restored the flg22-induced *FRK1* induction to the WT level (Fig. 4.1E). In addition, the complementation lines restored the susceptibility to *Pst* infection to the WT level (Fig. 4.1F).

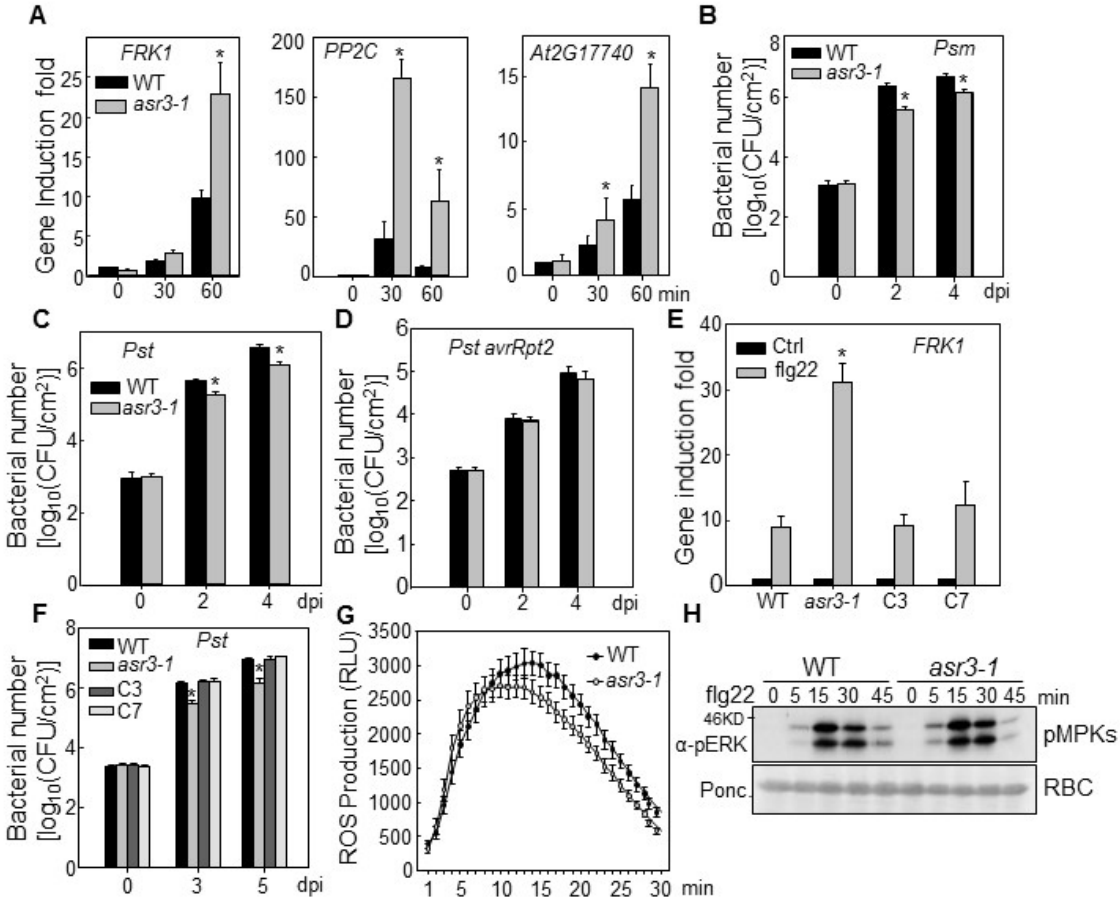

Fig. 4.1 Enhanced disease resistance and immune gene activation in *asr3*. (A) flg22-induced marker gene expression in WT and *asr3-1* mutant. Ten-day-old seedlings were treated with 100 nM flg22 for 30 and 60 min for qRT-PCR analysis. (B) and (C) The *asr3-1* mutant is more resistance to *Psm* and *Pst* infection. Four-week-old WT and *asr3-1* mutant plants were hand-inoculated with bacterial suspension at density of 5×10^5 cfu/ml, and bacterial population was quantified at 0, 2 and 4 dpi. (D) Bacterial growth of avirulent strain *Pst avrRpt2*. (E) ASR3 complements *asr3-1* mutant for *FRK1* gene inductionl. Ten-day-old seedlings from Col-0 WT, *asr3-1* mutant and complementation lines C3 and C7 were treated with 100 nM flg22 for 60min for qRT-PCR analysis. (F) ASR3 complements *asr3-1* mutant in *Pst*-mediated pathogen infection assay. Four-week-old plants were spray-inoculated with *Pst* at 10^8 cfu/ml, and bacterial counting was performed 0, 3 and 5 dpi. (G) flg22-induced ROS burst in WT and *asr3-1* mutant. Leaf discs from 5-week-old plants were treated with water or 100 nM flg22 over 30min. The data are shown as means ± SE from 24 leaf discs. (H) flg22-induced MAPK activation in WT and *asr3-1* mutant. Ten-day-old seedlings were treated with 100 nM flg22 and collected at the indicted time points. MAPK activation was analyzed by immunoblot with α-pERK antibody (top panel), and the protein loading is shown by Ponceau S staining for Rubisco (RBC) (bottom panel). The data in (A) to (F) are shown as mean ± SD from three independent repeats and asterisks (*) indicates significant difference with Student's t-test ($P < 0.05$) when compared to WT. The above experiments were repeated 3 times with similar results.

Together, these results suggest that ASR3 negatively regulates immune gene expression and disease resistance to virulent bacterial pathogens. However, flg22-induced ROS burst and MAPK activation did not show a detectable difference in WT

and *asr3-1* plants (Fig. 4.1G, H), suggesting that ASR3 functions either downstream or independently of MAPK activation and ROS production in FLS2 signaling.

4.4.2 The flg22 perception induces ASR3 phosphorylation

To reveal underlying mechanism of ASR3 in plant immune signaling, we ectopically expressed ASR3 in Arabidopsis protoplasts and transgenic plants. Interestingly, when expressing in protoplasts, ASR3 protein displayed a rapid and dynamic mobility shift upon flg22 treatment as detected by immunoblotting (Fig. 4.2A). The mobility shift of ASR3 proteins could be detected as early as 3 min, peaked at 15 min, gradually decreased at 30 min, and returned to the unshifted form at 2 h of flg22 treatment. The flg22-induced ASR3 mobility shift was also detected in ASR3-HA transgenic plants (Fig. 4.2B). In addition to flg22, other MAMPs, including elf18, chitin and LPS also induced ASR3 mobility shift although to a less extend (Fig. 4.2C). By contrast, ectopic expression of bacterial effectors AvrRpt2 and AvrRps4 did not induce a detectable mobility shift of ASR3 (Fig. 4.2D). In addition, abiotic stresses, such as treatment with low temperature (4°C) or excessive heat (42°C), did not induce a demonstrable ASR3 mobility shift (Fig. 4.2E). Thus, the mobility shift of ASR3 seems to be specifically induced in plant PTI signaling.

The flg22-induced ASR3 mobility shift was not observed in *fls2* and *bak1* mutant protoplasts (Fig. 4.2F). Importantly, expression of FLS2 in *fls2* mutant protoplasts or BAK1 in *bak1* mutant protoplasts restored the flg22-induced ASR3 mobility shift, suggesting the requirement of the functional flagellin receptor complex (Fig. 4.2F). By

contrast, expression of the FLS2 kinase-inactive mutant, FLS2Km, failed to complement ASR3 mobility shift in the *fls2* mutant, indicating that the FLS2 kinase activity is required for ASR3 mobility shift (Fig. 4.2F). Consistent with those results, the ASR3 mobility shift was blocked in the presence of a general kinase inhibitor K252a (Fig 4.2G). Since K252a likely interferes with multiple phosphorylation steps in FLS2 signaling, we applied phosphatase treatments of ASR3 proteins from flg22-induced samples to examine whether its mobility shift was caused by phosphorylation. Treatment of ASR3 proteins with Lamda protein phosphatase (λPP), a Mn^{2+}-dependent protein phosphatase with activity towards phosphorylated serine, threonine and tyrosine residues, was able to completely restore the flg22-induced mobility shift of ASR3 to the unmodified form. NaF, a phosphatase inhibitor, compromised λPP phosphatase activity (Fig 4.2H). Treatment of calf intestinal alkaline phosphatase (CIP), a phosphatase that preferentially alters phosphotyrosine residues, did not significantly affect the flg22-induced ASR3 mobility shift, although it completely restored the mobility of phosphorylated BIK1 to that of the unmodified form (Fig 4.2I) (Lu et al., 2010). This is consistent with the report that BIK1 possesses tyrosine phosphorylation activity (Lin et al., 2014; Xu et al., 2013). These results imply that ASR3 undergoes phosphorylation modification, likely on serine and threonine residues upon flg22 perception.

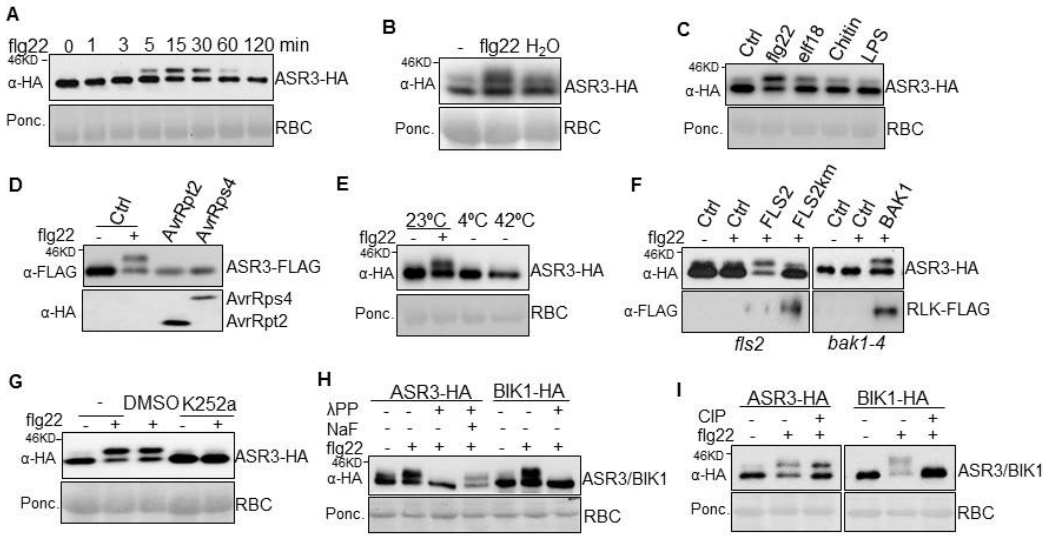

Fig. 4.2 The flg22 perception induces ASR3 phosphorylation. (A) ASR3 displays a mobility shift upon flg22 treatment. Protoplasts were transfected with HA-tagged ASR3 for 12 h and treated with 100 nM flg22 for the indicated amount of time. RBC, Rubisco. (B) The flg22 treatment induces ASR3 mobility shift in *35S::ASR3-HA* transgenic plants. The leaves from four-week-old *ASR3-HA* transgenic plants were hand-inoculated with 100 nM flg22 or water for 30 min. Ctrl "-" denotes the leaves without inoculation. (C) Multiple MAMPs trigger ASR3 mobility shift. Protoplasts were transfected with ASR3 for 12 h and treated with 100 nM flg22, 100 nM elf18, 50 μg/mL chitin or 5 μg/mL LPS for 15 min. (D) AvrRpt2 or AvrRps4 does not induce ASR3 mobility shift. Protoplasts were cotransfected with ASR3-FLAG and AvrRpt2-HA or AvrRps4-HA. (E) Cold or heat treatment does not induce ASR3 mobility shift. Protoplasts were transfected with ASR3-HA for 8 h at 23°C and incubated for additional 2 h at 23, 4, or 42°C. (F) The flg22-induced ASR3 mobility shift depends on functional FLS2/BAK1 receptor complex. Protoplasts isolated from *fls2* or *bak1-4* mutants were co-transfected with ASR3-HA and empty vector control (Ctrl), FLAG-epitope tagged FLS2, FLS2 kinase mutant (FLS2km) or BAK1. (G) Kinase inhibitor K252a blocks flg22-induced ASR3 mobility shift. K252a was applied 30 min before flg22 treatment. The controls were nontreatment (-) or solvent DMSO. (H) Lamda protein phosphatase removes the flg22-induced mobility shift of ASR3. Protein extracts from protoplasts transfected with ASR3-HA or BIK1-HA were treated with λPP following the standard protocol. NaF, a phosphatase inhibitor, compromised λPP phosphatase activity. (I) CIP treatment abolishes the mobility shift of BIK1 but not ASR3. Protoplasts were transfected with ASR3-HA or BIK1-HA and treated with or without 100 nM flg22 for 30 min. The above experiments were repeated three times with similar results.

4.4.3 Flg22 induces *in vivo* ASR3 phosphorylation at Thr-189

To identify the flg22-induced in vivo ASR3 phosphorylation site, we performed series of deletion/mutation and mass spectrometry analysis of ASR3. The N-terminal deletion (ΔN), but not the C-terminal deletion (ΔC), still exhibited a mobility shift upon flg22 treatment (Fig. 4.3A), implying that the phosphorylation underlining the mobility shift occurs at the C terminus of ASR3. To map the phosphorylated residues, we generated a series of truncation mutants each with about ~35 amino acids deleted, which in total span the entire C-terminal half of ASR3 (Fig. 4.3B). Interestingly, ΔC1 (156-190

amino acids) or ΔC2 (191-221 amino acids), but not ΔC3 (222-254 amino acids) nor ΔC4 (255-288 amino acids), completely blocked the flg22-induced mobility shift (Fig. 4.3B). There are multiple serine (S) and threonine (T) residues in C1 and C2 regions. We further mutated some of individual serine or threonine residues to alanine (A) in these regions. Remarkably, T189A mutant, but not S169A, S175A, S182A nor T196A mutant, blocked the flg22-induced ASR3 mobility shift (Fig. 4.3C). Deletion of the C2 (191 to 221) region may impose a conformational change on the nearby Thr-189 residue, there by abolishing flg22-induced mobility shift. Taken together, the data suggest that T189 is an important phosphorylation site of ASR3 in response to flg22 treatment.

Furthermore, we performed liquid chromatography-tandem mass spectrometry (LC-MS/MS) analysis with FLAG epitope-tagged ASR3 protein expressed in Arabidopsis protoplasts with or without flg22 treatment (Fig. 4.3D). The ASR3 proteins were immunoprecipitated with α-FLAG agarose and subjected for SDS-PAGE and silver staining analysis. Compared with the vector control-transfected protoplasts, a discrete band with the molecular mass of ~35 kD was observed in the ASR3-transfected protoplast samples (Fig. 4.3D). Another band with molecular mass of ~38 kD could be detected upon flg22 treatment. Immunoblot analysis using an α-FLAG antibody with a small aliquot of the same protein samples were used for silver staining confirmed that these bands were likely unphosphorylated and phosphorylated ASR3. We enriched the phosphorylated peptides and analyzed them by LC-MS/MS analysis. The LC-MS/MS analysis of the upper band derived from flg22-treated samples revealed that 13 peptides contain Thr-189 as the phosphorylation site (Fig. 4.3E, F; Supplemental Table 1). The

data in large part support our deletion and mutation analysis findings that ASR3^{T189A} mutant no longer exhibited the mobility shift upon flg22 treatment. There are three peptides containing Ser-230 as a high confidence phosphorylation site (Supplemental Table 1). However, the ASR3^{S230A} mutation did not block flg22-induced ASR3 mobility shift (Fig. 4.3G). In addition, ASR3 Thr-189 phospho-mimetic mutant (ASR3^{T189D}) with a substitution of aspartic acid (D) showed constitutive mobility shift in the absence of flg22 treatment (Fig. 4.3G). Taken together, the data indicate that Thr-189 is a major phosphorylation residue of ASR3 induced by flg22 treatment.

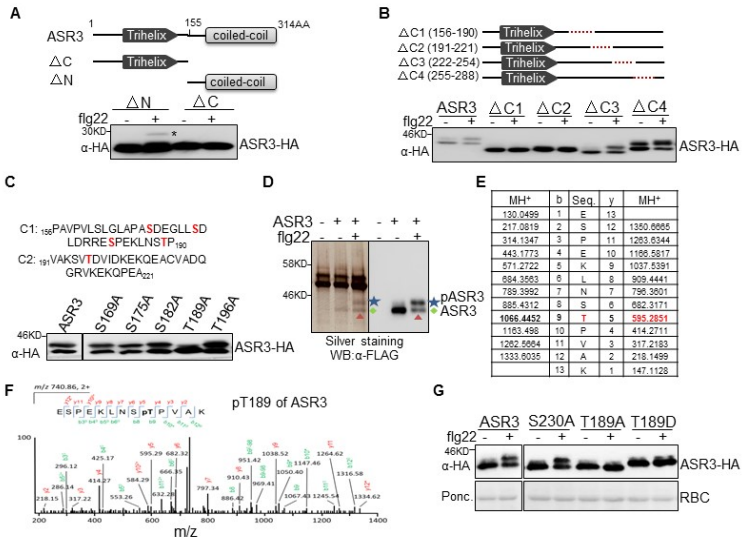

Fig. 4.3 Flg22 induced ASR3 phosphorylation at Thr-189. (A) The flg22-induced ASR3 phosphorylation occurs at its C-terminal half. The top panel shows schematic diagrams of deletion mutants with the putative trihelix and coiled-coil motifs labeled. The deletion was made at 155-amino acid position of ASR3. (B) C1 and C2 regions are required for flg22-induced ASR3 phosphorylation. The top panel shows schematic diagrams with the dashed red line indicating the deleted sequence. Protoplasts were transfected with different ASR3 truncation variants for 12 h and treated with 100 nM flg22 for 15 min. (C) ASR3^{T189A} mutation abolishes the flg22-induced ASR3 phosphorylation. Protoplasts were transfected with ASR3 point mutation variants and treated with 100 nM flg22 for 30 min. The amino acid sequences and potential phosphorylation residues (in red) in C1 and C2 regions are listed on the top. (D) Silver staining and immunoblot analysis of immunoprecipated ASR3-FLAG from Arabidopsis protoplasts. Protoplasts expressing ASR3-FLAG were treated with or without 100 nM flg22 for 15 min. Protein lysis was subjected to immunoprecipitation with α-FLAG antibody followed by SDS-PAGE sliver staining or immunoblot with an α-FLAG-HRP antibody. (E) and (F) LC-MS/MS analysis showing that ASR3 Thr-189 is phosphorylated. The sequence of a doubly charged peptide ion at *m/z* 740.86 matches to ESPEKLNSpTPVAK of ASR3. (G) Thr-189 is an essential phosphorylation site induced by flg22 treatment. Different ASR3 mutants were expressed in protoplasts, treated with flg22, and detected by immunoblotting with an α-HA antibody. The above assays, except the mass spectrometry analysis, were repeated at least three times with similar results.

4.4.4 ASR3 is a substrate of MPK4

We further examined the signaling events that potentially regulate ASR3 phosphorylation. Various chemical inhibitors, which could specifically interfere with distinct early defense responses following receptor complex activation including calcium influx, ROS burst or MAPK activation, were used. The treatment of Ca^{2+} channel inhibitors lanthanum chloride ($LaCl_3$), gallium chloride ($GaCl_3$) or ruthenium red (RR) or the NADPH oxidase inhibitor diphenylene iodonium (DPI) did not affect flg22-induced ASR3 phosphorylation (Supplemental Fig. 2). However, the treatment with MAPK pathway inhibitor U0126 markedly reduced flg22-triggered ASR3 phosphorylation. In addition, coexpression of the MAPK phosphatase MKP almost completely abolished ASR3 mobility shift (Fig 4.4A). These data suggest that the MAPK cascade(s) is required for flg22-triggered ASR3 phosphorylation. Ectopic expression of full-length MEKK1, the most upstream kinase in the flg22-activated MAPK cascade, was sufficient to induce ASR3 phosphorylation in the absence of flg22 treatment (Fig 4.4A). Notably, the flg22-induced phosphorylation residue Thr-189 is a typical MAPK phosphorylation site in that it is followed by a proline (P) residue. Thus, the data suggest that ASR3 may function as a direct target of certain MAPKs in immune signaling. The Arabidopsis genome encodes 20 *MPK* genes (Hamel et al., 2006; Ichimura et al., 2002). To discern which MAPK(s) could phosphorylate ASR3, we screened individual Arabidopsis MAPKs for the ability to phosphorylate ASR3. The HA-tagged MAPKs were expressed in protoplasts, activated by flg22 treatment, and immunoprecipitated for an in vitro kinase assay using ASR3 protein fused to maltose

binding protein (MBP) as a substrate. Importantly, flg22-activated MPK4 strongly phosphorylated ASR3 in vitro (Fig. 4.4B).

A time-course study suggested that MPK4 exhibited the highest phosphorylation activity towards ASR3 at 5 to 15 min after flg22 treatment (Fig. 4.4C). MPK4 was unable to phosphorylate $ASR3^{T189A}$, which abolished the flg22-induced ASR3 mobility shift (Fig. 4.4D). By contrast, mutation of another putative MAPK phosphorylation site (S182A) did not impair its phosphorylation of ASR3 by MPK4 (Fig.4.4D). $ASR3^{S182}$ was also not detected as a confident phosphorylation site by LC-MS/MS analysis (Supplemental Table 1). These data suggest that MPK4 directly phosphorylates ASR3 at the Thr-189 residue during FLS2 signaling. Importantly, flg22-induced ASR3 phosphorylation was largely abolished in the *mpk4* mutant compared to WT (*Landsberg erecta* [*Ler*]) plants, providing the genetic evidence of involvement of MPK4 in flg22-induced ASR3 phosphorylation (Fig. 4.4E).

In addition, MPK4 coimmunoprecipitated with ASR3 when coexpressed in protoplasts (Fig. 4.4F). The association was also confirmed in ASR3-HA transgenic plants. Following immunoprecipitation with the α-HA antibody, endogenous MPK4 detected by the α-MPK4 antibody was observed in ASR3-HA transgenic plants but not in the empty vector control transgenic plants (Fig. 4.4G).

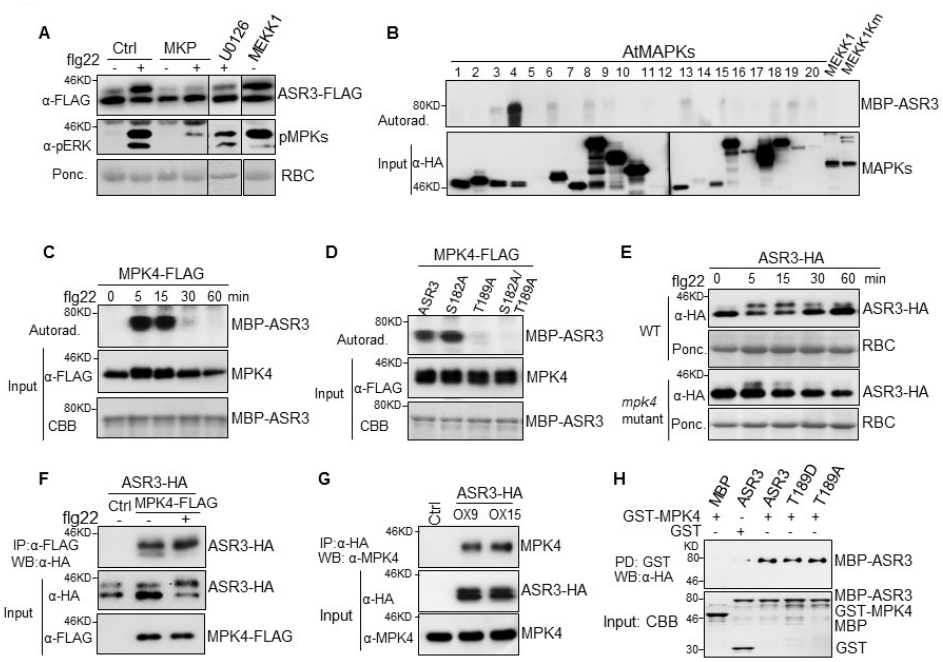

Fig. 4.4 MPK4 phosphorylates and interacts ASR3. (A) MPK-dependent ASR3 phosphorylation. Protoplasts were coexpressed with ASR3-FLAG and MAPK phosphatase MKP or MEKK1. MEK/MKK inhibitor U0126 was added to protoplasts 30 min before flg22 treatment. MAPK activation is shown by immunoblotting with α-pERK antibody (middle panel). (B) flg22-activated MPK4 phosphorylates ASR3. The individual MAPKs were expressed in protoplasts, activated by flg22 treatment, immunoprecipitated with α-HA antibody and subjected to an in vitro kinase assay using MBP-ASR3 as a substrate in the presence of [γ- ^{32}P]ATP. Proteins were separated with SDS-PAGE and analyzed by autoradiography (upper panel) and the MAPKs expression is shown by immunoblotting (bottom panel). (C) Time course of flg22-activated MPK4 phosphorylation on ASR3. The experiment was performed as in (B) with 100 nM flg22 treatment for the indicated time. MBP-ASR3 is shown by Coomassie blue staining (CBB). (D) Thr-189 is required for MPK4-mediated ASR3 phosphorylation. The experiment was performed as in (B) with different MBP-ASR3 mutants as substrates. (E) The *mpk4* mutant abolishes the flg22-induced ASR3 phosphorylation. Protoplasts were isolated from Ler and the *mpk4* mutant (in Ler background), transfected with ASR3-HA and treated with 100 nM flg22 for the indicated time. (F) ASR3 associates with MPK4 in Arabidopsis protoplasts. Protoplasts were cotransfected with ASR3-HA and MPK4-FLAG or an empty vector control (Ctrl). Co-IP was performed with α-FLAG antibody (IP: α-FLAG), and the proteins were analyzed using immunoblots with α-HA antibody (IB: α-HA). (G) ASR3 associates with MPK4 in *35S::ASR3-HA* transgenic plants. Ten-day-old seedlings from two independent transgenic lines (OX9 and OX15) were used for co-IP, and transgenic plants carrying an empty vector were used as the control (Ctrl). Co-IP assay was performed with α-HA antibody and the proteins were analyzed using immunoblot with an α-MPK4 antibody (top). The input of ASR3-HA and MPK4 proteins is shown by immunoblots (middle and bottom). (H) ASR3 directly interacts with MPK4 in in vitro pull-down assay. GST or GST-MPK4 immobilized on glutathione Sepharose beads was incubated with MBP, MBP-ASR3, MBP-ASR3^{T189D} or MBP-ASR3^{T189A} proteins. The beads were washed and pelleted for immunoblot analysis with α-HA antibody. PD, pull-down. The above experiments were repeated three times with similar results.

To test whether MPK4 directly interacts with ASR3, an in vitro pull-down assay was performed with glutathione S-transferase (GST)-tagged MPK4 immobilized on glutathione Sepharose beads as bait against MBP-ASR3 fusion protein with an HA epitope tag. As shown in Fig. 4.4H, MBP-ASR3 could be pulled down by GST-MPK4,

but not by GST alone. It appears that ASR3^{T189A} did not affect MPK4 and ASR3 interaction (Fig. 4.4H). Taken together, the data indicate that ASR3 directly interacts with MPK4 and is phosphorylated by MPK4 mainly on Thr-189 residue upon flg22 perception.

4.4.5 ASR3 is a transcriptional repressor

The putative trihelix DNA binding domain is located at its N terminus with three amphipathic α-helices and the conserved tryptophan (W) residues. The ASR3 C terminus is predicted to form a coiled-coil, which is loosely conserved within the clade (Fig 4.5A). Consistent with its potential function as a transcription factor, fluorescence signals derived from the green fluorescent protein (GFP) fusion of ASR3 were observed mainly in nucleus in *Nicotiana benthamiana* transient assays (Fig 4.5B). Similarly, stable Arabidopsis transgenic plants carrying ASR3-GFP under the control of Cauliflower Mosaic Virus *35S* promoter showed strong fluorescence signals in nucleus (Supplemental Fig. 3). There are two predicted nuclear localization signals (NLS) in ASR3, a bipartite NLS at N terminus and a monopartite NLS at C terminus (Fig 4.5A). Apparently, either NLS is sufficient to mediate ASR3 nuclear localization since both ASR3-ΔC and ASR3-ΔN were mainly localized in the nucleus when transiently expressed in Arabidopsis protoplasts (Fig 4.5C).

We also determined the transcriptional activity of ASR3 with an effector construct containing *35S* promoter-driven yeast transcription activator GAL4 DNA binding domain fused with ASR3 and a reporter construct containing the GAL4 upstream activation sequence (UAS) and the *35S* minimal promoter-driven a luciferase

reporter gene (Fig. 4.5D). Transactivation assays were performed by coexpression of the effector and the reporter constructs in Arabidopsis protoplasts. Surprisingly, compared with the empty vector control, expression of ASR3 resulted in ~3-fold reduction of luciferase activity, suggesting that ASR3 functions as a transcriptional repressor (Fig. 4.5E). In line with this observation, we identified two EAR motifs in ASR3 (Fig. 4.5A). The EAR motif with the consensus sequence of either LxLxL or DLNxxP has been reported to constitute a predominant form of transcriptional repression motif in plants (Kagale et al., 2010). Mutations in the conserved leucine (L) residues in the EAR motifs (*ear*-A: L161A/L163A/L165A or *ear*-B: L280A/L282A/L284A) impaired ASR3 transcriptional repressor activity (Fig. 4.5E), indicating that its repressor activity is largely conferred by the EAR motifs. Consistent with these results, expression of ASR3 in protoplasts suppressed flg22-induced *FRK1* promoter activity and this suppression activity depended on the EAR motifs (Fig. 4.5F). Together, the data indicate that ASR3 functions as a transcriptional repressor to suppress certain flg22-induced immune gene expression.

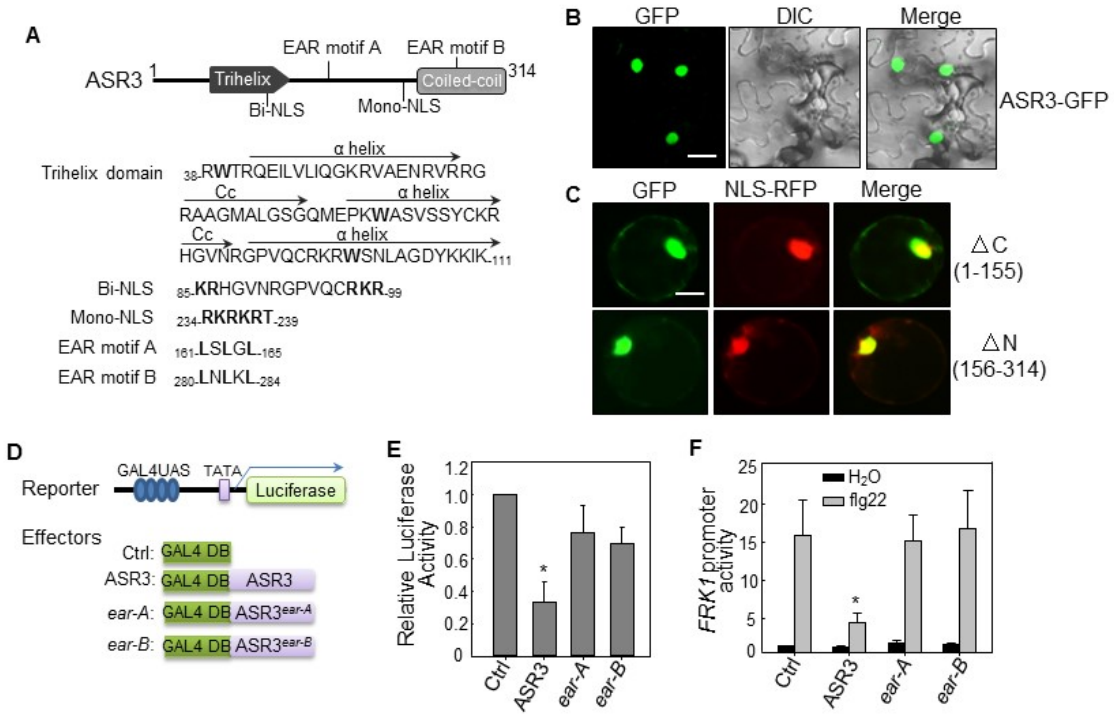

Fig. 4.5 ASR3 is a transcriptional repressor. (A) ASR3 is a putative trihelix transcription factor. The structure of ASR3 labeled with the putative protein motifs is shown on top and the amino acid sequence with the starting and ending positions for each motif is shown below. The trihelix domain contains three amphipathic α-helices with the conserved Trp residues in bold. Bi-NLS and Mono-NLS stand for bipartite NLS and monopartite NLS, respectively. The bold letters in the sequence indicate the conserved sites in the motifs. (B) ASR3-GFP localizes in nucleus. *N. benthamiana* leaves were infiltrated with *Agrobacterium tunefaciens* carrying *35S::ASR3-GFP* and the images were taken 2 dpi with a confocal microscope. Bar=10μm. (C) Both the N-terminal and C-terminal halves of ASR3 localize in nucleus. The GFP fusion of N-terminus half (△C) or C-terminal half (△N) was coexpressed with NLS-RFP in Arabidopsis protoplasts for 12h and the images were taken with a confocal microscope. NLS-RFP is a control for nuclear localization. Bar=10μm. (D) Schematic diagrams of the effector and reporter constructs used in transcription assay. The reporter construct contains four copies of GAL4-UAS, a minimal *35S* promoter (TATA) and a luciferase reporter gene. The effector constructs contain GAL4 DNA binding domain alone (Ctrl), or with *ASR3* WT ASR3, or *ear* mutants under the control of *35S* promoter. (E) Relative transcriptional activity of *ASR3* and *ear* mutants. Protoplasts were cotransfected with the reporter construct and different effector constructs. (F) Overexpression of *ASR3* in Arabidopsis protoplasts suppresses flg22-induced *FRK1* promoter activity. Protoplasts were cotransfected with *pFRK1::LUC* and *ASR3*, A*SR3*$^{ear\text{-}A}$, *ASR3*$^{ear\text{-}B}$ or empty control. In (E) and (F) *UBQ10-GUS* was included in all the transfections and served as an internal transfection control. The luciferase activity was normalized with GUS activity. The data are shown as mean ± SD from three independent repeats. The asterisk indicates significant difference with a Student's *t* test ($P < 0.05$) when compared with control. The above experiments were repeated three times with similar results.

4.4.6 ASR3 forms a homodimer

The C-terminal coiled-coil domain of trihelix transcription factors is predicted to be involved in protein dimerization (Kaplan-Levy et al., 2012; Qin et al., 2014)(Fig 4.5A). We tested the potential homodimerization of ASR3 and the involvement of the coiled-coil domain by yeast two-hybrid (Y2H) and coimmunoprecipitation (co-IP)

assays (Fig. 4.6A, B). ASR3 interacted with itself in Y2H assay (Fig. 4.6A). In addition, ASR3-FLAG could immunoprecipitate ASR3-HA when transiently expressed in Arabidopsis protoplasts (Fig. 4.6B). It appears that flg22-induced ASR3 phosphorylation did not affect ASR3 homodimerization (Fig. 4.6B). Consistent with this observation, both $ASR3^{T189A}$ (phospho-inactive mutant) and $ASR3^{T189D}$ (phospho-mimetic mutant) could interact with not only WT ASR3 (Supplemental Fig.s 4A, B) but also with themselves (Fig. 6C, D) in co-IP and Y2H assays. In line with the role of the C-terminal coiled-coil domain in protein dimerization, ASR3 △C, but not ASR3△N, lost the interaction with full-length ASR3 (Supplemental Fig. 4C). Furthermore, the △C4 (255-288) truncation mutant, of which the coiled-coil domain was deleted, blocked ASR3 homodimerization (Supplemental Fig. 4C). These data indicate that ASR3 forms a homodimer that is likely mediated by the C-terminal coiled-coil domain.

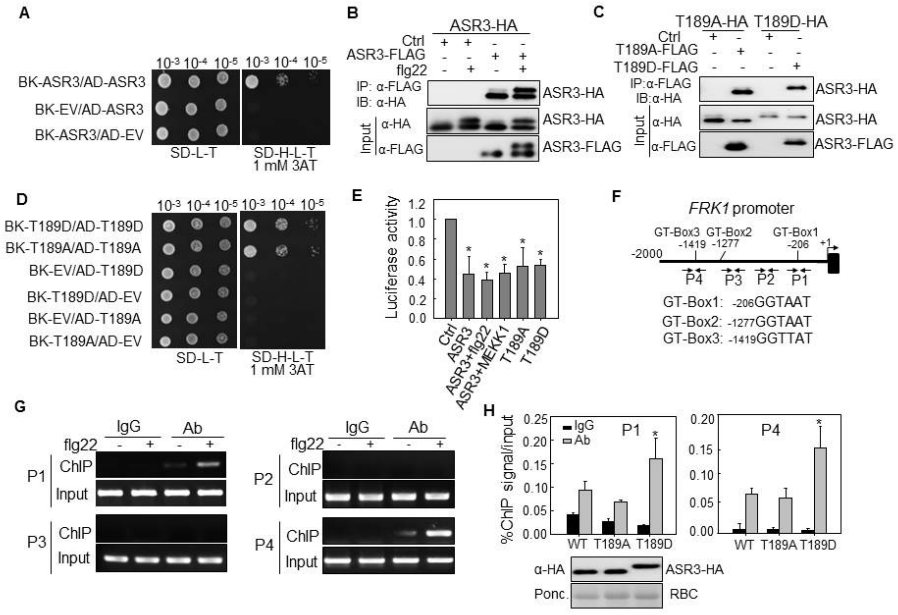

Fig. 4.6 Phosphorylation of ASR3 by MPK4 enhances its DNA binding activity. (A) ASR3 forms homodimmer in the Y2H assay. The interaction between pAD-ASR3 and pBK-ASR3 was tested on SD-H-L-T supplemented with 1 mM 3-amino-1,2,4-triazole (3AT). EV indicates the empty vectors for either pGADT7 or pGBKT7. Serial dilutions of the yeast colonies were plated. (B) ASR3 forms homodimmer in vivo. Co-IP was performed with Arabidopsis protoplasts coexpressing ASR3-HA and ASR3-FLAG or an empty vector control (Ctrl). (C) Neither ASR3^{T189A} nor ASR3^{T189D} exhibits altered homodimerization in co-IP assays. (D) Neither ASR3^{T189A} nor ASR3^{T189D} exhibits altered homodimerization in Y2H assay. (E) The effect of phosphorylation on ASR3 transcriptional regulation activity. All the transfections included the *UAS-LUC* (reporter construct), and *UBQ10-GUS* (internal transfection control), and different *ASR3* effector constructs. One sample was treated with 100 nM flg22 for 4 h, and one sample was cotransfected with MEKK1. The asterisk indicates a significant difference with a Student's t test ($P < 0.05$) when compared with control. (F) Schematic diagram of the *FRK1* promoter with the positions of putative GT-boxes and PCR primers for the ChIP assay. The sequence of each GT-box is shown with the starting nucleotide position. (G) ASR3 binds to the endogenous *FRK1* promoter in vivo based on ChIP assay. Twelve-day-old seedlings from *35S::ASR3-HA* transgenic plants were used for chromatin isolation. ASR3-chromatin complex was immunoprecipitated with α-HA antibody (with mouse IgG as negative control) and subjected to PCR analysis with primers as indicated in Fig. 4.6F. Sheared DNA before immunoprecipitation served as the input control. (H) Phosphorylation of ASR3 enhances its DNA binding activity. Twelve-day-old seedlings from WT ASR3-HA, ASR3^{T189D}-HA and ASR3^{T189A}-HA transgenic lines were used for chromatin isolation. ChIP- and input-DNA samples were quantified by PCR using P1 and P4 region primers. The ChIP results are presented as percentage of input DNA. Error bars indicate SD ($n = 3$). The asterisk indicates a significant difference with a Student's t test ($P < 0.05$) when compared with WT ASR3. The protein expression level of different ASR3 variants in transgenic plants is shown by immunoblot on the bottom.

4.4.7 Phosphorylation of ASR3 by MPK4 enhances its DNA binding activity

Our data suggest that flg22-activated MPK4 could directly phosphorylate ASR3 and that ASR3 possesses transcriptional repressor activity. Next, we determined whether MPK4-mediated ASR3 phosphorylation affects its repressor activity and/or DNA

binding activity. As shown in Fig. 4.6E, flg22 treatment or activation of ASR3 by MEKK1 did not affect its transcriptional repressor activity in the GAL4-UAS-based protoplast transactivation assay. In addition, the T189A and T189D mutants behaved similarly as WT ASR3 in terms of transcriptional repressor activity (Fig 4.6E). Apparently, phosphorylation of ASR3 may not regulate its transcriptional repressor activity.

It has been reported that trihelix transcription factors bind to the GT-like motif [GGT(A/T)(A/T)(A/T)] of target genes to regulate transcription (Kaplan-Levy et al., 2012). The *FRK1* promoter region (2 Kb upstream of the translational start site) contains three putative GT-like motifs (Fig 4.6F). We tested whether ASR3 is able to bind to any of these motifs in the *FRK1* promoter by chromatin immunoprecipitation (ChIP)-PCR assay with four pairs of primers amplifying different regions of *FRK1* promoter in transgenic plants expressing *35S::ASR3-HA*. ASR3 was able to bind to P1 and P4 regions of the *FRK1* promoter. Interestingly, the binding of ASR3 to these regions was enhanced upon flg22 treatment (Fig 4.6G). Furthermore, a ChIP-PCR assay with transgenic plants carrying *35S* promoter-driven WT *ASR3-HA*, *ASR3*^{T189A}*-HA* or *ASR3*^{T189D}*-HA* indicated that the phospho-mimetic form (ASR3^{T189D}) displayed higher DNA binding affinity than the WT ASR3 and phospho-inactive form (ASR3^{T189A}) (Fig 4.6H). The data support that flg22-induced ASR3 phosphorylation enhanced its binding to the *FRK1* promoter.

4.4.8 Overexpression of ASR3 compromises disease resistance to virulent bacterial pathogens

We further determined the disease phenotype of transgenic plants carrying *ASR3*^{T189D} with the a C-terminal HA epitope tag under the control of the constitutive *35S* promoter. We also generated transgenic plants carrying WT *ASR3-HA* under the control of *35S* promoter. Multiple lines of each construct were obtained and two lines with comparable transcript and protein expression levels for each were chosen for plant defense response assays (Supplemental Fig. 5A, B). OX9 and OX15 were the representative lines for *35S::ASR3-HA*, whereas OXD1 and OXD3 were the representatives for *35S::ASR3*^{T189D}*-HA* transgenic plants. We observed that transgenic plants overexpressing WT *ASR3* or *ASR3*^{T189D} were smaller in size than WT Col-0 or transgenic plants carrying an empty vector (Fig 4.7A). The transgenic plants overexpressing WT *ASR3* displayed slightly but statistically significant enhanced susceptibility to the infections by virulent bacterial pathogens *Pst* and *Psm* as measured by in planta bacterial multiplication (Fig. 4.7B, C). The enhanced susceptibility was more evident in plants overexpressing *ASR3*^{T189D} with over 10-fold bacterial population in transgenic plants than that in WT plants 4 dpi (Fig. 4.7B, C). The disease symptom were also more severe in the transgenic plants than in the WT (Fig. 4.7D). The flg22 treatment primed plant resistance against *Pst* infection in WT plants (Zipfel et al., 2004). However, flg22-induced resistance was blocked in *ASR3*^{T189D} overexpression plants (Fig. 4.7E). Consistent with the *asr3-1* mutant, overexpression lines showed unaltered disease resistance to avirulent pathogen *Pst* avrRpt2 (Fig. 4.7F).

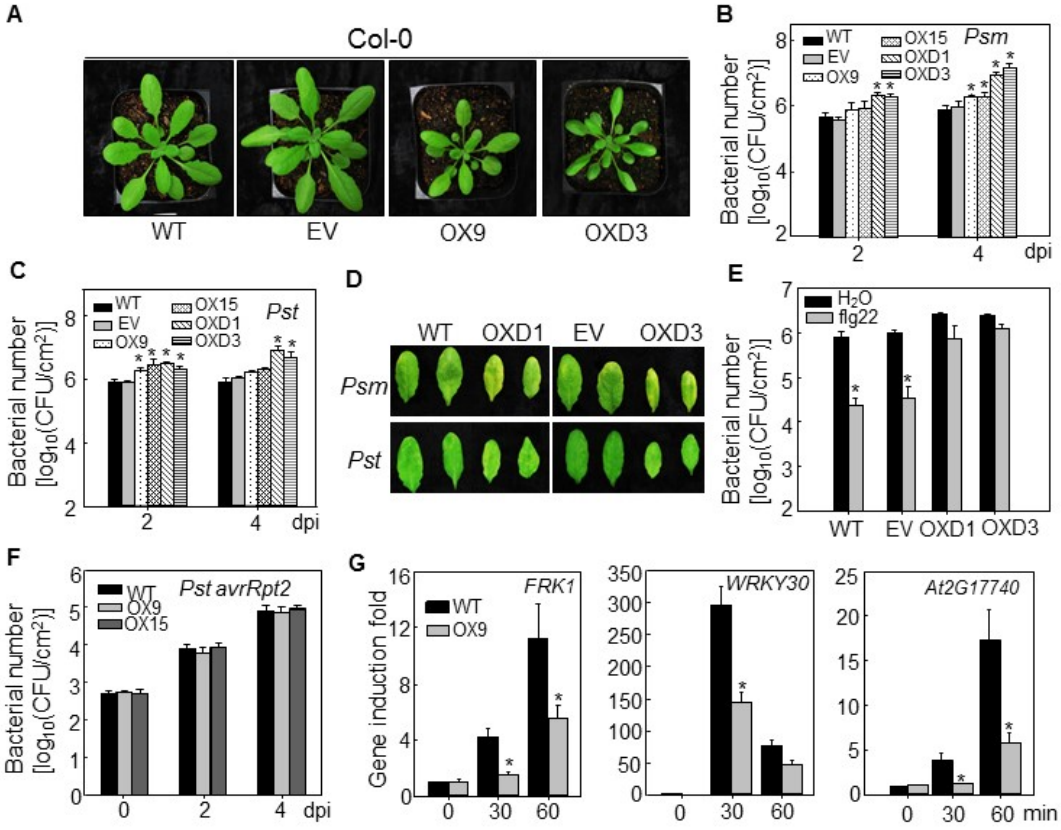

Fig. 4.7 Overexpression of ASR3 compromises disease resistance. (A) Morphological phenotype of WT, the empty vector control (EV), *35S::ASR3-HA* (OX9) and *35S::ASR3^{T189D}-HA* (OXD3) transgenic lines. Four-week-old soil-grown plants were shown. (B) and (C) Bacterial multiplication of *Psm* ES4326 (B) or *Pst* DC3000 (C) in WT, empty vector control, *35S::ASR3-HA* (OX9 and OX15) and *35S::ASR3^{T189D}-HA* (OXD1 and OXD3) transgenic plants at 2 and 4 dpi. Leaves from four-week-old plants were hand-inoculated with *Psm* or *Pst* at 5 x 10^5 cfu/ml and bacterial counting was performed at the indicated time points. (D) The disease symptom upon *Psm* or *Pst* infection. The pictures were taken at 4 dpi. (E) Compromised flg22-mediated immunity to *Pst* infection in *ASR3^{T189D}* overexpression lines. Leaves from four-week-old plants were hand-inoculated with water or 100 nM flg22, and 24h later hand-inoculated with *Pst* at 5 x 10^5 cfu/mL. Bacterial counting were performed at 3 dpi. (F) Bacterial growth of *Pst avrRpt2*. The bacteria at 5X3 10^5 cfu/mL were hand-inoculated into leaves of 4-week-old plants. (G) Reduced immune gene expression in *ASR3* overexpression lines. Ten-day-old seedlings were treated with 100 nM flg22 for 30 and 60 min for qRT-PCR analysis. Gene expression level was normalized with internal control *UBQ10*. The data in (B), (C), and (E) to (G) are shown as means ± SD from three biological repeats. The asterisk indicates a significant difference with a Student's t test ($p<0.05$) when compared with the WT or control treatment. The above experiments were repeated three times with similar results.

The data further indicate that ASR3 plays a negative role in plant PTI defense and that phosphorylation at Thr-189 is important for its function. Consistent with this, the transgenic plants overexpressing *ASR3* displayed reduced induction of immune-responsive genes *FRK1*, *WRKY30* and *At2G17740* upon flg22 treatment (Fig 4.7G).

4.4.9 ASR3 globally regulates flg22-induced immune genes

To further identify the ASR3-regulated flg22-induced genes, we performed RNA sequencing (RNA-seq) analysis with 10-d-old seedlings of WT, *asr3-1* and *35S:ASR3-HA* transgenic line OX9 with or without 100 nM flg22 treatment for 30 min. Samples from four independent biological repeats were collected and RNAs from two repeats were pooled for RNA-seq. The correlation coefficient (R) for the expression profiles of all transcripts between WT and *asr3-1*, and between WT and OX9 without flg22 treatment was close to linear (0.99), suggesting that ASR3 does not affect general gene transcription (Fig. 4.8A). Among 23,317 detectable transcripts, 48 genes showed differential expression (fold change $\geqslant$ 2, P value < 0.05) with 31 showing enhanced and 17 reduced expression in the *asr3-1* mutant compared with WT plants without treatment (Supplemental Data Set 1A). Compared with no treatment, flg22 treatment induced 1244, 1384 and 991 genes (fold change $\geqslant$ 2, p value < 0.05) in the WT, *asr3-1* and OX9 respectively, with 904 genes induced in all three genotypes (Fig. 4.8B, Supplemental Data Set 1B). Hierarchical clustering analysis with 1531 genes induced by flg22 treatment in any of the three genotypes suggested that the *asr3-1* mutant displayed overall enhanced flg22 response, whereas OX9 displayed an overall enhanced flg22 response compared with WT plants (Fig. 4.8C). We further analyzed the differential flg22-induced genes in the WT and *asr3-1* mutant, which were defined as ASR3-dependent flg22-induced genes and classified them into four groups: Group I, 109 genes as ASR3-required flg22-induced genes (genes induced in the WT, but not in *asr3-1*); Group II, 43 genes as ASR3-potentiated flg22-induced genes (genes induced in both the

WT and *asr3-1*with at least 1.5-fold higher induction in WT than *asr3-1*); Group III, 89 genes as ASR3-attenuted flg22-induced genes (genes induced in both WT and *asr3-1* with at least 1.5-fold higher induction in *asr3-1* than WT); and Group IV, 249 genes as ASR3-suppressed flg22-induced genes (genes induced in *asr3-1*, but not in WT) (Fig 4.8D, Supplemental Data Set 1C). Importantly, 338 out of 490 (69%) ASR3-dependent flg22-induced genes showed enhanced flg22-induction in *asr3-1* compared with WT plants. Notably, 227 out of 338 (67%) ASR3 negatively regulated flg22-induced genes displayed reduced flg22 induction in OX9 plants compared with that in the WT (Supplemental Data Set 1D). Enrichment analysis of Gene Ontology (GO) categories indicates that genes associated with defense response to stress, response to biotic stimulus, immune system response, and response to salicylic acid were significantly enriched (P value<0.01) in Group III and IV genes (Fig. 4.8E, Supplemental Data Set 1E). The elevated expression of several flg22-induced genes, including *At1G02360* (chitinase family protein), *At2G40180* (PP2C family phosphatase gene) and *At4G25110* (type I metacaspase gene), in *asr3-1* was confirmed with quantitative RT-PCR analysis (Fig. 4.8F).

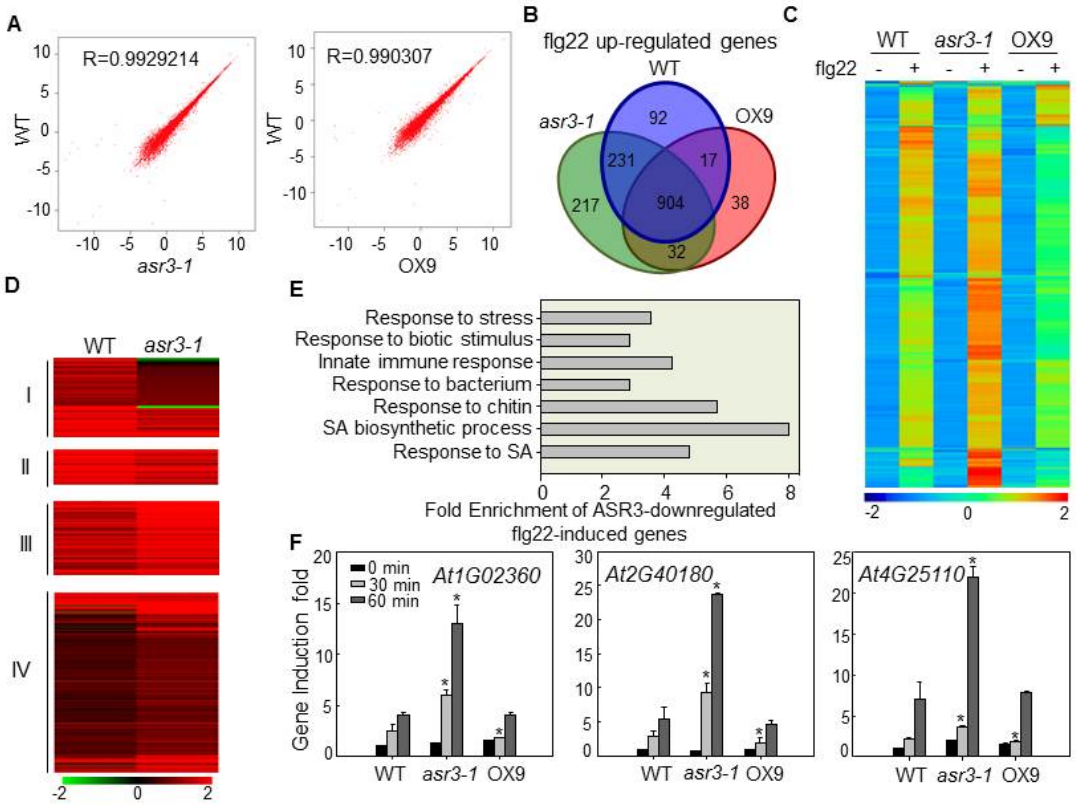

Fig. 4.8 ASR3 globally regulates flg22-induced gene expression. (A) Scatter plots of whole-genome transcript fragments per kilobase of transcript per million mapped reads (FPKM) in Col-0 (WT) versus *asr3-1* mutant (left) or OX9 transgenic plants (right). Gene expression levels were detected in 10-d-old seedlings without treatment. The y axis indicates gene expression in the wild type, and the x axis indicates gene expression in *asr3-1* or OX9 transgenic plants.(B) Venn diagram of flg22-induced genes (fold change ≥ 2 and P value < 0.05; 30 min after 100 nM flg22 treatment) in WT, *asr3-1*, or OX9 transgenic plants. (C) Heat map of flg22-induced genes in WT, *asr3-1*, or OX9 transgenic plants. The original FPKM values were subjected to data adjustment by normalized genes/rows and hierarchical clustering was generated with the average linkage method using MeV4.0. Red color indicates relatively high expression, and blue indicates relatively low expression. A list of flg22-induced genes is shown in Supplemental Data Set 1B. (D) Clustering display of ASR3-dependent flg22 upregulated genes in WT and *asr3-1* mutant plants. The four clusters are defined in the text. The flg22 induction fold of individual genes with the $\log_2$-transformed values was used for hierarchical clustering analysis with the average linkage method using MeV4.0. Red color indicates upregulation and green indicates downregulation with flg22 treatment. The gene list for this analysis is shown in Supplemental Data Set 1C. (E) Enrichment of genes with GO terms related to defense response for Group III and IV genes. The fold enrichment was calculated based on the frequency of genes annotated to the term compared with their frequency in the genome. (F) qRT-PCR analysis of ASR3-regulated genes. *At1G02360* encodes a chitinase family protein, *At2G40180* encodes a PP2C family phosphatase, and *At4G25110* encodes a type I metacaspase. Gene expression was normalized to internal control *UBQ10*. The data are shown as means ± SD from three biological replicates with a Student's t test. Asterisk indicates a significant difference with P < 0.05 when compared with the wild type.

There were 133 genes identified as flg22 down-regulated genes (fold change ⩾ 2, P value < 0.05) in either the WT, *asr3-1* or OX9 (Supplemental Data Set 1F). Compared with the WT (25 genes), OX9 (69 genes) had more downregulated genes and

enhanced fold change of downregulation, which is consistent with the idea that ASR3 functions as a transcription repressor. Thus, ASR3 appears to regulate both flg22-induced and flg22-reduced genes. Taken together, the global gene expression data suggest that ASR3 plays a negative role in regulating a large subset of flg22-regulated genes.

4.5 Discussion and conclusions

Proper transcriptional reprogramming of immune-related genes is critical for any organisms to achieve efficient defense responses against pathogen infections. Although more than 1000 genes are activated by MAMP treatments, the regulation of immune-related gene expression remains largely unknown. In this study, we report that a putative trihelix transcription factor, ASR3, plays a negative role in regulating immune-related gene expression and defense in FLS2 signaling. ASR3 functions as a transcriptional repressor via its EAR motifs. ASR3 directly interacted with MPK4 in vivo and in vitro. Upon flg22 perception, MPK4 rapidly phosphorylated ASR3 primarily on Thr-189 residue, which enhanced ASR3 DNA binding activity toward the promoters of target genes. *FRK1*, a PTI marker gene, is a direct target of ASR3 and its induction was suppressed by overexpression of ASR3. The *asr3* knockout mutant shows enhanced disease resistance to virulent *P. syringae* strains accompanied by the elevated immune-related gene induction. Thus, the data revealed that ASR3, as a new MPK4 substrate functions as a transcriptional repressor to downregulate expression of certain immune-related genes and negatively regulate PTI responses.

ASR3 was annotated as an unknown function protein containing a putative MYB-like DNA binding domain by TAIR10 (http://www.arabidopsis.org/) and does not bear significant similarity to any other proteins. ASR3 was not classified as a member of MYB or MYB-like gene family, as the individual helix motif of its DNA binding domain is significantly longer than the classical MYB or MYB-like domain and the target sequences are also different. It was recently shown that its DNA binding domain bears features of the trihelix DNA binding motif (Kaplan-Levy et al., 2012; Qin et al., 2014). In addition, ASR3 contains a conserved coiled-coil motif at its C terminus (Fig. 4.5A). Based on these features and phylogenetic analysis, ASR3 was classified as a member of SH4 clade in the trihelix transcription factor family (Kaplan-Levy et al., 2012). The *Arabidopsis* genome contains four SH4-related genes, and none of them has been assigned a function. ASR3 does not bear high sequence similarity to other *Arabidopsis* SH4-related proteins, with sequence identity of 22.6% to At4G31270, 20.2% to At2G35640, and 19.5% to At1G31310 at the amino acid level. Trihelix transcription factors appear to be specific to land plants and do not exist in algae, insects, and animals. In *Arabidopsis*, there are 30 members in this gene family. Compared with other transcription factor families, trihelix family transcription factors remain poorly characterized and most of them have not been assigned a function. Several characterized trihelix transcription factors have been reported to be involved in light response, plant development, and abiotic stress responses (Kaplan-Levy et al., 2012). The founding members of trihelix transcription factors, GT factors (GT-1 and GT-2), bind to the GT elements in the promoters of light-induced genes. Whether and how trihelix transcription

factors function in plant biotic stresses was not clear. It has been reported that *GT-3b*, a GT-1 clade of the trihelix transcription factor, is transcriptionally induced 30 min after *P. syringae* infection, although the biological function of this was unclear (Park et al., 2004). Here, we provide genetic evidence that ASR3, a SH-4 clade trihelix transcription factor, negatively regulates plant immune gene expression and defense. In contrast to GT-1 and GT-2, which function as transcriptional activators. ASR3 is a transcriptional repressor through its EAR motifs.

Transcription factors are often transcriptionally and/or posttranslationally regulated in response to internal and external stimuli. Transcripts of WRKY transcription factors are quickly activated upon pathogen infections. By contrast, transcripts of *ASR3* do not appear to change significantly upon flg22 treatment. Similarly, expression of GT-1 and GT-2 is constitutive and is not affected by light signals. It has been speculated that GT-1 and GT-2 are likely regulated by posttranslational modification in response to light. Indeed, in vitro phosphorylation of GT-1 by mammalian calcium/calmodulin kinase II increases its DNA binding activity, but the biological significance of this and the corresponding plant kinase remain unknown (Marechal et al., 1999). We found that MPK4 directly phosphorylated ASR3 and that the phosphorylation enhanced its DNA binding activity to the promoters of target genes. There are several putative GT-like elements in the promoter region of *FRK1*. We show that flg22 treatment or the phospho-mimetic form ASR3^{T189D} enhanced ASR3 binding to some of the GT-like elements in the *FRK1* promoter. It appears that different mechanisms underlie the phosphorylation-induced enhancement of DNA binding

activity of ASR3 and GT-1. The phosphorylation site of GT-1 is located in the DNA binding domain and structural modeling suggests that the phosphorylated side chain of GT-1 is involved in direct interaction with bases of the DNA (Marechal et al., 1999; Nagata et al., 2010). However, the MPK4-mediated phosphorylation occurs outside of the DNA binding domain of ASR3. The mechanistic details of how phosphorylation enhances the DNA binding activity of ASR3 await further elucidation.

The MEKK1-MKK1/MKK2-MPK4 cascade is considered to be a negative regulator in plant innate immunity (Gao et al., 2008). Recent functional study of constitutively active (CA) form of MPK4 further supports this hypothesis. CA-MPK4 transgenic plants show compromised disease resistance to virulent bacterial *Pst* DC3000 and non-pathogenic mutant *hrcC* infection (Berriri et al., 2012). Activation of the MPK4 pathway has been hypothesized to antagonize the MKK4/MKK5-MPK3/MPK6 pathway and balance the strength of defense response (Rodriguez et al., 2010). MPK4 phosphorylates and interacts with a VQ motif-containing protein, MPK4 SUBSTRATE1 (MKS1), which likely serves as a scaffold protein to form the MPK4-MKS1-WRKY33 complex (Andreasson et al., 2005). Upon pathogen signal perception, phosphorylation of MKS1 by MPK4 results in the complex disassembly, thereby releasing WRKY33 to bind to the promoters of its target genes, including *PAD3*, which encodes an enzyme required for the synthesis of phytoalexin camalexin (Qiu et al., 2008). Consistent with this, the *wrky33* mutant displayed reduced MAMP- or pathogen-induced *PAD3* expression and camalexin production. However, the *mks1* and *mpk4* mutants have no detectable change of camalexin levels (Qiu et al., 2008). Unlike the MPK4-MKS1-

WRKY33 complex, MPK4 and ASR3 interact constitutively and the phosphorylation status or pathogen signal perception does not appear to exert a demonstrable change in complex formation (Fig. 4.4F). In addition, the *mks1* mutant compromised plant basal defense to *Pst* DC3000 infection (Petersen et al., 2010), whereas the *asr3* mutant enhanced plant resistance to virulent bacterial infections. Apparently, ASR3 functions in parallel with MKS1-WRKY33 downstream of MPK4 to regulate plant defense genes.

REFERENCES

Albrecht, C., Russinova, E., Hecht, V., Baaijens, E., and de Vries, S. (2005). The Arabidopsis thaliana SOMATIC EMBRYOGENESIS RECEPTOR-LIKE KINASES1 and 2 control male sporogenesis. *The Plant Cell Online, 17*(12), 3337-3349.

Andreasson, E., Jenkins, T., Brodersen, P., Thorgrimsen, S., Petersen, N. H., Zhu, S., . . . Petersen, M. (2005). The MAP kinase substrate MKS1 is a regulator of plant defense responses. *The EMBO journal, 24*(14), 2579-2589.

Asai, T., Tena, G., Plotnikova, J., Willmann, M. R., Chiu, W. L., Gomez-Gomez, L., . . . Sheen, J. (2002). MAP kinase signalling cascade in Arabidopsis innate immunity. *Nature, 415*(6875), 977-983.

Ausubel, F. M. (2005). Are innate immune signaling pathways in plants and animals conserved? *Nature Immunology, 6*(10), 973-979. doi: 10.1038/ni1253

Axtell, M. J., and Staskawicz, B. J. (2003). Initiation of RPS2-specified disease resistance in Arabidopsis is coupled to the AvrRpt2-directed elimination of RIN4. *Cell, 112*(3), 369-377.

Berriri, S., Garcia, A. V., Frei dit Frey, N., Rozhon, W., Pateyron, S., Leonhardt, N., . . . Colcombet, J. (2012). Constitutively active mitogen-activated protein kinase versions reveal functions of Arabidopsis MPK4 in pathogen defense signaling. *Plant Cell, 24*(10), 4281-4293.

Bethke, G., Unthan, T., Uhrig, J. F., Poschl, Y., Gust, A. A., Scheel, D., and Lee, J. (2009). Flg22 regulates the release of an ethylene response factor substrate from MAP kinase 6 in Arabidopsis thaliana via ethylene signaling. *Proceedings of the National Academy of Sciences, 106*(19), 8067-8072.

Bhattacharjee, S., Halane, M. K., Kim, S. H., and Gassmann, W. (2011). Pathogen effectors target Arabidopsis EDS1 and alter its interactions with immune regulators. *Science, 334*(6061), 1405-1408.

Block, A., Li, G. Y., Fu, Z. Q., and Alfano, J. R. (2008). Phytopathogen type III effector weaponry and their plant targets. *Current Opinion in Plant Biology, 11*(4), 396-403.

Bohm, H., Albert, I., Fan, L., Reinhard, A., and Nurnberger, T. (2014). Immune receptor complexes at the plant cell surface. *Current Opinion Plant Biology, 20C*, 47-54.

Boller, T., and Felix, G. (2009). A Renaissance of Elicitors: Perception of Microbe-Associated Molecular Patterns and Danger Signals by Pattern-Recognition Receptors. *Annual Review of Plant Biology, 60*, 379-406.

Bonardi, V., and Dangl, J. L. (2012). How complex are intracellular immune receptor signaling complexes? *Frontier Plant Science, 3*, 237.

Boyle, E. I., Weng, S., Gollub, J., Jin, H., Botstein, D., Cherry, J. M., and Sherlock, G. (2004). GO::TermFinder--open source software for accessing Gene Ontology information and finding significantly enriched Gene Ontology terms associated with a list of genes. *Bioinformatics, 20*(18), 3710-3715.

Catanzariti, A.-M., Dodds, P. N., Ve, T., Kobe, B., Ellis, J. G., and Staskawicz, B. J. (2010). The AvrM effector from flax rust has a structured C-terminal domain and interacts directly with the M resistance protein. *Molecular Plant-Microbe Interactions, 23*(1), 49-57.

Chinchilla, D., Zipfel, C., Robatzek, S., Kemmerling, B., Nürnberger, T., Jones, J. D., . . . Boller, T. (2007). A flagellin-induced complex of the receptor FLS2 and BAK1 initiates plant defence. *Nature, 448*(7152), 497-500.

Chinchilla, D., Zipfel, C., Robatzek, S., Kemmerling, B., Nurnberger, T., Jones, J. D. G., . . . Boller, T. (2007). A flagellin-induced complex of the receptor FLS2 and BAK1 initiates plant defence. *Nature, 448*(7152), 497-U412.

Clarke, J. T., Warnock, R., and Donoghue, P. C. (2011). Establishing a time‐scale for plant evolution. *New Phytologist, 192*(1), 266-301.

Collier, S. M., and Moffett, P. (2009). NB-LRRs work a "bait and switch" on pathogens. *Trends in Plant Science, 14*(10), 521-529.

Cove, D. J., Knight, C. D., and Lamparter, T. (1997). Mosses as model systems. *Trends in Plant Science, 2*(3), 99-105.

Cui, F., Wu, S., Sun, W., Coaker, G., Kunkel, B., He, P., and Shan, L. (2013). The Pseudomonas syringae type III effector AvrRpt2 promotes pathogen virulence via stimulating Arabidopsis auxin/indole acetic acid protein turnover. *Plant Physiology, 162*(2), 1018-1029.

Dodds, P. N., and Rathjen, J. P. (2010). Plant immunity: towards an integrated view of plant-pathogen interactions. *Nature Reviews Genetics, 11*(8), 539-548.

Dou, D., and Zhou, J. M. (2012). Phytopathogen effectors subverting host immunity: different foes, similar battleground. *Cell Host Microbe, 12*(4), 484-495.

Fàbregas, N., Li, N., Boeren, S., Nash, T. E., Goshe, M. B., Clouse, S. D., . . . Caño-Delgado, A. I. (2013). The BRASSINOSTEROID INSENSITIVE1–LIKE3 signalosome complex regulates Arabidopsis root development. *The Plant Cell Online, 25*(9), 3377-3388.

Felix, G., Duran, J. D., Volko, S., and Boller, T. (1999). Plants have a sensitive perception system for the most conserved domain of bacterial flagellin. *The Plant Journal, 18*(3), 265-276.

Feng, F., and Zhou, J.-M. (2012). Plant–bacterial pathogen interactions mediated by type III effectors. *Current Opinion in Plant Biology, 15*(4), 469-476.

Flor, H. H. (1971). Current status of the gene-for-gene concept. *Annual Review Phytopathology, 9*(1), 275-296.

Gómez-Gómez, L., and Boller, T. (2000). FLS2: An LRR receptor–like kinase involved in the perception of the bacterial elicitor flagellin in Arabidopsis. *Molecular cell, 5*(6), 1003-1011.

Gao, M., Liu, J., Bi, D., Zhang, Z., Cheng, F., Chen, S., and Zhang, Y. (2008). MEKK1, MKK1/MKK2 and MPK4 function together in a mitogen-activated protein kinase cascade to regulate innate immunity in plants. *Cell Research, 18*(12), 1190-1198.

Gao, M., Wang, X., Wang, D., Xu, F., Ding, X., Zhang, Z., . . . Li, X. (2009). Regulation of cell death and innate immunity by two receptor-like kinases in Arabidopsis. *Cell Host and Microbe, 6*(1), 34-44.

Gao, X., Chen, X., Lin, W., Chen, S., Lu, D., Niu, Y., . . . Sheen, J. (2013). Bifurcation of Arabidopsis NLR immune signaling via Ca2+-dependent protein kinases. *PLoS Pathogens, 9*(1), e1003127.

Gassmann, W., and Bhattacharjee, S. (2012). Effector-Triggered Immunity Signaling: From Gene-for-Gene Pathways to Protein-Protein Interaction Networks. *Molecular Plant-Microbe Interactions, 25*(7), 862-868.

Goldberg, R. B., Beals, T. P., and Sanders, P. M. (1993). Anther development: basic principles and practical applications. *The Plant Cell, 5*(10), 1217.

Gou, X., Yin, H., He, K., Du, J., Yi, J., Xu, S., . . . Li, J. (2012). Genetic evidence for an indispensable role of somatic embryogenesis receptor kinases in brassinosteroid signaling. *PLoS Genetics, 8*(1), e1002452.

Halter, T., Imkampe, J., Mazzotta, S., Wierzba, M., Postel, S., Bucherl, C., . . . Kemmerling, B. (2014). The leucine-rich repeat receptor kinase BIR2 is a negative regulator of BAK1 in plant immunity. *Current Biology, 24*(2), 134-143.

Hamel, L.-P., Nicole, M.-C., Sritubtim, S., Morency, M.-J., Ellis, M., Ehlting, J., . . . Lee, J. (2006). Ancient signals: comparative genomics of plant MAPK and MAPKK gene families. *Trends in Plant Science, 11*(4), 192-198.

He, J.-X., Gendron, J. M., Sun, Y., Gampala, S. S., Gendron, N., Sun, C. Q., and Wang, Z.-Y. (2005). BZR1 is a transcriptional repressor with dual roles in brassinosteroid homeostasis and growth responses. *Science, 307*(5715), 1634-1638.

He, K., Gou, X., Yuan, T., Lin, H., Asami, T., Yoshida, S., . . . Li, J. (2007). BAK1 and BKK1 regulate brassinosteroid-dependent growth and brassinosteroid-independent cell-death pathways. *Current Biology, 17*(13), 1109-1115.

He, P., Shan, L., Lin, N. C., Martin, G. B., Kemmerling, B., Nurnberger, T., and Sheen, J. (2006). Specific bacterial suppressors of MAMP signaling upstream of MAPKKK in Arabidopsis innate immunity. *Cell, 125*(3), 563-575.

Hecht, V., Vielle-Calzada, J.-P., Hartog, M. V., Schmidt, E. D., Boutilier, K., Grossniklaus, U., and de Vries, S. C. (2001). The Arabidopsis SOMATIC EMBRYOGENESIS RECEPTOR KINASE 1 gene is expressed in developing ovules and embryos and enhances embryogenic competence in culture. *Plant Physiology, 127*(3), 803-816.

Hedges, S. B. (2002). The origin and evolution of model organisms. *Nature Reviews Genetics, 3*(11), 838-849.

Heese, A., Hann, D. R., Gimenez-Ibanez, S., Jones, A. M., He, K., Li, J., . . . Rathjen, J. P. (2007). The receptor-like kinase SERK3/BAK1 is a central regulator of innate immunity in plants. *Proceedings of the National Academy of Sciences, 104*(29), 12217-12222.

Howe, E. A., Sinha, R., Schlauch, D., and Quackenbush, J. (2011). RNA-Seq analysis in MeV. *Bioinformatics, 27*(22), 3209-3210.

Huffaker, A., Pearce, G., and Ryan, C. A. (2006). An endogenous peptide signal in Arabidopsis activates components of the innate immune response. *Proceedings of the National Academy of Sciences, 103*(26), 10098-10103.

Ichimura, K., Shinozaki, K., Tena, G., Sheen, J., Henry, Y., Champion, A., . . . Grp, M. (2002). Mitogen-activated protein kinase cascades in plants: a new nomenclature. *Trends in Plant Science, 7*(7), 301-308.

Jones, J. D., and Dangl, J. L. (2006). The plant immune system. *Nature, 444*(7117), 323-329.

Kadota, Y., Sklenar, J., Derbyshire, P., Stransfeld, L., Asai, S., Ntoukakis, V., . . . Zipfel, C. (2014). Direct regulation of the NADPH oxidase RBOHD by the PRR-associated kinase BIK1 during plant immunity. *Molecular Cell, 54*(1), 43-55.

Kagale, S., Links, M. G., and Rozwadowski, K. (2010). Genome-wide analysis of ethylene-responsive element binding factor-associated amphiphilic repression motif-containing transcriptional regulators in Arabidopsis. *Plant Physiology, 152*(3), 1109-1134.

Kaplan-Levy, R. N., Brewer, P. B., Quon, T., and Smyth, D. R. (2012). The trihelix family of transcription factors--light, stress and development. *Trends in Plant Science, 17*(3), 163-171.

Kaufmann, K., Muino, J. M., Osteras, M., Farinelli, L., Krajewski, P., and Angenent, G. C. (2010). Chromatin immunoprecipitation (ChIP) of plant transcription factors followed by sequencing (ChIP-SEQ) or hybridization to whole genome arrays (ChIP-CHIP). *Nature Protocol, 5*(3), 457-472.

Kim, M. G., da Cunha, L., McFall, A. J., Belkhadir, Y., DebRoy, S., Dangl, J. L., and Mackey, D. (2005). Two Pseudomonas syringae type III effectors inhibit RIN4-regulated basal defense in Arabidopsis. *Cell, 121*(5), 749-759.

Kim, T.-W., Guan, S., Burlingame, A. L., and Wang, Z.-Y. (2011). The CDG1 kinase mediates brassinosteroid signal transduction from BRI1 receptor kinase to BSU1 phosphatase and GSK3-like kinase BIN2. *Molecular Cell, 43*(4), 561-571.

Kim, T.-W., Guan, S., Sun, Y., Deng, Z., Tang, W., Shang, J.-X., . . . Wang, Z.-Y. (2009). Brassinosteroid signal transduction from cell-surface receptor kinases to nuclear transcription factors. *Nature Cell Biology, 11*(10), 1254-1260.

Kim, T.-W., and Wang, Z.-Y. (2010). Brassinosteroid signal transduction from receptor kinases to transcription factors. *Annual Review of Plant Biology, 61*, 681-704.

Krol, E., Mentzel, T., Chinchilla, D., Boller, T., Felix, G., Kemmerling, B., . . . Al-Rasheid, K. A. (2010). Perception of the Arabidopsis danger signal peptide 1 involves the pattern recognition receptor AtPEPR1 and its close homologue AtPEPR2. *Journal of Biological Chemistry, 285*(18), 13471-13479.

Lewis, L. A., and McCourt, R. M. (2004). Green algae and the origin of land plants. *American Journal of Botany, 91*(10), 1535-1556.

Li, B., Jiang, S., Yu, X., Cheng, C., Chen, S., Cheng, Y., . . . Shan, L. (2015). Phosphorylation of Trihelix Transcriptional Repressor ASR3 by MAP KINASE4 Negatively Regulates Arabidopsis Immunity. *The Plant Cell, 27*(3), 839-856.

Li, C., Zhou, A., and Sang, T. (2006). Rice domestication by reducing shattering. *Science, 311*(5769), 1936-1939.

Li, J., Wen, J., Lease, K. A., Doke, J. T., Tax, F. E., and Walker, J. C. (2002). BAK1, an Arabidopsis LRR receptor-like protein kinase, interacts with BRI1 and modulates brassinosteroid signaling. *Cell, 110*(2), 213-222.

Li, L., Li, M., Yu, L., Zhou, Z., Liang, X., Liu, Z., . . . Zhou, J. M. (2014). The FLS2-associated kinase BIK1 directly phosphorylates the NADPH oxidase RbohD to control plant immunity. *Cell Host Microbe, 15*(3), 329-338.

Lin, W., Li, B., Lu, D., Chen, S., Zhu, N., He, P., and Shan, L. (2014). Tyrosine phosphorylation of protein kinase complex BAK1/BIK1 mediates Arabidopsis innate immunity. *Proceedings of the National Academy of Science, 111*(9), 3632-3637.

Lin, Z., Griffith, M. E., Li, X., Zhu, Z., Tan, L., Fu, Y., . . . Sun, C. (2007). Origin of seed shattering in rice (Oryza sativa L.). *Planta, 226*(1), 11-20.

Liu, J., Elmore, J. M., Fuglsang, A. T., Palmgren, M. G., Staskawicz, B. J., and Coaker, G. (2009). RIN4 functions with plasma membrane H+-ATPases to regulate stomatal apertures during pathogen attack. *PLoS Biology, 7*(6), e1000139.

Lu, D., Wu, S., Gao, X., Zhang, Y., Shan, L., and He, P. (2010). A receptor-like cytoplasmic kinase, BIK1, associates with a flagellin receptor complex to initiate plant innate immunity. *Proceedings of the National Academy of Sciences, 107*(1), 496-501.

Lu, D. P., Lin, W. W., Gao, X. Q., Wu, S. J., Cheng, C., Avila, J., . . . Shan, L. B. (2011). Direct Ubiquitination of Pattern Recognition Receptor FLS2 Attenuates Plant Innate Immunity. *Science, 332*(6036), 1439-1442.

Lu, D. P., Wu, S. J., Gao, X. Q., Zhang, Y. L., Shan, L. B., and He, P. (2010). A receptor-like cytoplasmic kinase, BIK1, associates with a flagellin receptor complex to initiate plant innate immunity. *Proceedings of the National Academy of Sciences, 107*(1), 496-501.

Mackey, D., Belkhadir, Y., Alonso, J. M., Ecker, J. R., and Dangl, J. L. (2003). Arabidopsis RIN4 is a target of the type III virulence effector AvrRpt2 and modulates RPS2-mediated resistance. *Cell, 112*(3), 379-389.

Maekawa, T., Kufer, T. A., and Schulze-Lefert, P. (2011). NLR functions in plant and animal immune systems: so far and yet so close. *Nature Immunology, 12*(9), 817-826.

Mao, G., Meng, X., Liu, Y., Zheng, Z., Chen, Z., and Zhang, S. (2011). Phosphorylation of a WRKY transcription factor by two pathogen-responsive MAPKs drives phytoalexin biosynthesis in Arabidopsis. *Plant Cell, 23*(4), 1639-1653.

Marechal, E., Hiratsuka, K., Delgado, J., Nairn, A., Qin, J., Chait, B. T., and Chua, N. H. (1999). Modulation of GT-1 DNA-binding activity by calcium-dependent phosphorylation. *Plant Molecular Biology, 40*(3), 373-386.

Martin, G. B., Brommonschenkel, S. H., Chunwongse, J., Frary, A., Ganal, M. W., Spivey, R., . . . Tanksley, S. D. (1993). Map-based cloning of a protein kinase gene conferring disease resistance in tomato. *Science, 262*, 1432-1432.

Meng, X., and Zhang, S. (2013). MAPK cascades in plant disease resistance signaling. *Annual Review Phytopathology, 51*, 245-266.

Metzker, M. L. (2010). Sequencing technologies—the next generation. *Nature Reviews Genetics, 11*(1), 31-46.

Mora-García, S., Vert, G., Yin, Y., Caño-Delgado, A., Cheong, H., and Chory, J. (2004). Nuclear protein phosphatases with Kelch-repeat domains modulate the response to brassinosteroids in Arabidopsis. *Genes and Development, 18*(4), 448-460.

Mudgett, M. B. (2005). New insights to the function of phytopathogenic bacterial type III effectors in plants. *Annual Review of Plant Biology, 56*, 509-531.

Nagata, T., Niyada, E., Fujimoto, N., Nagasaki, Y., Noto, K., Miyanoiri, Y., . . . Katahira, M. (2010). Solution structures of the trihelix DNA-binding domains of the wild-type and a phosphomimetic mutant of Arabidopsis GT-1: mechanism for an increase in DNA-binding affinity through phosphorylation. *Proteins, 78*(14), 3033-3047.

Nam, K. H., and Li, J. (2002). BRI1/BAK1, a receptor kinase pair mediating brassinosteroid signaling. *Cell, 110*(2), 203-212.

Nishiyama, T., Fujita, T., Shin, T., Seki, M., Nishide, H., Uchiyama, I., . . . Shinozaki, K. (2003). Comparative genomics of Physcomitrella patens gametophytic

transcriptome and Arabidopsis thaliana: implication for land plant evolution. *Proceedings of the National Academy of Sciences, 100*(13), 8007-8012.

Noguchi, T., Fujioka, S., Choe, S., Takatsuto, S., Yoshida, S., Yuan, H., . . . Tax, F. E. (1999). Brassinosteroid-insensitive dwarf mutants of Arabidopsis accumulate brassinosteroids. *Plant Physiology, 121*(3), 743-752.

Ntoukakis, V., Schwessinger, B., Segonzac, C., and Zipfel, C. (2011). Cautionary notes on the use of C-terminal BAK1 fusion proteins for functional studies. *The Plant Cell Online, 23*(11), 3871-3878.

Park, H. C., Kim, M. L., Kang, Y. H., Jeon, J. M., Yoo, J. H., Kim, M. C., . . . Cho, M. J. (2004). Pathogen- and NaCl-induced expression of the SCaM-4 promoter is mediated in part by a GT-1 box that interacts with a GT-1-like transcription factor. *Plant Physiology, 135*(4), 2150-2161.

Petersen, K., Qiu, J.-L., Lütje, J., Fiil, B. K., Hansen, S., Mundy, J., and Petersen, M. (2010). Arabidopsis MKS1 is involved in basal immunity and requires an intact N-terminal domain for proper function. *PloS One, 5*(12), e14364.

Pitzschke, A., Schikora, A., and Hirt, H. (2009). MAPK cascade signalling networks in plant defence. *Current Opinion in Plant Biology, 12*(4), 421-426.

Postel, S., Küfner, I., Beuter, C., Mazzotta, S., Schwedt, A., Borlotti, A., . . . Nürnberger, T. (2010). The multifunctional leucine-rich repeat receptor kinase BAK1 is implicated in Arabidopsis development and immunity. *European Journal of Cell Biology, 89*(2), 169-174.

Prigge, M. J., and Bezanilla, M. (2010). Evolutionary crossroads in developmental biology: Physcomitrella patens. *Development, 137*(21), 3535-3543.

Qi, D., and Innes, R. W. (2013). Recent Advances in Plant NLR Structure, Function, Localization, and Signaling. *Front Immunology, 4*, 348.

Qin, Y., Ma, X., Yu, G., Wang, Q., Wang, L., Kong, L., . . . Wang, H. W. (2014). Evolutionary History of Trihelix Family and Their Functional Diversification. *DNA Res*earch, 10-15.

Qiu, J.-L., Zhou, L., Yun, B.-W., Nielsen, H. B., Fiil, B. K., Petersen, K., . . . Morris, P. C. (2008). Arabidopsis mitogen-activated protein kinase kinases MKK1 and MKK2 have overlapping functions in defense signaling mediated by MEKK1, MPK4, and MKS1. *Plant Physiology, 148*(1), 212-222.

Rensing, S. A., Lang, D., Zimmer, A. D., Terry, A., Salamov, A., Shapiro, H., . . . Kamisugi, Y. (2008). The Physcomitrella genome reveals evolutionary insights into the conquest of land by plants. *Science, 319*(5859), 64-69.

Rodriguez, M. C., Petersen, M., and Mundy, J. (2010). Mitogen-activated protein kinase signaling in plants. *Annual Review Plant Biology, 61*, 621-649.

Roux, M., Schwessinger, B., Albrecht, C., Chinchilla, D., Jones, A., Holton, N., . . . Zipfel, C. (2011). The Arabidopsis leucine-rich repeat receptor–like kinases BAK1/SERK3 and BKK1/SERK4 are required for innate immunity to hemibiotrophic and biotrophic pathogens. *The Plant Cell Online, 23*(6), 2440-2455.

Rubinelli, P., Hu, Y., and Ma, H. (1998). Identification, sequence analysis and expression studies of novel anther-specific genes of Arabidopsis thaliana. *Plant Molecular Biology, 37*(4), 607-619.

Sanders, P. M., Bui, A. Q., Weterings, K., McIntire, K., Hsu, Y.-C., Lee, P. Y., . . . Goldberg, R. (1999). Anther developmental defects in Arabidopsis thaliana male-sterile mutants. *Sexual Plant Reproduction, 11*(6), 297-322.

Schmidt, E., Guzzo, F., Toonen, M., and De Vries, S. (1997). A leucine-rich repeat containing receptor-like kinase marks somatic plant cells competent to form embryos. *Development, 124*(10), 2049-2062.

Schwessinger, B., and Ronald, P. C. (2012). Plant innate immunity: perception of conserved microbial signatures. *Annual Review of Plant Biology, 63*, 451-482.

Segonzac, C., Macho, A. P., Sanmartin, M., Ntoukakis, V., Sanchez-Serrano, J. J., and Zipfel, C. (2014). Negative control of BAK1 by protein phosphatase 2A during plant innate immunity. *Embo Journal*, 420-426.

Shan, L., He, P., Li, J., Heese, A., Peck, S. C., Nürnberger, T., . . . Sheen, J. (2008). Bacterial effectors target the common signaling partner BAK1 to disrupt multiple MAMP receptor-signaling complexes and impede plant immunity. *Cell Host Microbe, 4*(1), 17-27.

Shendure, J., and Ji, H. (2008). Next-generation DNA sequencing. *Nature Biotechnology, 26*(10), 1135-1145.

Shiu, S.-H., and Bleecker, A. B. (2001). Receptor-like kinases from Arabidopsis form a monophyletic gene family related to animal receptor kinases. *Proceedings of the National Academy of Sciences, 98*(19), 10763-10768.

Spoel, S. H., and Dong, X. (2012). How do plants achieve immunity? Defence without specialized immune cells. *Nature Review Immunology, 12*(2), 89-100.

Staskawicz, B. J., Dahlbeck, D., and Keen, N. T. (1984). Cloned avirulence gene of Pseudomonas syringae pv. glycinea determines race-specific incompatibility on Glycine max (L.) Merr. *Proceedings of the National Academy of Sciences, 81*(19), 6024-6028.

Sun, Y., Fan, X.-Y., Cao, D.-M., Tang, W., He, K., Zhu, J.-Y., . . . Oh, E. (2010). Integration of brassinosteroid signal transduction with the transcription network for plant growth regulation in Arabidopsis. *Developmental cell, 19*(5), 765-777.

Sun, Y. D., Li, L., Macho, A. P., Han, Z. F., Hu, Z. H., Zipfel, C., . . . Chai, J. J. (2013). Structural Basis for flg22-Induced Activation of the Arabidopsis FLS2-BAK1 Immune Complex. *Science, 342*(6158), 624-628.

Tang, W., Kim, T.-W., Oses-Prieto, J. A., Sun, Y., Deng, Z., Zhu, S., . . . Wang, Z.-Y. (2008). BSKs mediate signal transduction from the receptor kinase BRI1 in Arabidopsis. *Science, 321*(5888), 557-560.

Tena, G., Boudsocq, M., and Sheen, J. (2011). Protein kinase signaling networks in plant innate immunity. *Current Opinion in Plant Biology, 14*(5), 519-529.

Trapnell, C., Williams, B. A., Pertea, G., Mortazavi, A., Kwan, G., van Baren, M. J., . . . Pachter, L. (2010). Transcript assembly and quantification by RNA-Seq reveals unannotated transcripts and isoform switching during cell differentiation. *Nature Biotechnology, 28*(5), 511-U174.

Xin, X. F., and He, S. Y. (2013). Pseudomonas syringae pv. tomato DC3000: a model pathogen for probing disease susceptibility and hormone signaling in plants. *Annual Review Phytopathology, 51*, 473-498.

Xu, J. H., Wei, X. C., Yan, L. M., Liu, D., Ma, Y. Y., Guo, Y., . . . Shui, W. Q. (2013). Identification and functional analysis of phosphorylation residues of the Arabidopsis BOTRYTIS-INDUCED KINASE1. *Protein and Cell, 4*(10), 771-781.

Xu, X., Chen, C., Fan, B., and Chen, Z. (2006). Physical and functional interactions between pathogen-induced Arabidopsis WRKY18, WRKY40, and WRKY60 transcription factors. *Plant Cell, 18*(5), 1310-1326.

Yamaguchi, Y., Pearce, G., and Ryan, C. A. (2006). The cell surface leucine-rich repeat receptor for AtPep1, an endogenous peptide elicitor in Arabidopsis, is functional

in transgenic tobacco cells. *Proceedings of the National Academy of Sciences, 103*(26), 10104-10109.

Yin, Y., Vafeados, D., Tao, Y., Yoshida, S., Asami, T., and Chory, J. (2005). A new class of transcription factors mediates brassinosteroid-regulated gene expression in Arabidopsis. *Cell, 120*(2), 249-259.

Yu, X., Li, L., Zola, J., Aluru, M., Ye, H., Foudree, A., . . . Liu, P. (2011). A brassinosteroid transcriptional network revealed by genome‐wide identification of BESI target genes in Arabidopsis thaliana. *The Plant Journal, 65*(4), 634-646.

Zhang, J., Li, W., Xiang, T., Liu, Z., Laluk, K., Ding, X., . . . Chen, S. (2010). Receptor-like Cytoplasmic Kinases Integrate Signaling from Multiple Plant Immune Receptors and Are Targeted by a Pseudomonas syringae Effector. *Cell Host Microbe, 7*(4), 290-301.

Zhou, J., Wu, S., Chen, X., Liu, C., Sheen, J., Shan, L., and He, P. (2014). The Pseudomonas syringae effector HopF2 suppresses Arabidopsis immunity by targeting BAK1. *The Plant Journal, 77*(2), 235-245.

Zhu, Y., Mang, H.-g., Sun, Q., Qian, J., Hipps, A., and Hua, J. (2012). Gene discovery using mutagen-induced polymorphisms and deep sequencing: application to plant disease resistance. *Genetics, 192*(1), 139-146.

Zipfel, C., Kunze, G., Chinchilla, D., Caniard, A., Jones, J. D., Boller, T., and Felix, G. (2006). Perception of the bacterial PAMP EF-Tu by the receptor EFR restricts Agrobacterium-mediated transformation. *Cell, 125*(4), 749-760.

Zipfel, C., Robatzek, S., Navarro, L., Oakeley, E. J., Jones, J. D. G., Felix, G., and Boller, T. (2004). Bacterial disease resistance in Arabidopsis through flagellin perception. *Nature, 428*(6984), 764-767.

APPENDIX

SUPPLEMENTAL DATA

Supplemental Fig. 1. Characterization of *asr3* T-DNA Knockout Lines and Complementation Transgenic Lines.

Supplemental Fig. 2. The flg22-Induced ASR3 Phosphorylation Is Not Affected by Ca^{2+} Channel Inhibitor or NADPH Oxidase Inhibitor Treatment.

Supplemental Fig. 3. ASR3 Localizes to the Nucleus in *35S:ASR3-GFP* Transgenic Plants.

Supplemental Fig. 4. The Coiled-Coil Domain of ASR3 Is Required for ASR3 Homodimerization.

Supplemental Fig. 5. Characterization of *35S:ASR3-HA* and *35S:ASR3*^{T189D}*-HA* Transgenic Lines.

Supplemental Table 1. LC-MS/MS Analysis of in Vivo Phosphorylation of ASR3 upon flg22 Treatment.

Supplemental Table 2. Primers Used in This Study.

Supplemental Table 3. Elicitors and Chemical Inhibitors Used in This Study.

Supplemental Data Set 1A. List of ASR3-Regulated Genes without Treatment.

Supplemental Data Set 1B. List of flg22-Induced Genes in Either the WT, *asr3-1*, or OX9.

Supplemental Data Set 1C. Four Groups of ASR3-Dependent flg22-Induced Genes.

Supplemental Data Set 1D. The flg22-Induced Genes with Enhanced Induction in *asr3-1* Mutant and Reduced Induction in OX9 Plants Compared with WT Plants.

Supplemental Data Set 1E. GO Biological Process Enrichment of ASR3-Dependent flg22-Induced Genes.

Supplemental Data Set 1F. List of flg22-Reduced Genes in Either the WT, *asr3-1*, or OX9.